Politecnico di Torino

Master of Science in Energy and Nuclear Engineering

Joint M. S. in Nuclear Engineering at Politecnico di Milano (Poly2Nuc)

fondazione CNAO
Centro Nazionale di Adroterapia Oncologica per il trattamento dei tumori

Radio Frequency KnockOut (RFKO) extraction: hardware analysis and beam optics simulation and optimization

Supervisors: Prof. Sandra Dulla (PoliTo)
Prof. Stefano Agosteo (PoliMi)
Dr. Marco Pullia (CNAO)

Student: Giulia Russo

MARCH 2019

A mio papà.

Abstract

The aim of this thesis is the optimization of the CNAO synchrotron working point in order to achieve beam extraction with the RF-KO (Radio Frequency Knock-Out) technique. This method would reduce the time needed for patient treatment since the non-extracted beam is kept in the machine and could be re-accelerated in order to attain a new energy for the new irradiation field. At present, the re-acceleration of the non-extracted beam is not possible since the beam is de-bunched and the bunching process, i.e. trapping particles in the bucket, performed by the RF cavity, would induce great particle losses (almost 50%). With the RFKO technique the beam remains bunched so the RF cavity can accelerate it without losing half of the particles. As a nuclear engineer, particle physics, accelerators and beam dynamics were not part of my academic background. This is why the first two chapter of the thesis concern the physics of accelerator as well as beam dynamics, they contain a kind of summary of the topics studied and of the different references used. The third chapter is still a fully theoretical one since it contains the different techniques for beam extraction, in particular, the slow ones will be highlighted since the main topic of the thesis concerns the study of RFKO. From the fourth chapter on results will be presented. The analysis of the hardware was the first set of experimental measures performed and post-processed. At the beginning, different test benches have been built with the aim of optimizing of the connections between the different components, i.e. long or short cable connections (and so the location of the components themselves in the electronic or synchrotron room). Fourier analysis was part of the study in order to highlight the fundamental harmonics and their evolution as a function of the peak-to-peak inlet voltage signal. Then the numerical simulation step has been performed. Deterministic particle codes simulating beam extraction have already been developed. The post-processing code has been written on MatLab. Since first results seemed to be promising, the modification of the original codes has been started in order to try to improve the performances of the machine. Due to statistics the profile of the extracted beam is not constant (as required for medical application) therefore the code for the kicker ramp-up has been written using a Monte Carlo method for the random generation of kicks. An additional code to further study the extracted particles has been developed in order to monitor the last three turns of the particles before the extraction.

Riassunto

Lo scopo di questa tesi è l'ottimizzazione del punto di lavoro del sincrotrone del CNAO al fine di ottenere l'estrazione del fascio con la tecnica RF-KO (Radio Frequency Knock-Out). Questo metodo ridurrebbe il tempo necessario per il trattamento del paziente poiché il fascio non estratto viene tenuto nella macchina e potrebbe essere nuovamente accelerato al fine di ottenere la nuova energia per il nuovo campo di irraggiamento. Allo stato attuale, la ri-accelerazione del fascio non estratto non è possibile poiché il fascio è *de-bunched* longitudinalmente e il processo di *bunching*, cioè l'intrappolamento di particelle nel *bucket*, eseguito dalla cavità RF, indurrebbe grandi perdite di particelle (quasi 50 %). Con la tecnica RFKO il fascio è sempre *bunched* in modo che la cavità RF possa accelerarlo senza perdere metà delle particelle. Come ingegnere nucleare, la fisica delle particelle, gli acceleratori e le dinamiche del fascio non facevano parte del mio background accademico. Questo è il motivo per cui i primi due capitoli della tesi riguardano la fisica dell'acceleratore e la dinamica del fascio, contengono una sorta di riassunto degli argomenti studiati e delle diverse fonti utilizzate. Il terzo capitolo è ancora completamente teorico in quanto contiene una descrizione delle tecniche di estrazione del fascio, in particolare quelle lente saranno evidenziate dal momento che il tema principale della tesi riguarda lo studio della RFKO. Dal quarto capitolo in poi i risultati saranno presentati. L'analisi dell'hardware è stata la prima serie di misure sperimentali eseguite e post-elaborate. All'inizio, sono stati costruiti diversi banchi di prova con l'obiettivo di ottimizzare i collegamenti tra i diversi componenti, cioè i collegamenti con cavi lunghi o corti (e quindi la posizione dei componenti stessi nella sala elettronica o sincrotrone). L'analisi di Fourier faceva parte dello studio al fine di evidenziare le armoniche fondamentali e la loro evoluzione in funzione della tensione picco-picco del segnale in ingresso. Quindi è stata eseguita la fase di simulazione numerica. Erano già stati sviluppati codici deterministici per studiare il percorso delle particelle nell'acceleratore che dunque simulano l'estrazione del fascio. Il codice di post-elaborazione è stato scritto su MatLab. Dal momento che i primi risultati sembravano essere promettenti, la modifica dei codici originali è stata avviata al fine di cercare di migliorare le prestazioni della macchina. A causa della statistica, il profilo del fascio estratto non era costante (come richiesto per l'applicazione medica) quindi il codice per la rampa del kicker è stato scritto utilizzando un metodo Monte Carlo per la generazione casuale di kick. È stato infine sviluppato un codice ulteriore per studiare più nel dettaglio le particelle estratte al fine di monitorare gli ultimi tre giri delle stesse prima dell'estrazione.

TABLE OF CONTENTS

List of Tables

List of Figures

Figure **Page**

CHAPTER 1

HADRONTHERAPY AND CNAO

This chapter will give an introduction to radiobiology, useful to understand why the conventional radiotherapy could be (in selected cases) substituted with hadrontherapy. This medical treatment exploits the physics of particles beams and thus particles accelerators can be studied in a new context. Hadrons are particles composed by quarks and held together by the strong nuclear force,protons and neutrons are two of the elementary hadrons that compose most of the ordinary matter. In this context, the focus will be on protons and carbon ions. In the world there are several proton centres for cancer treatment, but just few of them are able to accelerate also carbon ions. There are just six (operative) centres around the world that use both the particle beams for treatments, but new ones are under construction or commissioning. One of these centre has been built in Pavia (PV - Italy) and it is called CNAO: National Centre for Oncological Hadrontherapy. At the and, the description of CNAO accelerating facility will be done.

1.1 Introduction to radiobiology

A cell can live, grow, reproduce and die thanks to the information contained in its DNA, perfectly enclosed in the nucleus. Among all the processes occurring within a cell the most important is its reproduction. Mitosis is the division process that brings the mother nucleus to divide in two daughters nuclei both with the same genetic information, other processes (occurring also in other parts of the human body) bring the cells to get specialized for a particular function. From embryo to old people, the velocity at which cells reproduce themselves strongly decreases, being one of the reasons of aging. This characteristic is also the reason of the different effects of radiation interactions with biological tissue. When the radiation reaches the tissue, it can interact with the local cells leading to different possible outcomes:

- No effects on the living cell;
- Delay in the division;
- Apoptosis: the cell dies before it divides or afterwards by fragmentation into smaller bodies, and it is then absorbed by the neighbouring cells;
- Reproductive failure: the cell dies when it tries the first or subsequent mitosis;
- Genomic instability: delayed form of reproductive failure as a result of induced genomic instability;
- Mutation: the cell survives but it contains genetic mutations:
- Transformation: the cell survives but the mutation leads to a transformed phenotype and possibly carcinogenesis;
- Bystander effects: an irradiated cell can send signal to neighbouring unirradiated cells and induce genetic damage in them;
- Adaptive responses: the irradiated cell is stimulated to react and become more resistant to subsequent irradiation.

A tumour consists in a small group of cells, with genetic mutation that doesn't respond to normal apoptosis and then undergoes to fast growth. The altered cells still look like normal ones, but their reproduction velocity is too high (hyperplasia). It can occur that one of the abnormal cells undergoes to a further mutation that increases again its reproduction velocity. If this happens, then an optical difference can be observed because that group of cells has a different form and orientation (dysplasia) with respect to the healthy tissue. If the growth continues and the boundaries of the local tissue is still not broken then the tumour is called *in-situ tumour*, otherwise it is an *invasive cancer*. In this latter case if abnormal cells reach the blood or the lymphatic system, they are able to set in another part of the body generating new tumour

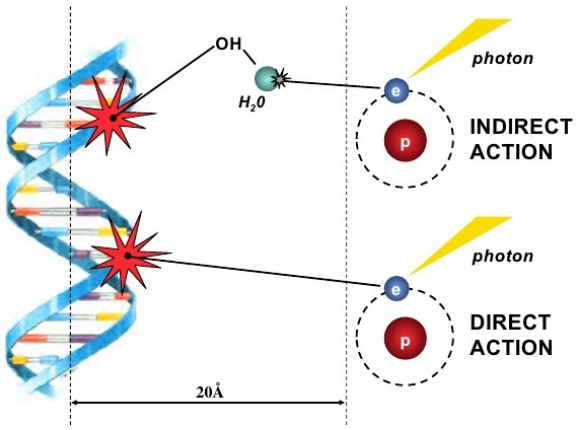

FIGURE 1.1. Schematic representation of DNA-radiation interaction highlighting the difference between direct and indirect action [23].

locations (metastases). The radiation interaction with biological tissue is one of the possible reasons why a cell can be subjected to genetic mutation. There are two main mechanisms of interactions, schematically shown in Figure 1.1:

- Direct action. The radiation interacts with the target causing ionization or excitation through coulomb interactions. This starts a chain of physical and chemical events that is typical of high LET particles.
- Indirect action. The radiation interacts with molecules producing free radicals (as hydroxyl radical) which can damage the DNA through diffusive process within the cell. The biological damage is caused by the rupture of chemical bonds substituted by new and abnormal ones. The high reactivity of the free radicals can be explained thanks to their unpaired valance electron. This type of interaction is characteristic of low LET particles.

To have a better understanding of the phenomenology it is important to explain the concept of LET. LET (Linear Energy Transfer) can be defined as the energy locally deposited, dE, in the medium by a charged particle of specified E_0 energy on a path length dl.

$$LET = \frac{dE}{dl}\bigg|_{E_0} \tag{1.1}$$

LET is expressed in keV/μm and it is common practice to divide it into two regions: low and high LET. The boundary is set around 10 keV/ μ m from sparsely ionizing (X and γ -rays, Co-60) to densely ionizing (i.e., heavy charged) particles. In Table 1.1 there are values of LET for different types of particles at different energies. The same particle can be considered a low LET particle or a high LET particle according to its energy. On the one hand, radiation can cause biological damages in the tissue, on the other hand if it is well controlled and accurately chosen it can be used for cancer treatment. The therapeutic index, also referred to as therapeutic ratio, defines

	Energy [MeV]	LET[$keV/\mu m$]
Electrons	0.01	2.30
	0.1	0.42
	1	0.25
Protons	2	16
	5	8
	10	4
Neutrons	5	3 - 30
Photons	1 -25	0.2 - 2
Carbon Ions	10 - 250 MeV/u	170 - 140

Table 1.1: LET for electrons, protons, neutron, photons and carbon ions for different energy values or ranges [24].

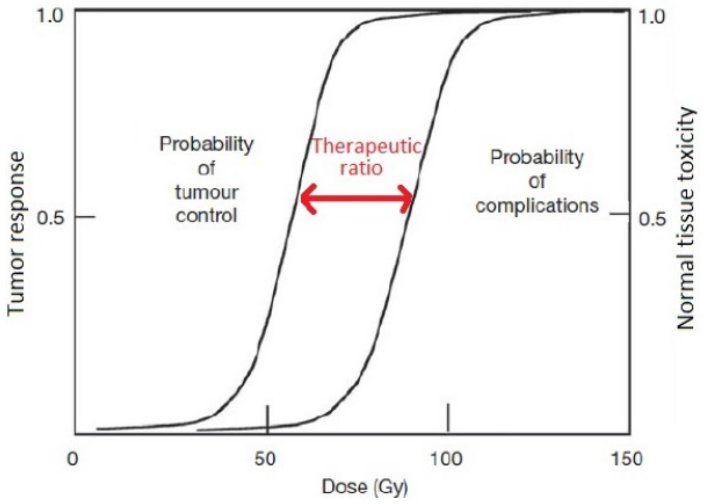

FIGURE 1.2. Survival fraction and tumor response versus dose in Gy [25].

the amount of agent (in this case, the dose) above which the side-effects arise (i.e., radiation is no longer helping in cancer treatment) and below which no effect can be seen. In Figure 1.2 it is represented how the therapeutic ratio changes with the dose. It is easy to understand how low doses induce no reactions in the tumour cells, as if they were almost insensible to lower doses. On the other hand, a too high dose could be able to kill the tumour cells but, at the same time, it is highly probable that it could produce side effects. There is so a quite thin line that separates benefits from drawbacks of such a treatment.

Interactions of heavy charged particles with matter is of interest because at CNAO tumours are treated using beams of protons and carbon ions. Due do their relatively high mass with respect to the one of electrons with which they interact, their flight direction is practically left unchanged after the collision. But as they move in matter, they continuously lose energy according

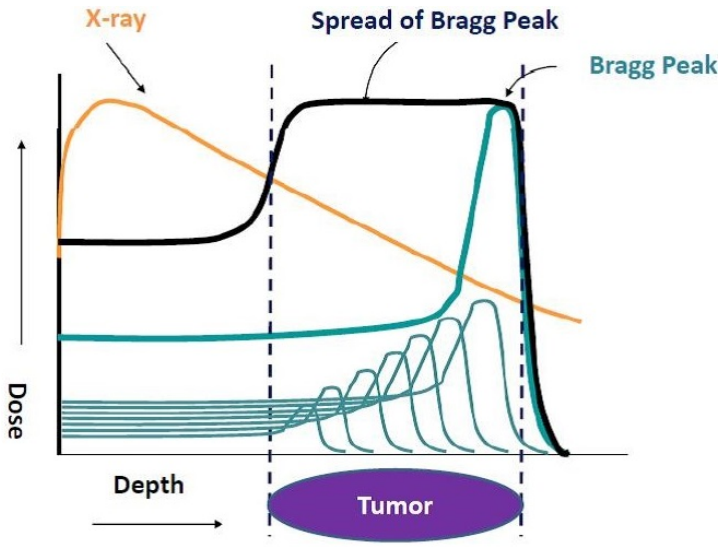

FIGURE 1.3. X-rays undergo to exponential decay with the deposition of the maximum dose at the skin level while beam of particles can deposit the the maximum dose at the Bragg peak, which position can be changed by changing the beam energy [3].

to the Bethe-Bloch formula, reported in Equation (1.6).

$$-\frac{dE}{dx} = 4\pi N_e r_e^2 m_e c^2 \frac{z^2}{\beta^2}\left(ln\frac{2m_e c^2\beta^2\gamma^2}{I} - \beta^2 - \frac{\delta(\gamma)}{2}\right) \tag{1.2}$$

The formula describes the mean energy loss (that justifies the minus sign) per distance travelled by the radiation across the medium. From a physical point of view, the kinetic energy lost by the particle (*Kerma*) can be different from the energy absorbed by the biological tissue (*Dose*). From Figure 1.3 it is possible to see this phenomenon in case of tumour treatment with conventional radiotherapy (X-rays). The dose delivered to the tissue increases as the radiation penetrates inside the body, it reaches a maximum and then it exponentially decreases. The initial growing trend is known as *skin sparing effect* and it is due to collisions that make the radiation non-collimated. On the contrary, when a beam of particles is considered a different phenomenology occurs. There is an initial region along which the energy loss is constant, then it rapidly increases reaching a maximum. The maximum energy lost (i.e., the **Bragg peak**) occurs at a certain distance within the matter and then the particle has not enough energy to travel so the energy loss falls to zero almost vertically and the particle is absorbed by the medium. This phenomenon can be observed in Figure 1.3 where different Bragg peaks for different energies of the incoming beam are represented. This feature is of great interest for medical applications since it allows the positioning of the maximum energy loss at the tumour location just by changing the beam energy. The combination of different Bragg peaks has to be carefully studied in order to match the energy loss with the medical dose. This procedure takes into account different drawbacks as the non perfectly mono-energetic beam, the penumbra region, the tumour shape and even more. As

Type of radiation	**weighting factors**
X-rays and γ -rays for all energies	1
Electrons and muons for all energies	1
Protons @ energy>2Mev	5
Alphas, fission fragments, heavy nuclei	20
Neutrons @ energy<10keV	5
Neutrons between 10keV and 100keV	10
Neutrons between 100keV and 2MeV	20
Neutrons between 2MeV and 20MeV	10
Neutrons @ energy>20Mev	5

Table 1.2: RBE for different particles at particular energies [18]

the exponentially decay is the characteristic feature of *x-rays* used in conventional radiotherapy, the Bragg peak is the main physical characteristic of heavy charged particles interactions with matter, and it is the main reason why it can be easily exploited to release the highest amount of energy at the tumour location. This type of treatment is known as *hadrontherapy* or highly precise radiotherapy. The amount of energy able to produce biological damages in the tumour site is of fundamental importance in the treatment planning stage. It could be useful to compare the dose necessary to produce the same biological damage by different type of radiations: this information is collected in the Relative Biological Effectiveness (RBE) defined in Equation (1.7). It should be considered that the RBE strongly depends on the radiation, as shown in Table 1.2.

(1.3)
$$RBE = \frac{D_X}{D_R} = \frac{reference\ absorbed\ dose\ of\ a\ standard\ type\ X}{absorbed\ dose\ of\ type\ R\ that\ causes\ the\ same\ amount\ of\ biological\ damage}$$

The content of oxygen in cancer treatment is fundamental, in fact cell that are not fully oxygenated require a higher dose (with respect to fully oxygenated cells) to obtain the same biological effect. This behaviour is numerically expressed by the Oxigen Enhanced Ratio (OER) is defined in Equation (1.8).

(1.4)
$$OER = \frac{dose\ to\ produce\ a\ given\ effect\ without\ oxygen}{dose\ to\ produce\ the\ same\ effect\ with\ oxygen} \geq 1$$

The reason why a hypoxic cell has a different behaviour compared with an oxic cell, leading then to a different radiotherapy response, could be due to the way the oxygen molecules affect indirect actions, in particular the combination of free radicals (OH^- and H^+) with the molecules themselves, making a chain reaction to build up. It is important to highlight that there is still not unanimous agreement in the scientific community to explain how oxigen affect the radiotherapy response. Assuming to deliver the same dose to the tissue (for example look at the red line in Figure 1.9), the fraction of hypoxic cells that survive to the irradiation is larger than the one

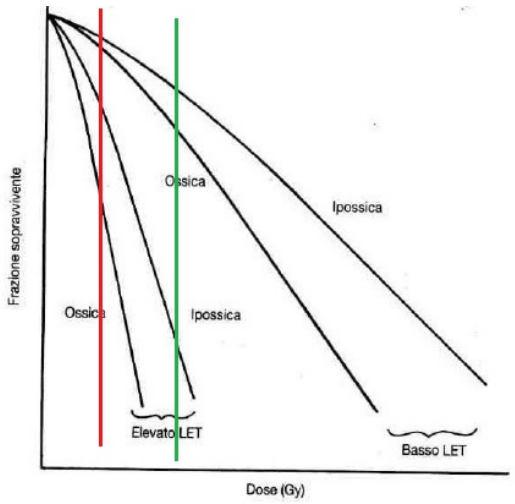

FIGURE 1.4. Fraction of survival cells vs. dose as a function of oxygen content. Focus on different behavious of oxic and hypoxic cells when the same dose is delivered and on the different dose necessary to kill a cell (of a certain family) when irradiated with low or high LET particles [25].

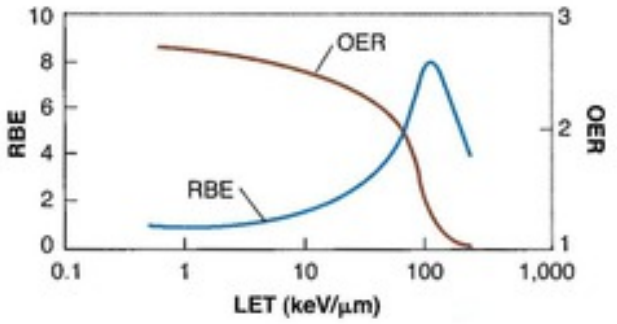

FIGURE 1.5. RBE and OER vs LET comparison [9].

of oxic one, no matter if the irradiation is performed with high or low LET particle. It further confirms the idea that the first type of cell (hypoxic) shows a higher resistance to radiation treatment. In addition, considering just hypoxic or oxic cells the probability they survive to low LET particle irradiation is higher than the case of high LET particle irradiation. This means that the effect of oxygen content is more relevant in case of low LET particle treatment. By the comparison between OER and RBE with respect to LET, as shown in Figure 1.10, it is possible to conclude that high LET particles have a smaller OER but a higher RBE, which means that the effective dose absorbed by the tissue is relevant but the effect on hypoxic cells is small; on the other hand, low LET particles have higher OER so they have a greater effect on low oxygen content cells but the biological damage they can induce is small.

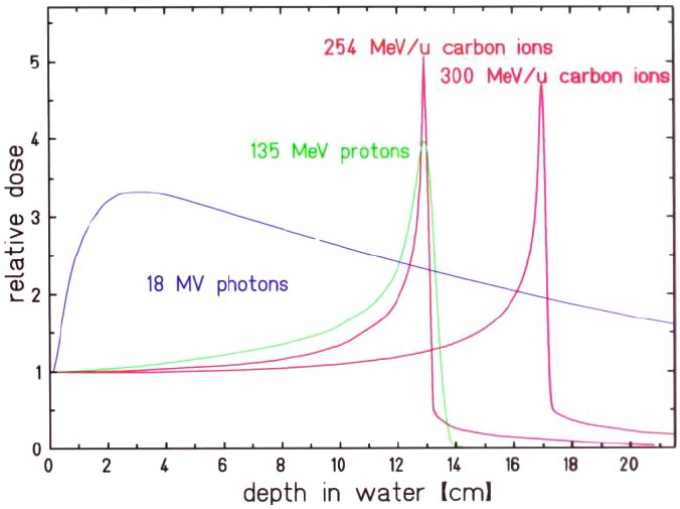

FIGURE 1.6. Penetration length versus relative dose for photons at 18Mev, protons at 135MeV and carbon ions at 254Mev/u and 300MeV/u. At 0cm corresponds the skin of the patient. [26].

1.2 Hadrontherapy

Hadrontherapy is an innovative radiotherapy which first date back to 1946 [26]. The term hadrons refers to those particles composed by quarks held together by the strong nuclear force. Protons and neutrons are the two fundamental hadrons that compose most of the ordinary matter. Among the different medical procedures for oncological patients, the main difference between conventional radiotherapy and hadrontherapy can be observed in Figure 1.6. Photons show the highest dose release between 2.5cm and 3.5cm well above the tumour position; a beam of protons or carbon ions with specific energy shows the characteristic Bragg peak at the desired position. From Figure 1.6, it is possible to understand that to totally cover the tumour, it is necessary to irradiate the patient with beams at different energies and to assess that the cells receive the required dose to be killed. The overlapping of the dose curves of mono-energetic beams in depth will issue an expanded Bragg peak, or “spread-out Bragg peak” (SOBP), which will guarantee the conformation of the dose delivered to the target volume in the direction of beam penetration and, simultaneously, a narrow distal penumbra as shown in Figure 1.8. By the knowledge of the specific ion RBE, for every value of energy, i.e. the RBE at various depths of SOBP as shown in Table 1.2, physical dose may be conformed to obtain a uniform biological dose along the SOBP and avoid regions with high dose and high RBE outside the tumour volume. In both cases (photons and protons/carbon ions), the tissue in front of the tumour interacts with the particles and receives a certain dose. This side-effect can be handled, in fact, if in the front of the tumour there are organ at risks (organs sensible to irradiation and fundamental for patient life), the patient can be irradiated from another direction or with multiple beams in order to reduce as much

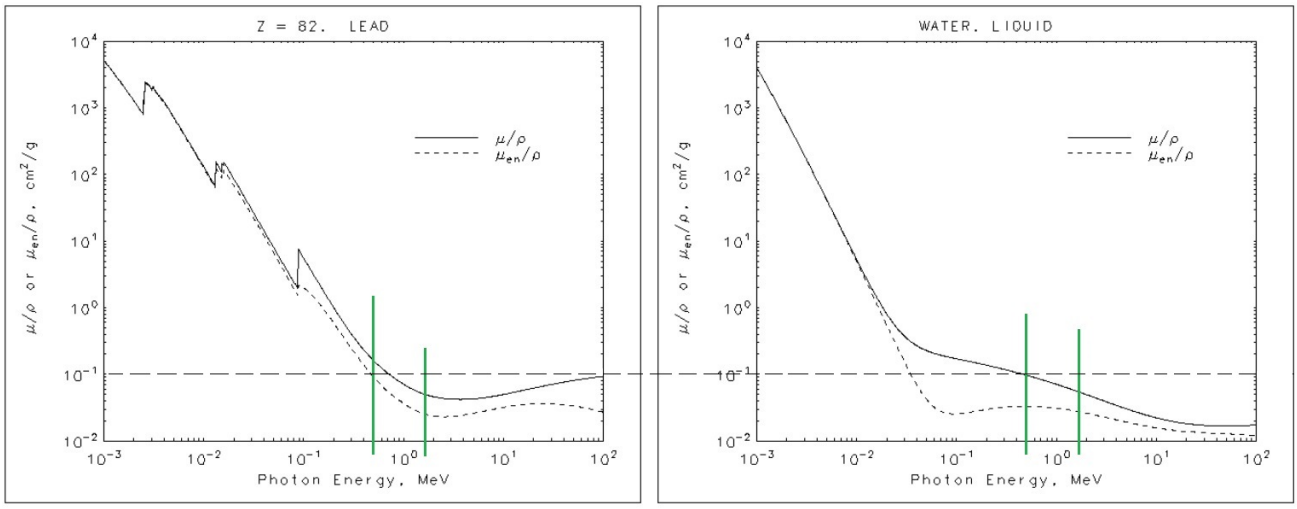

FIGURE 1.7. Comparison attenuation coefficients of water and lead in the energy range for radiotherapy [14].

as possible the dose deposited in the sensible region. A fundamental drawback of conventional radiotherapy is that photons have an infinite range, i.e. their intensity is exponentially reduced as it passes by the medium and it goes to zero as the travelled path approches to infinte, meaning that all the "thickness" of the patient receives a dose that must be minimized as much as possible. In the energy range of interest for radiotherapy, water has a smaller attenuation coefficient than lead (frequently used to shield radiation in medical X-ray scanning technique), that globally explains why photons have the slowly decreasing trend in Figure 1.6.

Obviously, cancer treatment with hadrons is not always possible. The tumour has to be of a specific kind, very resistant to conventional radiotherapy (or other therapies), and localized. In Table 1.2 there is a row where generic heavy nuclei are considered, to this category pertains carbon ions too. The reason why it is difficult to assess a weighting factor to each of those particles is due to the way they interact with matter. On the one hand, as Figure 1.6 shows, carbon ions have a narrower Bragg peak than the one of protons, meaning that they release the highest energy in a very limited region. On the other hand, they release a higher amount of energy in the region behind the tumour because as they pass in the medium they undergo to fragmentation, producing an additional but unnecessary dose released in the tissue; this phenomenon leads to a non-zero dose released smaller than the one given by photons in the same range.

Figure 1.9 shows the different dose distribution to the tumour and the surrounding healthy tissue when the patient (either paediatric or adult) is irradiated with protons (on the right hand side of each group of pictures) or with IMRT (Intensity-Modulated Radiation Therapy). In the paediatric case study, the tumour is in the upper part of the body (thoracic tumour) near critical organs like heart, lungs, cord and testes, and it is well confined in the left-hand side of the body.

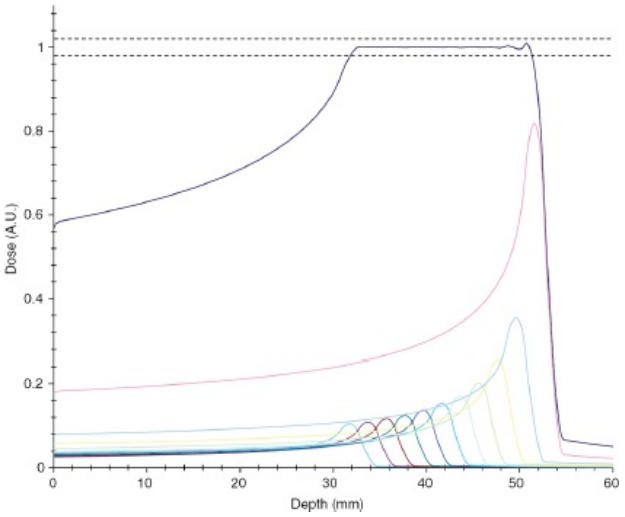

FIGURE 1.8. Spread-Out Bragg Peak (SOBP) [21].

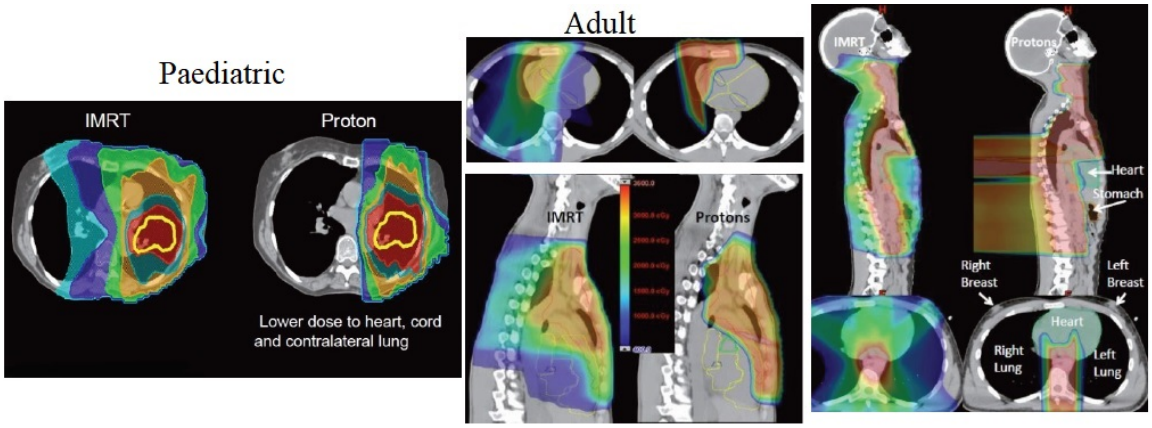

FIGURE 1.9. Comparison between Hadrontherapy and IMRT in paediatric and adult critical tumour location. From the left to the right there are: an abdominal paediatric tumour, two case of lungs tumour in adults. The different dose distribution for the two treatment strategies has to be strongly highlighted. To the blue colour is associated the lowest dose delivered to the patient, whereas the red one corresponds to the highest one [7].

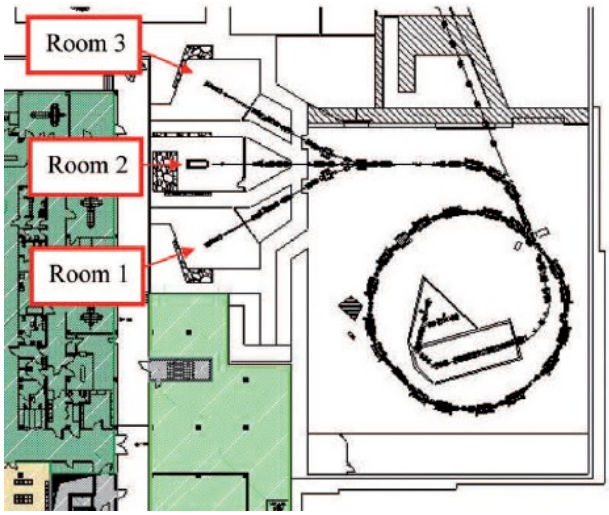

FIGURE 1.10. Schematic representation of the CNAO synchrotron and treatment rooms [27].

The use of IMRT gives the highest dose to the tumour, but also the critical organs around it, the use of protons beam ensures the highest dose in the required region, leaving the cord and part of the testes unirradiated. In the same way, two different case of lungs tumour in adults are shown. The use of protons succeeds in avoiding heart, stomach (on the right side of Figure 1.9) and cord (on the left side) to be irradiated by the beam.

1.3 CNAO facility

CNAO (Italian acronym for National Centre for Oncological Hadrontherapy)[27] is a facility conceived to supply hadrontherapy treatments to patients recruited all over the Country and it has been realised in Pavia, Italy. It is constituted by three operating treatment rooms with four beam lines (three horizontal and one vertical) and one experimental room under installation.

The construction of the CNAO facility has been completed at the beginning of 2010 and on October 2010 the Italian Ministry of Health approved the beginning of the Phase 1 of clinical trial, i.e. the dosimetry and radiobiology programme necessary for the qualification of the two types of beams. The particle beams accelerated in the synchrotron are extracted and send alternately in one of the treatment rooms. In particular, proton beams have an energy range between 60MeV and 250MeV, while carbon ions have an energy between 120MeV/u and 400MeV/u. Energies of such beams will cover a range in water up to about 27 cm, complying with the requirements of clinical use. As far as the main characteristics of CNAO synchrotron are concerned, it is a circular accelerator, of about 25m in diameter. Inside the ring, the sources, the injection lines (particles are injected at 7MeV/u) and a linear accelerator are housed. Outside the ring there are four extraction lines, about 50m each, leading the extracted beam into one of the treatment rooms.

FIGURE 1.11. Real image of CNAO synchrotron. The blue components are the dipoles, while at the centre is possible to observe the LINAC in pink, the electric instrumentation in orange, the sources of hydrogen and bioxide carbide in grey. [27].

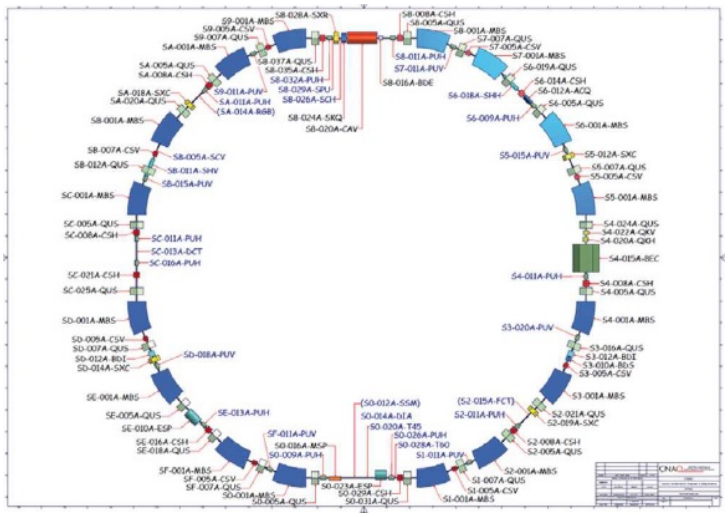

FIGURE 1.12. Schematic representation of CNAO lattice sequence. [27].

In each of the two side rooms (Room 1 and Room 3), in Figure 1.15, a horizontal beam is driven, while in the central one (Room 2) the beam can be directed both horizontally and vertically. The lattice, i.e. the sequence of magnets building up the accelerator, is based on two symmetric arcs joined by two non-dispersive straight sections. The resulting geometry is illustrated in Figure 1.17. In the synchrotron there are sixteen dipoles and twenty-four quadrupoles. The dipoles are powered in series, the quadrupoles have been divided into three families of eight quadrupoles each and there are also three sextupoles. The independent power supply configuration of the three families allow the necessary flexibility to obtain the two non-dispersive regions. The injection

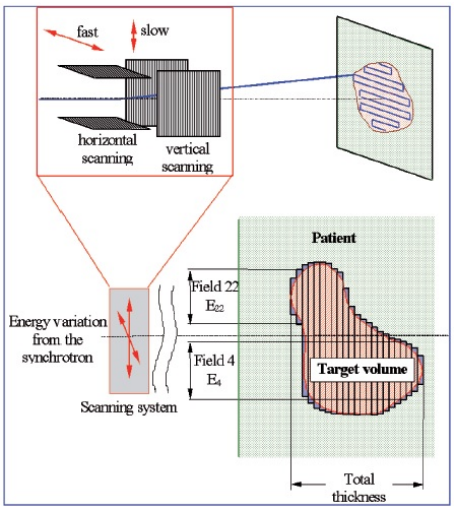

FIGURE 1.13. Active dose distribution. Fast horizontal and slow vertical scanning. [27].

scheme is multi-turn in the horizontal plane and the beam acceleration is provided by a single RF cavity located in the non-dispersive region. The extraction procedure is the most critical step of the whole synchrotron project. An extracted beam (often called spill) as much as possible uniform in time and constant in transverse distribution is a necessary requirement for a clinical use. In this scheme a circulating beam, having a momentum spread, is extracted by pushing it into resonance with a betatron accelerator (the detailed explanation of the extraction process will be discussed in the next chapters). The location of the betatron core is not critical and it has been placed in a free straight section of the synchrotron lattice. CNAO is designed for a fully active dose distribution system, as Figure 1.13 shows. This means that the tumour is ideally divided into “slices”, i.e. into regions that are reached by particles of the same energy; the energy change of the beam for each slice is performed by the synchrotron. Each slice is then irradiated by “painting” it with a pencil beam. In this way the beam is directed to the various points of the tumour, delivering the correct number of particles prescribed by the treatment plan. The position of the beam is controlled in real time thanks to a system of monitors that measure the position of the beam and the number of particles received by each elementary volume element. Patient set-up verification and motion management in particle therapy is a critical issue as the required accuracy level is higher than in conventional photon radiotherapy.

CHAPTER 2

BEAM DYNAMICS

An accelerator has one dimension which is dominant with respect to the other two. This dimension defines the direction along which the particle undergoes to revolutions within the machine and it is called longitudinal direction. The other two are called transverse directions. The particle is accelerated along the longitudinal direction and the study of the phenomena is part of the longitudinal beam dynamics. Even if this topic is of great interest, a brief explanation of the phenomenology will be performed only at the end of this section. The main focus will be on the other two directions and the study of this motion is called transverse beam dynamics.

The chapter will be divided in different subsection, at the beginning there will be a brief description of the different accelerators and of the most common magnets for adjust and control particle position and particle motion; then a detailed derivation of the motion equation will be presented. Thus, the concept of dispersion function will be introduced as the particular solution of the particle motion equation. It will follow a description of particles beams, new concepts will be introduced and other will need to be redefined, so it will be possible to observe common points and differences with respect to single particle motion. At the end, fundamental machine parameters will be mathematically defined and briefly described since they will be strongly used in the next chapters.

2.1 Accelerators

A particle accelerator is a device that increases particle energy using electromagnetic fields. A group of particles with almost the same energy and that is kept well-confined in the machine is called beam. Accelerators can be classified according to different criterions. At first the simplest and more intuitive one is: the geometrical shape. Accelerator can be linear or circular. The design of linear accelerators (named also LinAcs) strongly depends on the type of particle to be accelerated, electrons, ions or protons which strongly differs on their mass. Although this topic is interesting it will not be treated in this context because the focus will be on circular accelerators. They are usually connected to a Radio Frequency (RF) cavity that allows particles to be accelerated up to the required energy. According to this classification an important exception exists: betatron is a circular accelerator that increases the beam energy using the magnetic induction principle. As particles energy is increased they lose part of it due to electromagnetic radiation: the synchrotron radiation. This emission gets more and more important as lighter particles are accelerated.

When a charged particle moves in an electromagnetic field, it is subjected to a force that is called Lorentz force:

$$\mathbf{F} = q(\mathbf{E} + \mathbf{v}x\mathbf{B}) \tag{2.1}$$

A component of the force is in the same direction of the electric field, the other one is proportional to the cross product between the particle velocity and the magnetic field. Obviously, if the particle is subjected just to one between the electric and the magnetic field, then Equation (2.1) simplifies as well as the particle motion.

2.1.1 Electrostatic accelerators

A charged particle is subjected to the action of a constant and time independent electric field, thus, in a non-relativistic case Equation (2.1) simplifies into:

$$\mathbf{F} = q\mathbf{E} = m\mathbf{a} \tag{2.2}$$

It was one of the first accelerator to be designed and its first construction can be dated back to 1932 by J.D. Cockcroft and E.T. Walton. It exploits the physical principle of electrostatic acceleration: it works by accelerating a particle through a constant potential difference V. The particle acceleration can be retrieved being the potential difference directly proportional to the electric field by the particle charge. The strong limitation of such a device is due to physical properties of capacitors and diodes, it leads to a maximum potential difference of 700kV. Higher energies could be obtained with a Van de Graaff accelerator. Moreover, being the electric field conservative, it is not possible to impose too high potential difference otherwise a disruptive electric discharge occurs. In order to have particle beams at higher energies it is necessary to make the electric field time dependent.

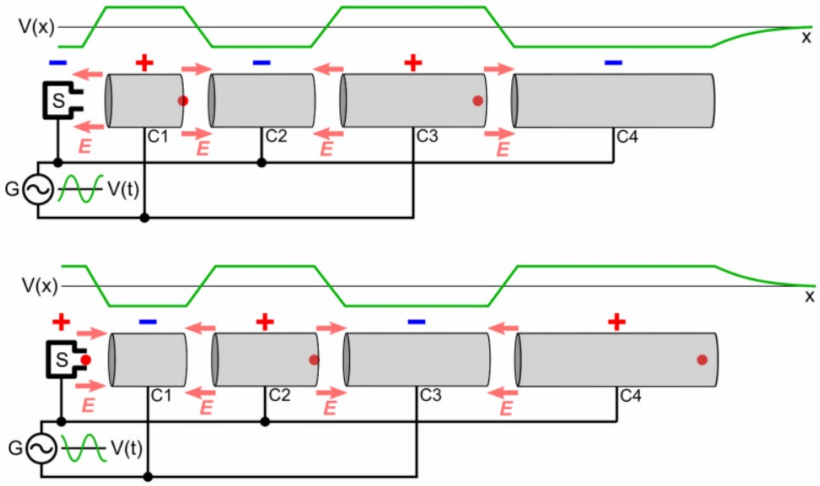

FIGURE 2.1. Working principle of a LINear ACcelerator. It is highlighted the fact that frequency of the voltage generator is synchronous to the passage of the particle in the free flight region [1].

2.1.2 LinAcs

LinAcs are Linear Accelerators where particles are subjected to a time dependent electric field. In this context and under the assumption of not considering relativistic particles, Equation (2.1) is written as:

$$\mathbf{F} = q\mathbf{E}(t) = m\mathbf{a} \tag{2.3}$$

Linear accelerators are constituted by two different components: drift tubes and space between them. Drift tubes are connected to the voltage generator that imposes a sinusoidal potential difference, in particular, consecutive drifts are connected to the two opposite sides of the generator. They work like a Faraday cage, so when the beam crosses them, it does not feel any potential difference, and so, any electric field. Instead, when it moves in the space between the drifts its motion is influenced by the periodic wave of the voltage generator. For this reason, it is necessary to perform opportune changes in such a way that the electric field vector points in the same direction of the particle momentum. So, a change in the length of the drift tubes or in the frequency of the generator is mandatory. If the aim of the accelerator is producing a continuous particle beam at the required energy, then the best choice is changing the length of the drift tubes so that the previous conditions are satisfied. Between two drifts the particle has to be accelerated, this means that if it enters this space while the generator is imposing an electric field which direction is coherent with the particle motion, then it will enter the next drifts with a higher energy. By keeping drifts of the same length would mean that particles always need less time to cross them and so they will pass in the space between drift always at different times and soon the direction of the electric field will not be any more coherent with the direction of the particle

motion (the particle could be decelerated instead of being accelerated). For this reason, the length of the drift tube is increased so that the particle can be always accelerated when it moves in the space between drifts. Otherwise, the change of the generator frequency is possible too, but having clear in mind that in this configuration is not possible to achieve a continuous beam. In this latter case, the frequency is adapted to the transit time of the particle in the free flight region. Usually drifts are connected to only one RF generator, so when the frequency is adapted to allow the acceleration of particles exiting the drift *n*, those that are going out from the drift *n-1* will have a lower energy so they will see the accelerating field for a lower time. Performing the same reasoning for particles exiting the first drift, if the difference in energy is significant, they could enter the free drift space when the field is in the opposite direction, being so decelerated. This is the reason why in this last configuration is not possible to accelerate in a coherent way all the particle, so it is not possible to have a continuous beam but just a bunch of particles.

2.1.3 Cyclotron

It belongs to cyclic RF accelerators. It has a fixed magnetic field imposed by an external electromagnet, that it is responsible for curving particle trajectories, and a time dependent electric field made by a RF generator that accelerates particles. Thus Equation (2.1) turns into:

$$\mathbf{F} = q(\mathbf{E}(t) + \mathbf{v}x\mathbf{B}) \tag{2.4}$$

In the Figure 2.2, it is reported a schematic representation of a cyclotron accelerator. There are two electromagnets imposing the external magnetic field which direction can point upward or downward according to the polarization of the electromagnets themselves. In the region between the magnets there are two (or more) electrodes, called dees. The dees are connected to an alternating RF voltage generator that give rise to a potential difference between the electrodes. In the space between the dees, the particle perceives the electric field, whereas once it is inside the structures it is shielded (they work as Faraday Cages). The ion source is located (red dot in Figure 2.2) in the horizontal plane that contains the dees, and it is also the plane where particles motion occurs. In particular, we can distinguish two main regions: the one inside one of the two dees and the space between the dees themselves. In the first one, the particle is totally shielded from the electric field, so it undergoes only to the motion imposed by the presence of the magnetic field. The motion equation (for particles with $v << c$) is found by the balance between the Second Newton's law and the magnetic component of the Lorentz force:

$$F = ma = \frac{mv^2}{r} = qvB \tag{2.5}$$

From the force balance described in Equation (2.4), the curvature radius can be computed:

$$r = \frac{mv}{qB} = \frac{p}{qB} \tag{2.6}$$

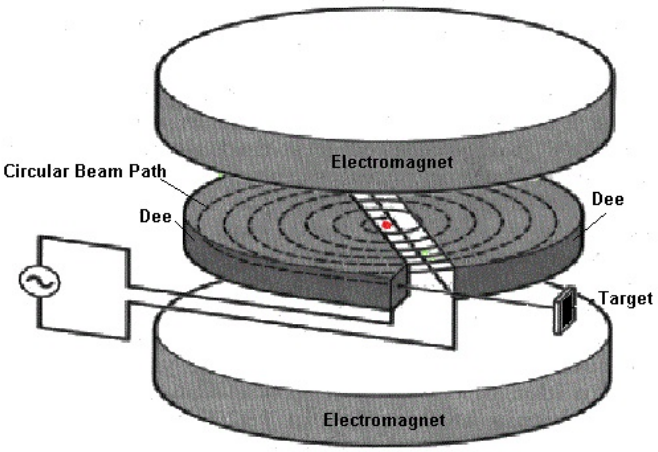

FIGURE 2.2. Schematic representation of a cyclotron from [4].

Once the particle leaves the dee, it perceives the electric field and in the space between the dees and so it is accelerated. Due to the change in its velocity, when it enters the next dee, the curvature radius will be different and it will change according to Equation (2.2). So, it results in a spiral motion of the particle towards higher radii. The frequency of the motion is called gyro-frequency and can be computed as written in Equation (2.5).

$$f = \frac{qB}{2\pi m} \tag{2.7}$$

Usually, a cyclotron is designed according to the maximum particle energy, so that it can reach the required value at the last spiral step, slightly before it is deflected and extracted. The main characteristic of this kind of accelerator is that it continuously accelerates particles, resulting in a beam of particles of almost the same energy. Their are mainly used for proton therapy, but due to the constant energy of the extracted beam it is necessary to put degraders before the beam reaches the patient in order to get the right energy for the treatment. This feature leads to the impossibility to use cyclotrons with heavy charged particles, as carbon ions. More sophisticated cyclotrons have been built. It is possible to find multi-dees cyclotrons with curved edges in order to ensure beam fusing and higher maximum energy.

In the Figure 2.3 it is possible to observe a cyclotron of Paul Scherrer Institut (PSI - Switzerland) which has eight curved dees (eight sector cyclotron) and four accelerating cavities. In this new configuration, a particle is accelerated four times before it passes again by the same electrode. The general result is that cyclotrons of the same dimensions (i.e. equal extraction radius) but with a different number of accelerating sections will generate particles beams of different energies.

FIGURE 2.3. PSI Cyclotron from [8].

2.1.4 Synchrocyclotron

The main defect of cyclotrons is detectable when light particles, i.e. electrons, are accelerated. In this case, when the particle approaches the speed of light, its mass reduces according to relativistic laws. So, to account for this changes, the rest mass of the particle is corrected adding the ratio between the particle speed and the speed of light (known as β, one of the two Lorentz factors). The mathematical expressions is found in Equation (2.8).

$$m = \frac{m_0}{\sqrt{1-(\frac{v}{c})^2}} = \frac{m_0}{\sqrt{1-\beta^2}} \tag{2.8}$$

A synchrocyclotron is a circular accelerator that accelerates particles with RF cavities and it can be said to be the first one that solves the problem of relativistic effects in light particles acceleration. In this condition, the mass reduces according to Equation (2.8) so the gyro-frequency increases according to Equation (2.7). In order to keep a constant gyro-frequency there are two available options: the magnetic field can be changed or a reduction of the RF voltage generator could be performed. Usually this last option is preferred. So, a synchrocyclotron works with a constant frequency up to the moment when particles start to get closer to the speed of light, i.e. relativistic mass reduction becomes important, then the frequency is reduced. In this configuration a continuous beam can not be obtain, because as the frequency is adapted to relativistic particles, those near to the centre of the accelerator, that are still not relativistic, will not be accelerated in a coherent way. So, only “packages” of particles are accelerated up to the required energy the others can be considered to be lost. Obviously, one of the main cons of this accelerator is to have a non-continuous beam and dimensions that depend of the maximum energy.

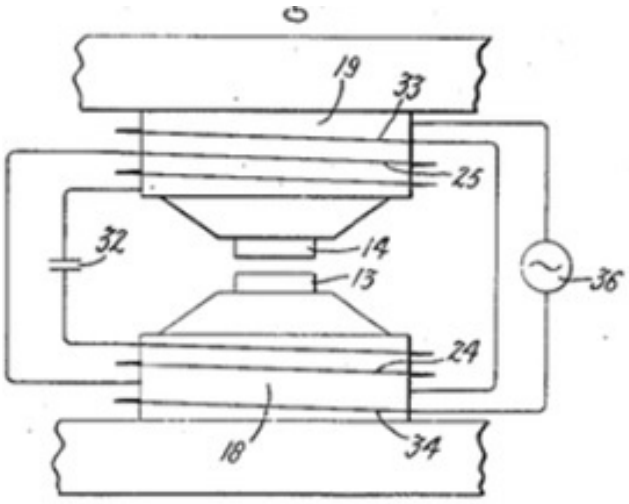

FIGURE 2.4. Betatron schematic representation from [11].

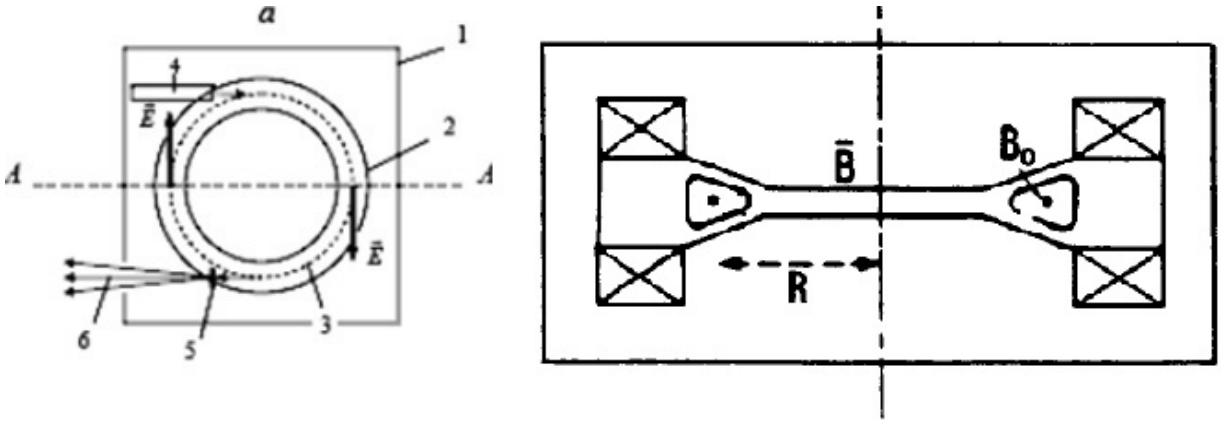

FIGURE 2.5. Transverse and longitudinal section of a betatron from [6, 28].

2.1.5 Betatron

As the names says, a betatron is an accelerator for beta particles, i.e. electrons. The main feature of a betatron is in the way it accelerates particles: it does not exploit the RF cavity principle, i.e. a RF electric field, but it practically works as a transformer. It has a toroidal shape and makes the beam work as the secondary winding. In Figure 2.4, primary winding is highlighted with the number 24 and 25: it is connected to an AC generator (number 36) and it is twisted around two electromagnets (number 18 and 19). In this configuration, the magnetic field varies in time according to the time dependent current in the winding. This field imposes the circular trajectories on which electrons move inside the torus and it also induces in the secondary of the transformer, i.e. the beam, a time dependent electric field that accelerate the particles. It is

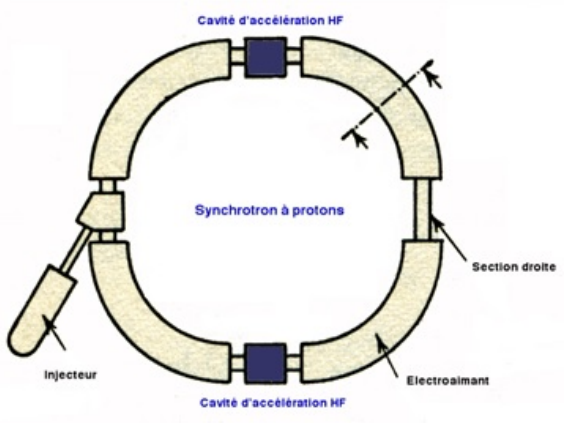

FIGURE 2.6. Schematic representation of a synchrotron from [2].

possible to observe the torus from above on the right hand side of Figure 2.5, while on the left hand side there is a representation of its transverse sections. At the centre particles are subjected to the nominal field that progressively decreases moving towards the outer region. Looking at the behaviour of light particles in a betatron, different discoveries have been made. When a particle is accelerated it loses part of its energy by radiation emission: the synchrotron radiation or magnetobremsstrahlung radiation. It is characteristic of those acceleration phenomena where the acceleration occurs on a closed circular path, i.e. it occurs both in the cyclotrons and synchrotrons. It has been detected the first time during the acceleration of an electron beam and it is easy to measure for almost relativistic particles. As far as particle optics is concerned, particles in a beam do not follow exactly a circular path and when they move from the equilibrium orbit they are subjected to restoring forces that bring them back to the stable orbit. This phenomenon was studied at first in betatron. Hence the name of betatron oscillations for the particle motion around the reference orbit, but this topic will be studied in detail in the next chapter.

2.1.6 Synchrotron

In a synchrotron, Figure 2.6, particles can move on a closed circular path which radius is constant and they reach the required energy after the acceleration step; both goals are achieved by a time dependent magnetic field that increases in time. The process is done in such a way that the electric current in the magnets, and so the magnetic field generated, is always synchronous with the actual kinetic energy of particles, thus the name of synchrotron. Once the beam has reached the desired energy, the machine provides a constant magnetic field to keep particles well confined in space. Particle motion in the longitudinal direction (i.e. along the main circumference of the accelerator) is characterized by the accelerating phenomenon achieved by RF cavities. The bending function in the longitudinal direction is ensured by a magnet made by just two poles: dipole magnet. The magnetic field is vertically directed, and it can point upwards or downwards

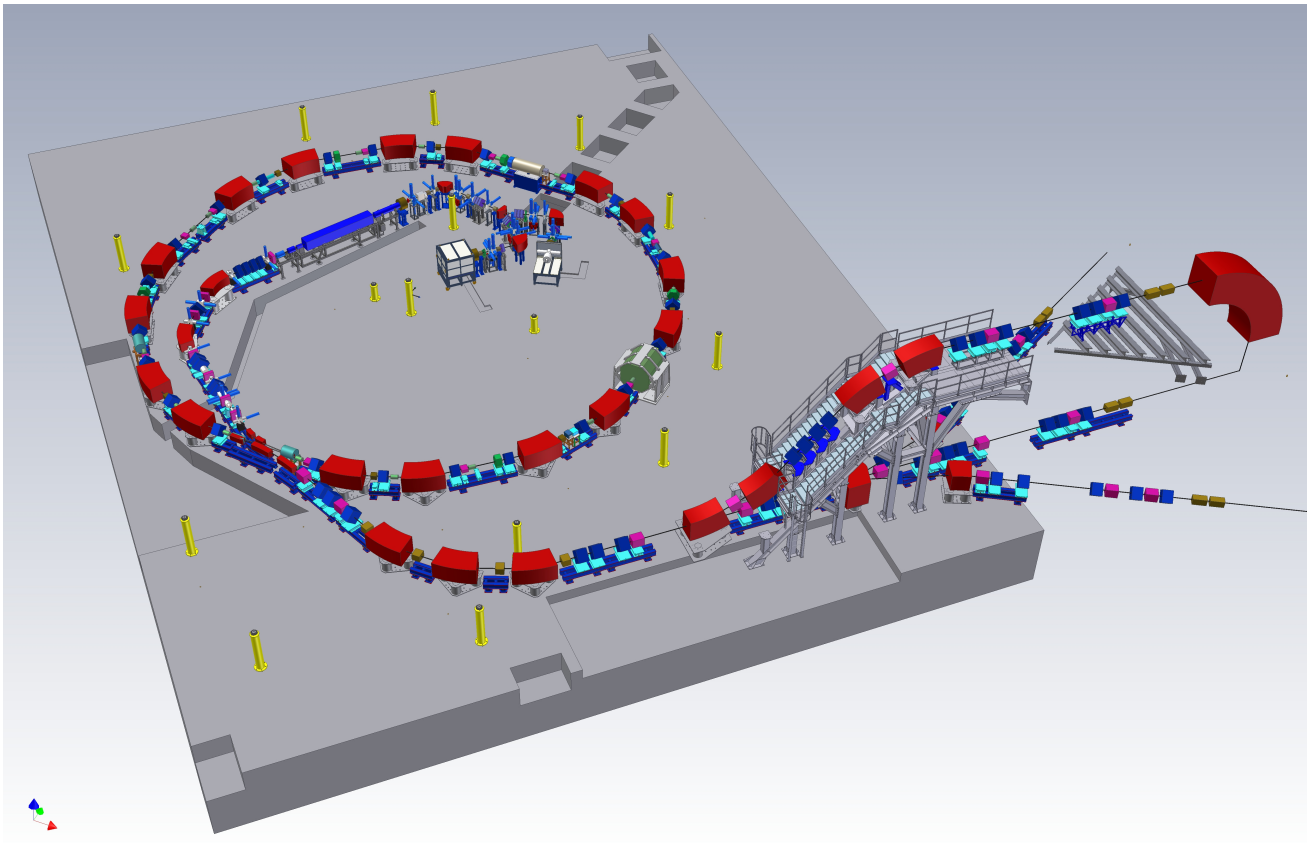

FIGURE 2.7. CNAO accelerating facility - schematic

according to the way the magnet is connected to the electric grid, but the bending magnitude, i.e. the angles, strongly depends on the particle's charge too. On the transverse direction, other phenomena occur. The particle is subjected to the Lorentz force which direction is given by the cross product between the particle velocity and the magnetic field. The confinement of the beam in the transverse direction is mainly ensured by quadrupoles that impose focusing and defocusing forces. A synchrotron is usually composed by section that repeats N times until the whole circumference is covered. This feature can be observed in Figure 2.6, where there are four elementary sections connected by a straight one on the right side and the injection septa on the left side; while in the other two are located the RF cavities. According to the description performed in the previous chapter, a similar structure can be found in CNAO synchrotron too. It is possible to observe that there are almost two symmetric sections connected by the injection and extraction septa, located on the right hand side of the Figure 2.7 and, on their opposite side there is the RF cavity. Moreover, at the middle of each section there is an almost straight section which host the betatron (used for the beam extraction) on one side and a kicker for RFKO extraction on the other side.

2.2 Magnets for accelerators

In order to further study the particle motion in a circular accelerator a synchrotron will be considered. It is a complex machine and its description is quite hard, but starting from a simple and schematic representation there are three main components that are necessary to obtain an energetic well confined beam of particles on a limited space:

- RF cavities: accelerate particles up to the required energy;
- Dipoles: bend the beam in the longitudinal plane so that it can follow the studied path. They are used in general to let the beam move on a specific path, it could be the longitudinal plane or the extraction line, in order to move the beam to treatment rooms or to change the irradiation direction (common practice in medical accelerators, more specifically for CNAO);
- Quadrupoles: focus the beam in the two transverse planes;
- Sextupoles: influences the momentum spread of a beam, i.e. the width of its (almost) gaussian distribution.

RF cavities influence particle motion in the longitudinal plane so they will be treated at the end of the chapter as previously explained. Instead, the other two components are of great interests.

A dipole is a magnet constituted by just two poles. Its function is to bend the beam in the required direction. An example can be obserbed is Figure 2.8 where it is reported a real image of a dipole magnet (left side of the picture) and its schematic working principle (on the righ side). In the case represented in the figure, the magnet bend the particle in the longitudinal plane making it follow, for example, a circular path. Assume to consider a simplified configuration where the magnetic field is constant and uniform along all the magnet, then the particle motion is influenced by just one component of the Lorentz force:

$$\mathbf{F} = q\mathbf{v}x\mathbf{B} \tag{2.9}$$

According to the vectors represented in Figure 2.8, the force direction (given by the cross product between velocity and magnetic field) is towards the centre of the accelerator when a negative charged particle is accelerated. It easy to observe that changing the direction of the particle velocity, or the polarization of the magnet, the force would be directed on the opposite side leading the particle to move outwards the circumference and soon being lost if nothing else is done to bring it back.

The other component to study is a quadrupole and as the name says, it is constituted by four poles. Assume that the magnet is connected to the electric grid in such a way that the electromagnets generate magnetic poles as represented on the right hand side of Figure 2.9. If a positively charged particle moving along the direction outgoing from the page plane is considered,

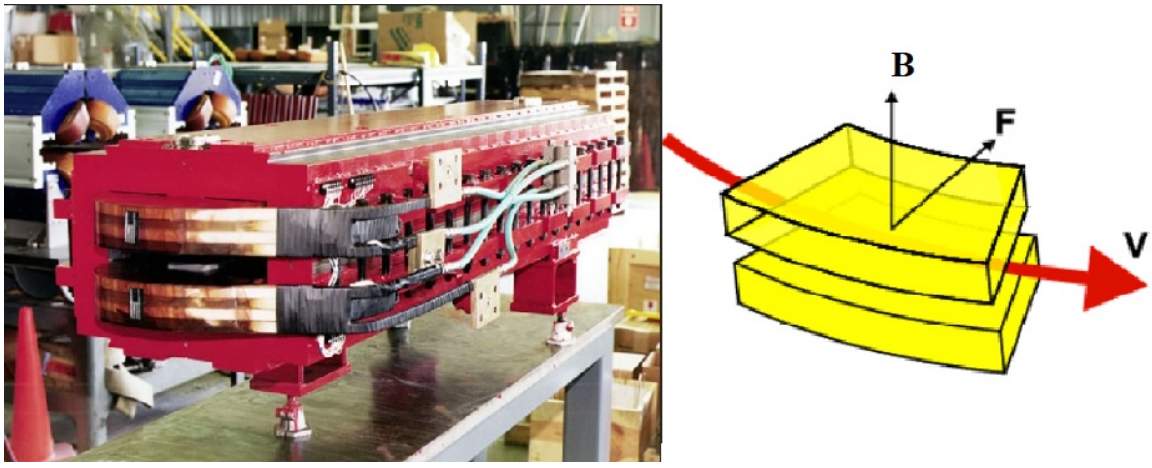

FIGURE 2.8. The figure represents the image of a real bending dipole (on the left) and the way it works when it is installed in the longitudinal plane of an accelerator. The direction of the force can be justified if the particle accelerated has a negative charge, as electrons. [10]

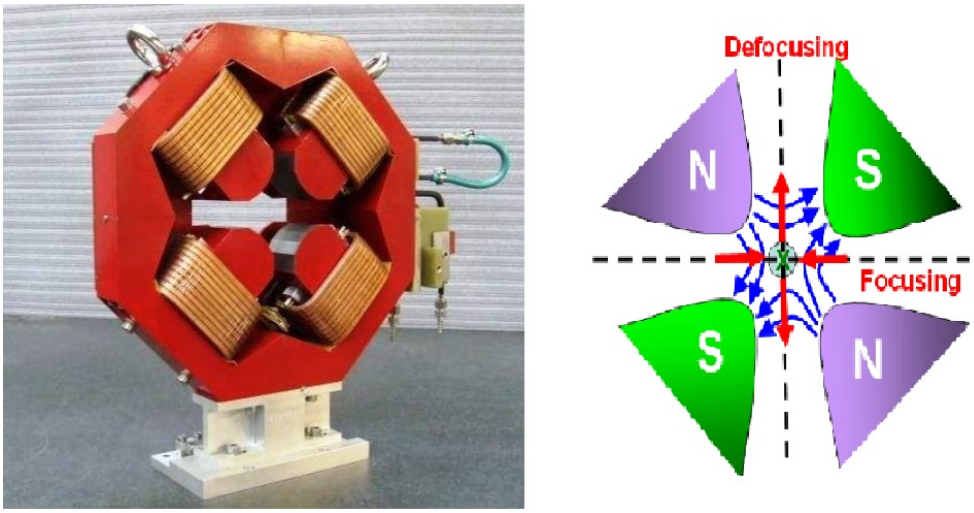

FIGURE 2.9. Real image of a quadrupole and its schematic representation. The blue lines represents the magnetic field line whereas the red ones show the direction of the Lorentz force in the magnet, considering a particle moving with a velocity directed in the outgoing direction from page plane. [12]

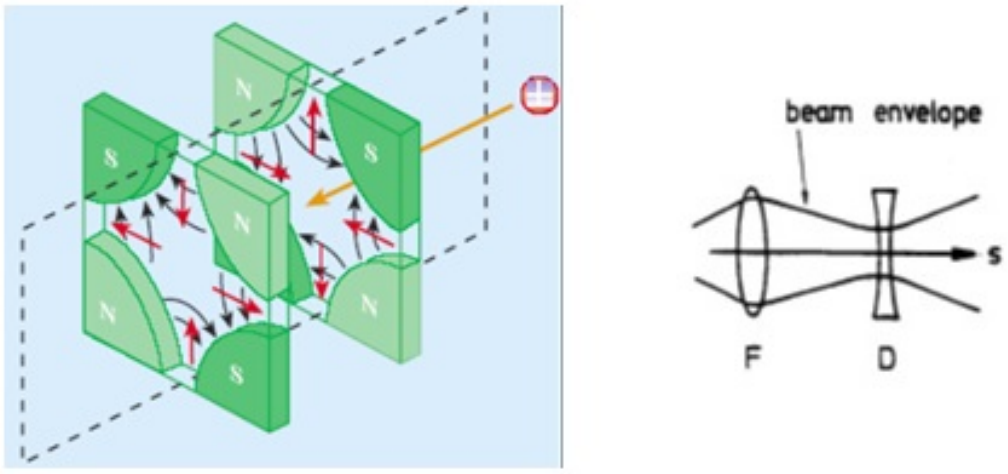

FIGURE 2.10. Focusing and defocusing quadrupoles: schematic representation and beam envelope from [5, 28].

then it is subjected to a Lorentz force directed as the red line. So, if the particle is horizontally displaced, the force will move it back towards the centre leading to a focusing action on the particle; on the contrary, if the particle is vertically displaced, it will be further pushed away because of the defocusing effect of the force in that direction. Imagine now to change the way the magnet is connected to the electric grid, then the electromagnets will have opposite polarization with respect to the one represented in the schematic, i.e. the magnetic field lines (in blue) will be directed in the opposite way. This means, that if the chosen particle is always the same (same charge, same velocity direction), the focusing/defocusing effect induced by the Lorentz force will act in the opposite way to the one represented in the Figure 2.7. The first kind of quadrupoles (horizontally focusing and vertically defocusing) is called Focusing Quadrupoles (QF) while the others (vertically focusing and horizontally defocusing) are called Defocusing Quadrupoles (QD). According to Figure 2.10, it is possible to understand that according to particle position within the vacumm chamber, it undergoes to strong or weak focusing or defocusing forces. The sequence of a QF and QD allows a focusing action along the direction in which the previous quadrupole induced a defocusing action. Thus, in the beam it is possible to observe a generally focusing effect.

Sextupoles are magnets composed by six poles as shown on the left side of Figure 2.11. When a particle enters a quadrupole with a displaced position with respect to the centre of the vacuum chamber, then it undergoes to a strong focusing along one of the two transverse directions. Considering a group of particles, each of them with a different displaced position, then the focal spot of the quadrupole won't be anymore a dot. It is a common phenomenon that can be observed also in normal optics, the result is a blurred image. In order to overcome to this chromatic aberration, sextupoles are introduced. They induce an additional focusing or defocusing action

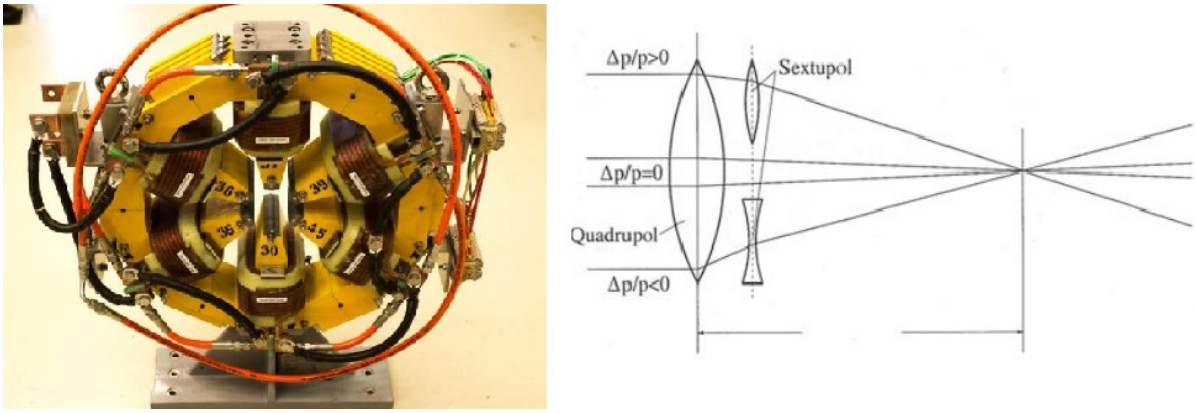

FIGURE 2.11. Sextupole and its working principle [12, 13].

leading to have a constant and not blurred focal spot.

The way a particle (and later on, a beam) moves in an accelerator is studied in beam optics, in particular as far as dipoles and quadrupoles are considered the optics is linear whereas the addition of other magnets with more than four poles (sextupoles, octupoles, ...) induce interactions between the motion in the two transverse planes leading to a non-linear beam optics.

2.3 Beam optics

In a circular accelerator dipoles and quadrupoles are arranged so that a particle can move on a close circular trajectory. Usually the radius of this trajectory is called ρ and it is the design value for the orbit along which particles (theoretically) would have to move on as shown in Figure 2.12. The motion is stable if restoring forces spontaneously arise when the particle moves from the design path. In a magnetic field with no dependencies on the azimuthal direction, it is possible to express this relation in terms of a force balance between the Lorentz force and the centrifugal one:

$$\mathbf{v}x\mathbf{B}: \begin{cases} > \frac{mv^2}{r}, & if \quad r > \rho \\ < \frac{mv^2}{r}, & if \quad r < \rho \end{cases} \tag{2.10}$$

Particles that move on an arc with curvature radius slightly larger than the reference one will experience a Lorentz force bigger than the centrifugal one, this ensure the particles to move back to the nominal path. On the contrary, those particles that move at radii smaller than ρ will experience a bigger centrifugal force that will make them move towards the nominal trajectory. A similar rational can be adopted for all those particles that are vertically displaced with respect to the plane where the nominal orbit lays. When in an accelerator a beam of particles is considered, those that are vertically or horizontally displaced with respect to the design orbit will undergo

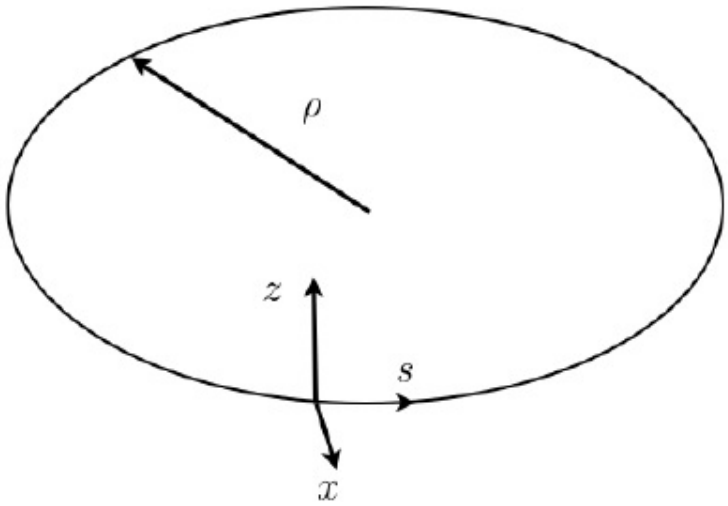

FIGURE 2.12. Circular path of a generic charged particle moving in a magnetic field pointing in the outgoing direction with respect to the page plane. Modified from [5].

to oscillations around it. These oscillations are called *betatron oscillations* and the number of oscillations per turn in the machine is called **betatron tune** or **Q-tune**. This quantity is a fundamental characteristic of the beam and it will be analyzed in detailed later on in this chapter.

2.3.1 The Hill's equation

In order to determine the motion equation, the particle position has to be expressed in terms of the design value radius of the reference orbit (ρ), as a function of radial position (to account any possible horizontal displacement) and vertical one (to consider vertical displacements too):

$$\mathbf{R} = \rho + r\mathbf{u_r} + z\mathbf{u_z} \tag{2.11}$$

Then deriving two times with respect to time the previous expression, it is possible to obtain the acceleration:

$$\ddot{\mathbf{R}} = (\ddot{r} - r\dot{\theta}^2)\mathbf{u_r} + (2\dot{r}\dot{\theta} + r\ddot{\theta})\mathbf{u}_\theta + \ddot{z}\mathbf{u_z} \tag{2.12}$$

A particle that moves in an electromagnetic field with the acceleration computed in Equation (2.12) has a confined motion if the condition expressed in Equation (2.10) is respected. So, each component of the force at which the particle is subjected has to be compared with the magnetic part of the Lorentz force (it's the one that ensure the particle confinement):

$$m(\ddot{r} - r\dot{\theta}^2) = q(v_\theta B_z - v_z B_\theta) \tag{2.13}$$

$$m(2\dot{r}\dot{\theta} + r\ddot{\theta}) = q(v_z B_r - v_r B_z) \tag{2.14}$$

$$m\ddot{z} = q(v_r B_\theta - v_\theta B_r) \tag{2.15}$$

The previous formulae are the balance equations respectively in the radial Equation (2.13), longitudinal (or azimuthal) Equation (2.14) and vertical direction Equation (2.15). The second one can be neglected since it was said that longitudinal dynamics will be discussed later on, so focus on the other two. They can be further simplified considering that:

- The magnetic field does not depend on θ, i.e. the azimuthal direction;
- The component of the particle velocity on the azimuthal direction is the dominant one with respect to the others and it can be referred just as v.

So Equation (2.13) and Equation (2.15) turn into:

$$m(\ddot{r} - r\dot{\theta}^2) = q v_\theta B_z \tag{2.16}$$

$$m\ddot{z} = q v_\theta B_r \tag{2.17}$$

An additional simplification can be performed by substituting the radial magnetic field with the one in the x direction; it is only a matter of notation since changing the reference system the radial direction is coincident with the x one. In addition, even if it is not totally correct, from a physical point of view it is more interesting to observe how variables change along the longitudinal axes of the machine (s) instead of their time variation, so:

$$\frac{d}{dt} \to v\frac{d}{ds}$$

$$\frac{d^2}{dt^2} \to v^2\frac{d^2}{ds^2}$$

Then Equation (2.16) and Equation (2.17) can be written as:

$$\begin{cases} mv^2\frac{d^2x}{ds^2} - mv^2\frac{d\theta}{ds} = -ev(B_0 - gx) \\ mv^2\frac{d^2z}{ds^2} = -ev(gz) \end{cases} \tag{2.18}$$

The last passage to be performed before looking for a solution is defining the following quantities:

$$k(s) = \frac{eg}{mv} = \frac{eg}{p} \quad \text{quadrupole normalized strength} \tag{2.19}$$

$$\frac{1}{\rho(s)} = \frac{eB_0}{mv} = \frac{eB_0}{p} \quad \text{dipole strength} \tag{2.20}$$

From the mathematical definition of arc of circumference, it is possible to perform a Taylor expansion of the radius and the momentum. By the substitution of definitions (2.19) and (2.20) the set of Equations (2.18) assumes the following form:

$$\begin{cases} \frac{d^2x}{ds^2} - (k(s) - \frac{1}{\rho(s)^2}) = \frac{1}{\rho}\frac{\Delta p}{p_0} \\ \frac{d^2z}{ds^2} + k(s)z = 0 \end{cases} \tag{2.21}$$

If only the homogeneous part of Equation (2.18) is considered, then they can be written in a compact form as:

$$y''(s) + K(s)y(s) = 0 \tag{2.22}$$

This equation is called the Hill's equation.
Where the parameter *K(s)* assumes different forms according to the considered direction (x or z).

$$K(s) = \begin{cases} -\left(k(s) - \frac{1}{\rho(s)^2}\right), & y = x \\ +k(s), & y = z \end{cases} \tag{2.23}$$

The determination of the solutions is quite complex if the parameter *K(s)* depends on s. But considering a small section of an accelerator along which *K(s)* can be considered constant with respect to s, then the solution of the Equation (2.22) is:

$$y(s) = AC(s) + BS(s) \tag{2.24}$$

In this case the Hill's equation is called piece-wise constant Hill's equation, where A and B are constants to be determined by imposing the initial conditions on *y(s)* and its derivative *y'(s)* at *s=0*. When this step is performed, the final form of the solution is:

$$y(s) = y_0 C(s) + y_0' S(s) \tag{2.25}$$

And it is called Sine-like Cosine-like solution. Another way to write the solution is adopting a matrix formalism:

$$\begin{pmatrix} y \\ y' \end{pmatrix} = \begin{pmatrix} C(s) & S(s) \\ C'(s) & S'(s) \end{pmatrix} \begin{pmatrix} y_0 \\ y_0' \end{pmatrix} \tag{2.26}$$

2.3.2 Matrix formalism

The matrix that describes how particle position and particle divergence changes when it passes through a segment of length s in an accelerator is called Transfer matrix. The sign of K defines the type of sine-like and cosine-like functions to be adopted. In fact, when *K>0* the solution is a linear combination of sine and cosine, whereas when K is negative, then the functions are hyperbolic sine and hyperbolic cosine. Equation (2.26) can be further developed as follows (the coefficients in front of the functions come from the integration constants, the detailed calculations are not reported here to avoid a too heavy notation).

$$For \quad K > 0: \qquad \begin{pmatrix} y \\ y' \end{pmatrix} = \begin{pmatrix} \cos\sqrt{K}s & \frac{1}{\sqrt{K}}\sin\sqrt{K}s \\ -\sqrt{K}\sin\sqrt{K}s & \cos\sqrt{K}s \end{pmatrix} \begin{pmatrix} y_0 \\ y_0' \end{pmatrix} \tag{2.27}$$

$$For \quad K < 0: \qquad \begin{pmatrix} y \\ y' \end{pmatrix} = \begin{pmatrix} \cosh\sqrt{|K|}s & \frac{1}{\sqrt{|K|}}\sinh\sqrt{|K|}s \\ \sqrt{|K|}\sin\sqrt{|K|}s & \cosh\sqrt{|K|}s \end{pmatrix} \begin{pmatrix} y_0 \\ y_0' \end{pmatrix} \tag{2.28}$$

Without removing the assumption of piece-wise constant Hill's equation, the transport matrix for those accelerator components (quadrupoles, dipoles) that allow a linear particle optics can be derived. Moreover, a new component will be added but its description is quite intuitive: the free drift.

2.3.2.1 Free drift

A free drift is a segment in which the particle is not subjected to any magnetic field. The particle just "flies" from one point to another one. The transfer matrix describes the position and divergence transformation at which the particle undergoes when it passes through this element. The free drift is represented as a space of length l with *K=0*, so the transfer matrix is easy to write, with the only exception of the element (1,2) that requires the use of a notable special limit.

$$M_{fd} = \begin{pmatrix} 1 & l \\ 0 & 1 \end{pmatrix} \tag{2.29}$$

2.3.2.2 Quadrupole

Since quadrupoles can focus the beam horizontally and, at the same time, defocus it vertically (QF type, $k > 0$) or viceversa (QD type, $k < 0$); two different matrices have been obtained (for the specifications on K look to Equation (2.23)):

$$K < 0, \quad k > 0 \qquad M_{QF} = \begin{pmatrix} \cos\sqrt{k}l & \frac{1}{\sqrt{k}}\sin\sqrt{k}l \\ -\sqrt{k}\sin\sqrt{k}l & \cos\sqrt{k}l \end{pmatrix} \tag{2.30}$$

$$K > 0, \quad k < 0 \qquad M_{QD} = \begin{pmatrix} \cosh\sqrt{|k|}l & \frac{1}{\sqrt{|k|}}\sinh\sqrt{|k|}l \\ \sqrt{|k|}\sin\sqrt{|k|}l & \cosh\sqrt{|k|}l \end{pmatrix} \tag{2.31}$$

The matrices can be simplified if the *thin lens approximation* is adopted; this assumption leads to consider a magnet of almost zero thickness and same focal length:

$$l \to 0 \qquad kl = const$$

So the sequence of a focusing and defocusing quadrupole (having the same focal length) separated by a free drift space, as reported in Figure 2.13, can be represented by:

- Horizontal plane: $M = M_{QD} * M_{fd} * M_{QF} = \begin{pmatrix} 1-\frac{l}{f} & l \\ -\frac{l}{f^2} & 1+\frac{l}{f} \end{pmatrix}$
- Vertical plane: $M = M_{QF} * M_{fd} * M_{QD} = \begin{pmatrix} 1+\frac{l}{f} & l \\ -\frac{l}{f^2} & 1-\frac{l}{f} \end{pmatrix}$

A particle that passes through a lattice composed by sequence of components described above it tends to be simultaneously focused on both the vertical and horizontal direction. This particular lattice sequence is commonly known as the FoDo Lattice (Focusing-Defocusing lattice).

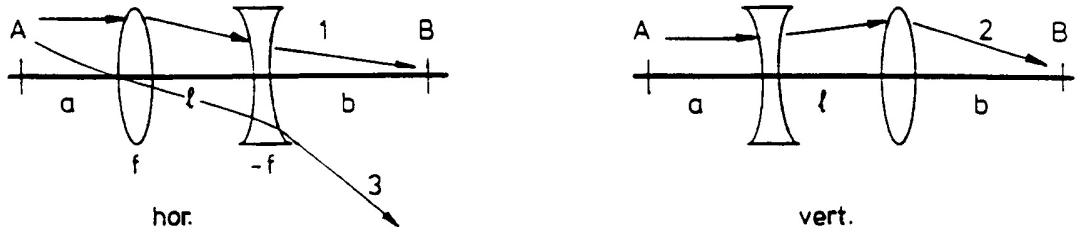

FIGURE 2.13. Tendency of simultaneously focusing on horizontal and vertical direction. The opposite sequence of quadrupoles in the two directions is due to the fact that a horizontally focusing quadrupole is also vertically defocusing and viceversa [28].

2.3.2.3 Dipole

It is the magnet responsible for the beam bending, and according to the inclination of the exit and entry surfaces (with respect to the beam trajectory), it can fulfill a further focusing function. The first type of magnet considered will be the one with both the entry and exit surfaces perpendicular to the beam trajectory. In this case the magnet only bends the beam in the longitudinal plane, leading the parameter K to be equal to $\frac{1}{\rho^2}$; and it leaves the motion in the other transverse direction unperturbed. So, considering our purpose of bending the particles in the x direction the matrices assume the following form:

$$M_x = \begin{pmatrix} \cos\frac{l}{\rho} & \rho\sin\frac{l}{\rho} \\ -\frac{1}{\rho}\sin\frac{l}{\rho} & \cos\frac{l}{\rho} \end{pmatrix} \qquad M_z = \begin{pmatrix} 1 & l \\ 0 & l \end{pmatrix} \tag{2.32}$$

This type of magnet is called dipole sector magnet in opposition with a rectangular dipole magnet which ensures also a focusing function, their schematic representation can be found in Figure 2.14. In a rectangular dipole, the entrance and exit surface can be rotated along two directions as reported in the Figure 2.15. The case reported in Figure 2.14 represents a rotation of an angle δ around the yellow axes with a sight from above, in order to have a clearer outline of the configuration. So the particle sees a magnetic wedge as it enters the dipole and its trajectory is changed according to its radial and vertical position (or displacements with respect to the reference orbit). In particular, for the case study defined before, the particle passes by a horizontally defocusing lens, a dipole sector and again a horizontally defocusing lens. The global result is that while particle is bended it is also horizontally defocused while vertically focused.

$$M_x = \begin{pmatrix} 1 & \rho\sin\frac{l}{\rho} \\ 0 & 1 \end{pmatrix} \qquad M_z = \begin{pmatrix} \cos\frac{l}{\rho} & \rho\sin\frac{l}{\rho} \\ -\frac{1}{\rho}\sin\frac{l}{\rho} & \cos\frac{l}{\rho} \end{pmatrix} \tag{2.33}$$

If now a rectangular dipole magnet with entrance and exit surfaces rotated around the green axes is considered, the situation will be reversed, i.e. during the bending process the particle undergoes to a vertical defocusing and a horizontal focusing. From a mathematical point of view, matrices in Equation (2.33) will exchange their subscripts.

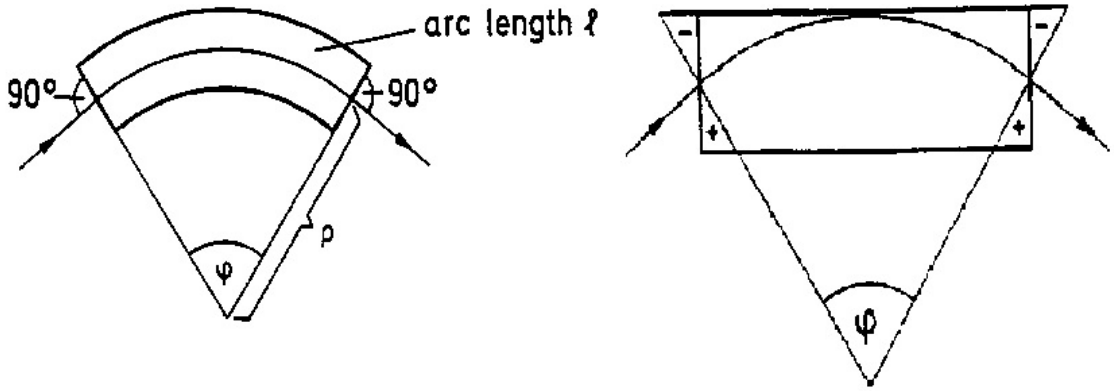

FIGURE 2.14. Comparison between a sector dipole (on the left side) that only bends the beam in the required direction and a rectangular one (on the right side) that can also ensure a focusing function. [28]

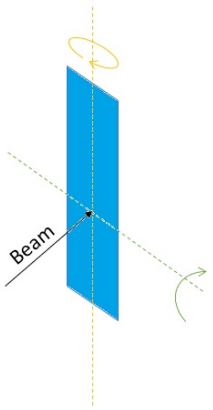

FIGURE 2.15. Possible ways to rotate entry/exit surface of a rectangular dipole. The case represented in Figure 2.14 is a rotation around the yellow axes.

.

2.3.3 Stability condition

The matrix formalism introduced before is helpful to write how the particle position and divergence change when the particle passes through elementary components like a dipole, a free drift space or a quadrupole. In particular, an ordered sequence of these elements can be analytically reproduced by a matrix product. Figure 2.16 represents a possible beam line composed by a combination of eight different components. Once the particle has undergone to that sequence its position and divergence can be obtained from:

$$\begin{pmatrix} y \\ y' \end{pmatrix} = M \begin{pmatrix} y_0 \\ y'_0 \end{pmatrix}$$

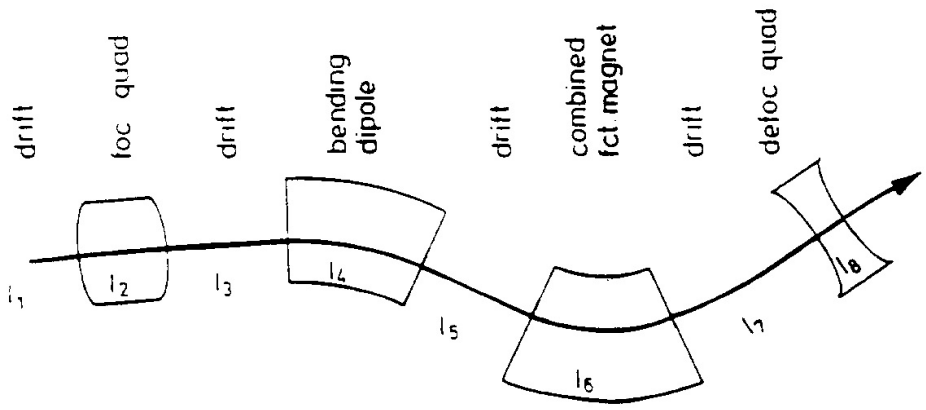

FIGURE 2.16. Example of a beam line composed by the sequence of eight elementary components: dipoles, quadrupoles, free drifts [28].

Where M is the total transfer matrix and its equal to:

$$M = M_8 * M_7 * M_6 * M_5 * M_4 * M_3 * M_2 * M_1$$

The subscript of each matrix corresponds to the component in the Figure 2.16. If an accelerator can be considered as made by N identical sections, each one characterized by the same ordered sequence of components, then:

$$C = N * L \tag{2.34}$$

Where L is the Lattice, i.e. the length of the section of elementary components, and N is the number of times the lattice has to be repeated to cover the whole longitudinal length of the accelerator C, i.e. the circumference.

A fundamental characteristic of an accelerator is to keep particle confined on a closed orbit. This requirement has to be successfully satisfied every time the particle does a turn in the machine; it means that it is necessary that all the elements of the matrices have to be limited as the number of turns in the machine increases. Thus, it is fundamental to retrieve a mathematical relation for the stability condition of the total transfer matrix evaluated at the n-th turn. At first the matrix after the particle completed a single turn in the machine has to be determined:

$$M\left(s + N\frac{L}{s}\right) = \left(M(s)\right)^N$$

But the stability condition has to be retrieved from the matrix that describes the particle at the n-th turn:

$$(M(s))^{N*n} \tag{2.35}$$

In order to have the total transfer matrix with limited elements, all its elements do not have to diverge as the number of turns tends to infinite. The problem can be solved assessing the eigenvalue problem:

$$M\mathbf{y} = \lambda\mathbf{y}$$

So at first the eigenvalues are computed:

$$det(M - \lambda I) = 0$$

$$\lambda^2 - \lambda(a+d) - (ad - bc) = 0 \tag{2.36}$$

As far as the study of the coefficients of Equation (2.36) is concerned, a meaning to both of them can be given. The second term $(a+d)$ is the trace of the matrix M, while for the other one $(ad-bc)$ more considerations have to be done. If the Wronski determinant of the general solution of the motion equation is computed then it can be shown it depends just on the initial conditions, in particular functions that satisfy the settings are the sin-like and cosine-like solutions. This leads to the simplification of the third term of Equation (2.36), that is just equal to unity. If the eigenvalues are written in a general form like λ_1 and λ_2, then the trace is also the sum of the eigenvalues themselves. In addition, the previous determinant is the product of the eigenvalues, so it is possible to write the condition as:

$$\lambda_1\lambda_2 = 1 \tag{2.37}$$

That it is satisfied for:

$$\lambda_1 = \lambda_2 = 1 \tag{2.38}$$

Or

$$\lambda_1 = e^{i\mu} \qquad \lambda_2 = e^{-i\mu} \tag{2.39}$$

Then the eigenvalues can be found solving Equation (2.36) then imposing that the argument of the root is real:

$$\sqrt{\frac{(a+d)^2}{4} - 1} > 0$$

Which leads to:

$$\frac{a+d}{2} < 1 \tag{2.40}$$

The sum of the coefficients a and d is the trace of the matrix M, which remains always the same also when the matrix is diagonalized; that is the reason why the previous expression is also equal to the following one once the eigenvalues in Equation (2.39), written in terms of sine and cosine, are substituted inside:

$$\frac{1}{2}(a+d) = \frac{1}{2}Tr(M) = \cos\mu \tag{2.41}$$

In conclusion, the elements of the matrix M are limited and they keep to be limited as the particle performs n turns in the machine if:

$$\cos\mu < 1 \tag{2.42}$$

2.4 Dispersion function

When a beam of particles is considered, it is necessary totake into account that particles are distributed in space and energy around the one moving on the reference (or equilibrium) orbit. In section 2.3.1 the homogeneous solution of the motion equation has been found. The particular solution can be found by introducing the concept of dispersion functions. Betatron oscillation has been already introduced: these oscillation arise from the vertical and/or horizontal displacement (i.e. non zero initial conditions) of particles with nominal momentum. So, according to their relative position with respect to the reference orbit, particles are subjected to different bending and focusing/defocusing forces, since the equilibrium orbit passes exactly at the centre of all dipoles and quadrupoles. The spatial distribution necessarily leads to an energy spread, especially in the acceleration process. Here the discussion has to be split in two, according to the direction along which the particle motion is observed.

In the transverse direction , particles can be spatially displaced with respect to the reference orbit (and in this case they undergo to betatron oscillations) and they can also have a different momentum with respect to the nominal value (that will be studied here below). It is equally probable to have particles with slightly larger and lower momentum, for this reason it is common to use the momentum deviation or its relative value:

$$dp = p - p_0 \qquad or \qquad \frac{dp}{p_0} = \frac{p - p_0}{p_0}$$

In both cases, particles will need a different trajectory on which they can move, for $dp > 0$ particles will move on an orbit of larger radius,otherwise the orbit will have a smaller radius. Also in this case, particles can have non zero initial conditions which means that they will undergo to betatron oscillations around the orbits defined before. In particular, if the maximum and minimum momentum is used in the evaluation of the dp, and so of the closed orbits, then the dotted lines in Figure 2.17 represent the beam envelope. So now it is possible to derive the motion equation for particles with different momentum. They satisfy the inhomogeneous form of the Hill's equation, i.e. Equation 2.19. The global solution is given by the linear combination of the solution to the homogeneous ode and the particular one. The first one has already been derived, so here it will be studied the particular integral. In Equation (2.40) is reported a modified version of the Equation 2.22 in order to avoid the reader to look for it:

$$\frac{d^2x}{ds^2} + K(s)x = \frac{1}{\rho}\frac{\Delta p}{p_0}, \qquad K(s) = -\left(k(s) - \frac{1}{\rho(s)^2}\right) \tag{2.43}$$

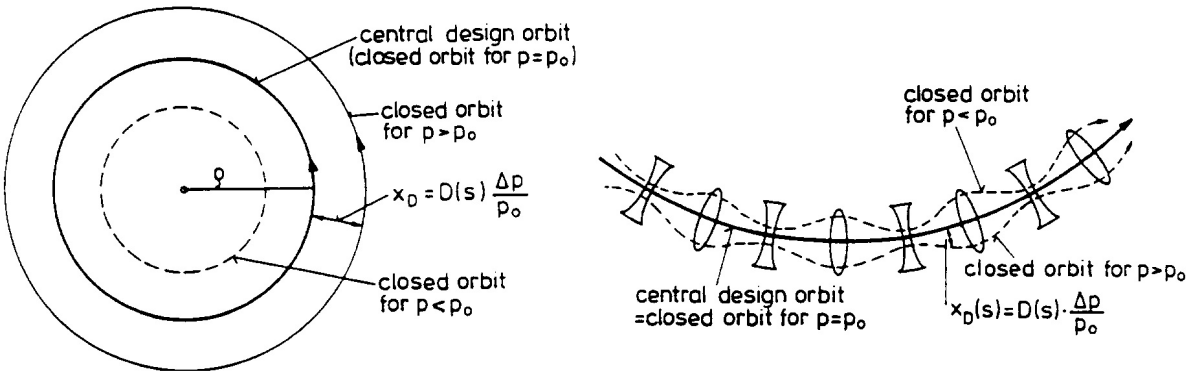

FIGURE 2.17. On the left hand side, it is possible to observe the equilibrium orbit and the two closed orbits. On the right hand side, it is highlighted that the reference orbit passes at the centre of all the magnets, while the other orbits undergo to focusing and defocusing actions [28].

The particular solution has to have the same mathematical shape of the forcing therm in the previous equation. Thus, it has to be proportional to the relative momentum spread times a function that depends on the longitudinal coordinate s:

$$x_p(s) = D(s)\frac{\Delta p}{p_0} \tag{2.44}$$

Equation (2.44) describes the deviation of the closed orbit for particles with momentum $dp + p_0$. In order to find the mathematical expression for the function D(s) (the *periodic dispersion*) the particular integral has to be substituted in the starting equation. Thus, Equation 2.40 becomes a second order differential equation in D(s):

$$D''(s) + K(s)D(s) = \frac{1}{\rho(s)} \tag{2.45}$$

The discussion can be further generalized considering that also along the vertical direction (previously called z) there could be a forcing term due to misalignment of the magnets, so it is better to go back to the previous notation, where the variable y was used to refer to both the transverse directions:

$$y''(s) + K(s)y(s) = F(s) \tag{2.46}$$

Also in this case periodic boundary conditions can be used but an additional specification is mandatory: K(s) and $\rho(s)$ both are periodic functions with period L (the length of the sequence of elementary components) while F(s) is a periodic function on the accelerator length (i.e. $C = NL$). F(s) is a generic function that represents the right hand side of Equation (2.45) if the x direction is considered; otherwise, along the z direction, it represents the error in the magnets alignment.

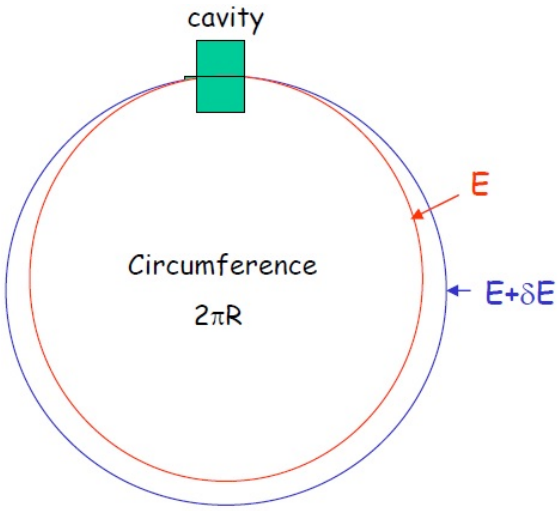

FIGURE 2.18. The red orbit at energy E is the reference one while the blue at energy E+δE refers to a closed dispersion one [17].

The general solution of Equation (2.46) is then:

$$y(s) = \frac{\sqrt{\beta(s)}}{2sin(\pi Q)} \oint \sqrt{\beta(s')} F(s') cos(\Phi(s') - \Phi(s) - \pi Q) ds' \tag{2.47}$$

The whole demonstration is not reported here but it could be found in [28].

In the longitudinal direction, particles with a momentum difference with respect to the nominal value will move on a different path (smaller or bigger circumference) that is called *dispersion orbit*, and also along this orbit betatron motion occurs. Obviously, the momentum spread of the particle make it move on a different path with a different velocity with respect to the particle on the equilibrium orbit, leading then to a different frequency of revolution f_r inside the machine. In Equation (2.48) and (2.49) two important quantities are defined:

- Slip factor:

$$\eta = \frac{df_r/f_r}{dp/p} \tag{2.48}$$

- Momentum compaction factor:

$$\alpha_c = \frac{dL/L}{dp/p} = \frac{1}{L} \oint_C \frac{D_x(s)}{\rho(s)} ds_0 \tag{2.49}$$

The slip factor gives information on the relative change of the revolution frequency with respect to the momentum spread, while the momentum compaction factor relates the change of the path length with the momentum spread. The two previous factors can be related in order to find a

relation for the relative change of the revolution frequency.

$$f_r = \frac{v}{2\pi R} = \frac{\beta c}{2\pi R} \rightarrow \frac{df_r}{f_r} = \frac{d\beta}{\beta} - \frac{dR}{R} = \frac{d\beta}{\beta} - \alpha_c \frac{dp}{p}$$

From the definition of the revolution frequency it is possible to obtain the relative change with respect to the nominal value by the evaluation of the differential of the frequency with respect to the Lorentz factor β and the path length (circumference length and radius are directly proportional). The last step is performed by the substitution of the definition of the momentum compation factor. The relative change of the Lorentz factor β can be obtained from the differential of the momentum, as follows:

$$p = mv = m\beta c = \frac{E_0}{c^2}\gamma\beta c = \frac{E_0}{c}\gamma\beta \rightarrow \frac{dp}{p} = \frac{d\beta}{\beta} + \frac{\beta d\beta}{(1-\beta^2)} = \gamma^2 \frac{d\beta}{\beta}$$

In the end, it is possible to obtain the following relation:

$$\frac{df_r}{f_r} = \left(\frac{1}{\gamma^2} - \alpha_c\right)\frac{dp}{p} = \left(\frac{1}{\gamma^2} - \frac{1}{\gamma_{tr}^2}\right)\frac{dp}{p} \tag{2.50}$$

What it is important to underline is that it exist a value of α_c or γ_{tr} at which the slip factor is zero. From a physical point of view, it means that in this configuration the change of velocity of the particle is perfectly compensated by the change in the path length, leading then to have the frequency spread independent from the momentum one. For positive values of the slip factor, an increase of the particle velocity leads to an increase of the revolution frequency; on the contrary, for negative values of the slip factor the increase in velocity does not compensate the increase in the path length. This concept will be really important in the description of longitudinal dynamics that will be performed soon.

2.5 Transverse beam dynamics

As far a group of particles is considered the phenomenon at which they undergo can be handled in a easier way if the matrix formalism is adopted. Moreover, the use of parametric equation allow the description of a particle beam with s single equation rather than one equation for each particle.

The total transfer matrix can be written in terms of $\cos\mu$ and $\sin\mu$, and the form it assumes is called Twiss Matrix:

$$M = I\cos\mu + J\sin\mu = I\cos\mu + \begin{pmatrix} \alpha & \beta \\ -\gamma & -\alpha \end{pmatrix}\sin\mu$$

Where I is the identity matrix. By the use of the transport matrix in the Twiss form it is possible to determine a relation between the Twiss parameters: α, β and γ. At first is used again the condition that the Wronski determinant is equal to unity, and it leads to:

$$\gamma = \frac{1+\alpha^2}{\beta} \tag{2.51}$$

Then, using the Floquet theory [19] for solutions to periodic linear differential equations, the particle position can be written as:

$$\begin{pmatrix} y \\ y' \end{pmatrix} = M(s|s_0)\begin{pmatrix} y_0 \\ y'_0 \end{pmatrix} = y(s)e^{\pm i\mu}$$

This particular form is of great importance since it will lead to demonstrate that there is an *invariant* of the motion. Where the notation $M(s|s_0)$ means the particle motion is considered from position s_0 to the generic position s. Writing down the previous equation in an explicit way and doing a separation between real and imaginary part, an equation relating α and β can be obtain. The relation between the two parameters is:

$$\alpha = -\frac{\beta'}{2} \tag{2.52}$$

After some mathematical passages, the particle position can be written as a function of the β parameter:

$$y(s) = A\sqrt{\beta(s)}\exp\left(\pm\int\frac{1}{\beta(s')}ds'\right) \tag{2.53}$$

Studying the periodicity of the previous expression, it is possible to retrieve the definition of two fundamental quantities:

- Phase advance per turn:

$$\mu(s) = \int\left(\frac{1}{\beta(s')}ds'\right) \tag{2.54}$$

- Q-tune or betatron tune, that has been already defined but it has never been done from a mathematical point of view:

$$Q(s) = \frac{1}{2\pi}\int\left(\frac{1}{\beta(s')}ds'\right) \tag{2.55}$$

- Chromaticity is a characteristic parameter that can be changed with sextupole magnets. Off-momentum particles undergo to a different focusing/defocusing action of quadrupoles, this changes are resumed in the *natural* chromaticity. It is defined as:

$$\xi = \frac{\delta Q/Q}{\delta p/p} \tag{2.56}$$

  Furthermore, a non-zero chromaticity leads to have a off-momentum beam and so a tune spread. But, above all, it can define if some amplitude-dependent phenomenon are stable or not. The chromaticity control leads to switch on magnets that induce non-linear effects in the beam optics, thus it ends up to be a really important but critical parameter.

Taking the real part of the Equation (2.53):

$$y(s) = A\sqrt{\beta(s)}\cos(\Phi(s) - \delta) \tag{2.57}$$

It is possible to write the particle motion equation in the accelerator. Note that the integral in Equation (2.53) has been substituted with $\Phi(s)$ in Equation (2.57) above to make the mathematical notation lighter, when a single revolution in the machine is considered then $\Phi(s)$ is equal to $\mu(s)$. Since the particle has always been described by its position and its divergence, it can be demonstrated that the set of this two equation constitute a parametric representation of an ellipse in the phase-space (y,y'):

$$\begin{cases} y(s) = A\sqrt{\beta(s)}\cos(\Phi(s) - \delta) \\ y'(s) = -\frac{A}{\sqrt{\beta(s)}}\Big[\sin(\Phi(s) - \delta) + \alpha(s)\cos(\Phi(s) - \delta)\Big] \end{cases} \tag{2.58}$$

The equation can be expressed also in terms of the Twiss parameters:

$$\gamma y^2 + 2\alpha y y' + \beta y'^2 = const. \tag{2.59}$$

And as the Equation (2.59) shows, they right hand side is a constant of the particle motion, i.e. an invariant: the Courant-Snyder invariant. So, as a particle moves in the machine it draws an ellipse in the phase-space plane and it remains unchanged as the particle moves in the accelerator, i.e. it is invariant with respect to the longitudinal coordinate s.
Different particles oscillates with different amplitudes (i.e., they have a different value of the constant A in Equation (2.58)) and each of them has its own ellipse on which it moves as it makes turns in the machine. So the parametric equations (2.59) can describe the motion of a particle beam too. In particular, as the ensemble of particle passes trough magnets or free drift spaces, the “shape” of the beam in the phase-space changes:

- Drift: Looking to the matrix representation reported in section 2.3.2.1, the particle is elongated while its divergence remains constant, so it tends to diverge
- Quadrupole: For a quadrupole the situation is a bit more complex since it focuses the beam on one plane and it defocuses on the other one. In Figure 2.20 a QF is considered: if the beam enters the quadrupole with a divergent trajectory in the direction along which the quadrupole imposes its focusing action, then it exits the magnet being convergent because of the rotation at which particles undergo while they move in the quadrupole.

As can be observed from Figure (2.19) and (2.20) it seems that the area of the ellipse enclosing the beam remains constant. In fact, the mathematical set of equations derived before is still valid for a beam since the maths has not changed. So, what before was called Courant-Snyder invariant (or single particle emittance) is said to be the beam emittance when an ensemble of particles is considered. The definition of beam emittance is not unique, it can be considered as

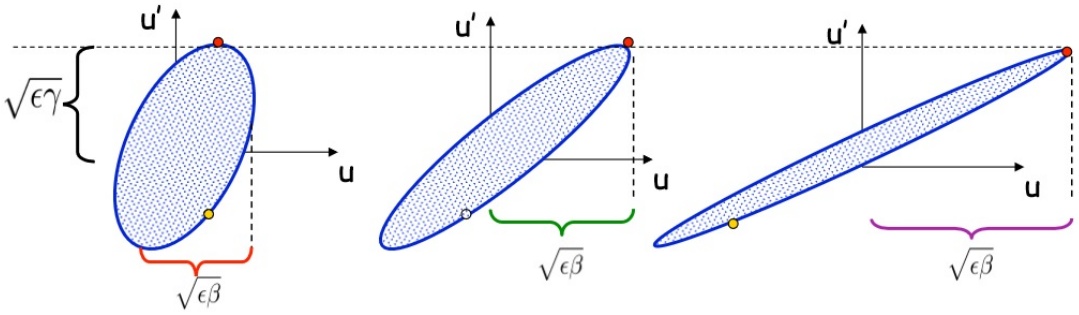

FIGURE 2.19. Example of a beam ellipse elongation as it passes trough a free drift from [13].

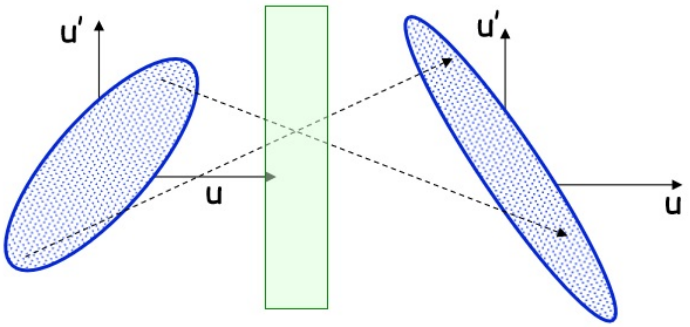

FIGURE 2.20. Example of a beam ellipse rotation, i.e. focusing on a specific direction as the beam passes in a focusing quadrupole [13].

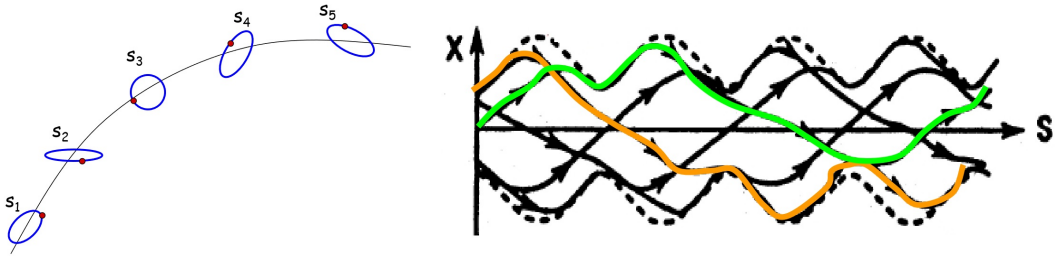

FIGURE 2.21. Representation of how particles oscillate on ellipses [13].

the smallest between all the ellipses that contains all the beam, or the ellipse that contains the 95% of all the particles constituting the beam itself. Considering what has been said till now, the particle motion in a beam is really much more complex than the description performed. Particles move on their ellipses, they occupy different position inside the beam envelope as they move in the accelerator and ellipses themselves evolve and change as they pass through magnets.

On the right side of Figure 2.21, it is possible to observe that particle trajectories evolve along

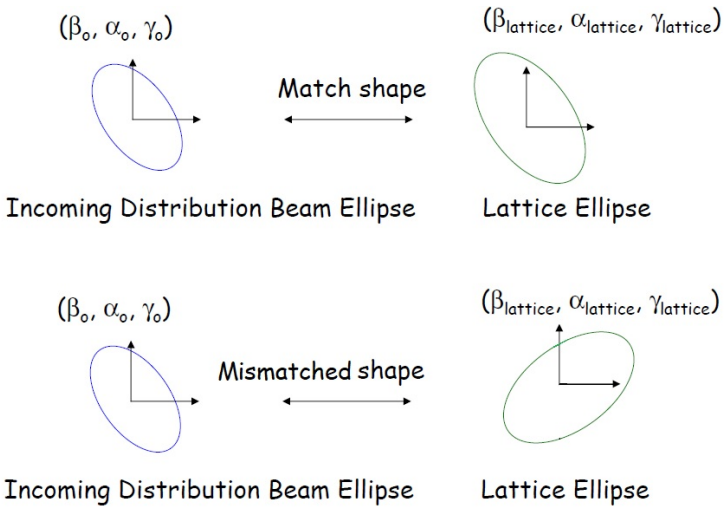

FIGURE 2.22. Comparison between matched and unmatched beam and lattice ellipse [13].

the longitudinal direction as a combination of sine and cosine (as was mathematically derived before) and, in addition, the combination of all particles trajectories form what is called the beam envelope (dotted black line), i.e. the physical region occupied by the beam. Particles move also inside the beam envelope occupying different position within it. If one could track the position of a single particle in the accelerator and also the beam envelope, then he will see the particle moving on the ellipse, except in the case of a lost or extracted particle because it will not be any more part of the beam envelope. On the left side of the previous picture is reported a general evolution of the particle ellipse along the longitudinal direction, any rotation and/or elongation is due to its passage in a quadrupole or free drift (as explained above).
Liouville's theorem is a fundamental theorem for the distribution of particles within the emittance and its conservation (constant area), it states that:

"*In an electromagnetic, along a particle trajectory the phase-space particle density is constant*".

A synchrotron has a periodic structure, as was previously explained in Equation (2.34), so when the optic of the beam is studied there is no need to impose boundary conditions because the only requirement is to have a Twiss parameter at point s equal to the one evaluated at $s+C$. In the context of partial differential equations, this problem is said to have periodic boundary conditions. Usually the β parameter is chosen because it is the one from which it is possible to retrieve information on the transverse beam dimension and, moreover, it is another way to ask for limited values of the total transfer matrix elements. Here a fundamental step occurs: once the emittance of the beam has been determined and the lattice structure has been fixed, then it is possible to identify the emittance that represents the outermost ellipse containing a predefined percentage of the beam particles (any other definition is accepted, like referring to the rms); and the Twiss

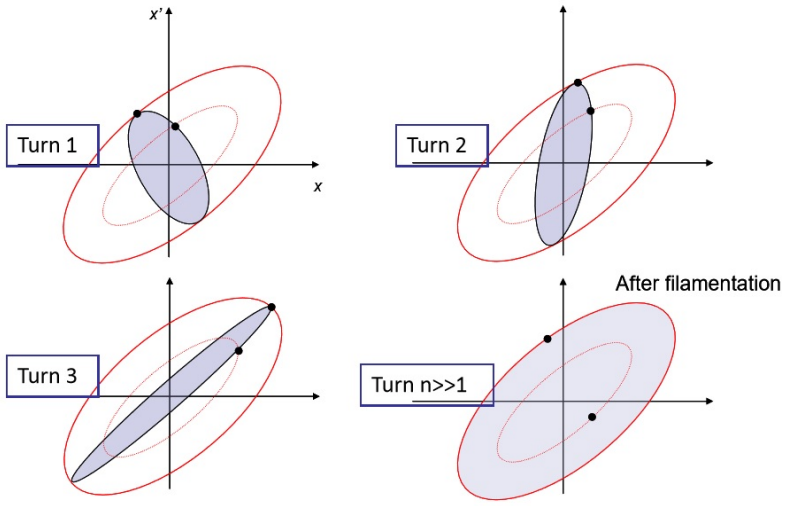

FIGURE 2.23. Schematic representation of how the beam adapts to the lattice ellipse undergoing to the filamentation process [13].

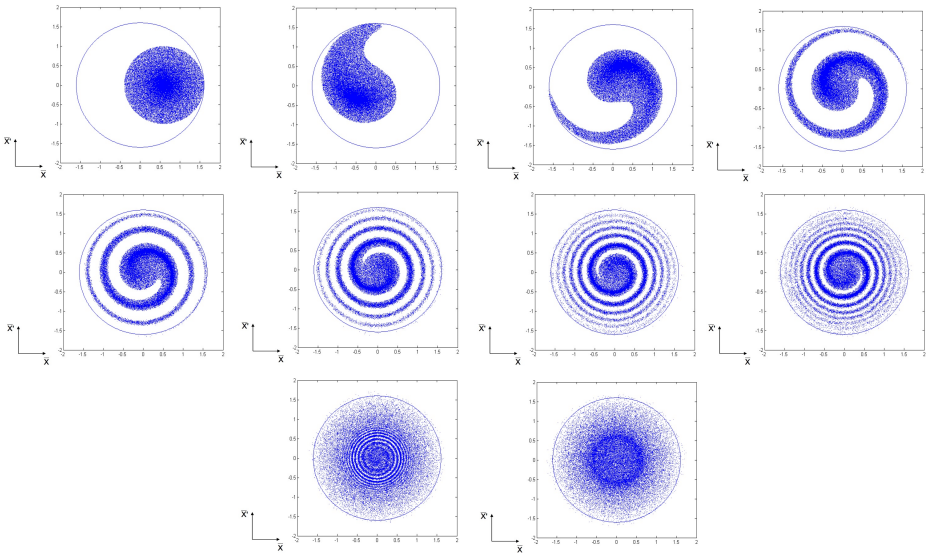

FIGURE 2.24. Simulation of the filamentation process represented in the normalized phase space [13].

parameters of the lattice components at which it is possible to associate an ellipse. In Figure 2.22 it is possible to have a graphical representation of matched and mismatched ellipses. In the first case, the beam undergoes to the transformations imposed by the lattice without suffering any important losses; in the other case this is not anymore true. Due to the mismatched ellipses, the beam undergoes to a complex motion within the lattice ellipse until particles cover all the area. A schematic representation of the evolution is reported in Figure 2.23 and Figure 2.24, it shows how the injected beam tries to adapt to the unmatched ellipse of the lattice. As it makes

turns in the machine, it undergoes to what is known as filamentation. This problem has to be faced up every time the beam is injected in the machine, if the machine parameters are kept constant (i.e., the elements of the total transfer matrix are constants) and the beam does not undergo to any instability, then filamentation does not occur. Liouville's theorem requires the phase space density to be conserved and in a strict mathematical sense this is true, since as the figure becomes more wound-up the spiral arms become narrower and the area is indeed constant. However it does not take long before the beam is apparently uniformly distributed over the matched ellipse and for all practical purposes the beam emittance has been increased [Beam transfer lines, P. J. Bryant, [28]].

2.6 Introduction to longitudinal beam dynamics

For the sake of completeness, a brief discussion on the longitudinal dynamics of the beam will be performed. In this direction the beam is accelerated by one (or more) radio-frequency (RF) cavities. A RF cavity is a closed structure in which electromagnetic waves move, being reflected (with a certain efficiency) by the walls of the chamber. The way electromagnetic waves are generated is out of the context of this thesis, but as an example, they could be generated by klystron (particular linear beam vacuum chamber for RF amplification) and then transported by wave-guides till the RF cavity. Once the wave reaches the cavity it is amplified until it reaches a steady state condition at the resonance frequency of the chamber: in this case the wave is called *standing wave*. The amplitude and the profile does not change in space but it oscillates in time and the frequency at which the wave oscillates is called f_{RF}. The interaction between the particle and the electromagnetic wave in the cavity could lead to the acceleration of the particle itself. It is possible to associate to a generic electromagnetic wave both an electric field and a magnetic field, but just the electric field is responsible for the increase in the particle velocity. So, it is necessary to make the particle cross the cavity when the direction of the (electric) field is equal to the direction of the particle motion.

A synchrotron can be considered as a sequence of a RF cavity and a free acceleration region, which is made by all the components that do not accelerate the beam as dipoles, quadrupoles, sextupoles, octupoles, free drifts, kickers, correction magnets, etc. Also in this case it is necessary to have the electric field in the cavity that points in the same direction of the particle motion when the beam crosses the cavity. The working principle is different because, a part from being accelerated, the particle has to be confined and bended to move on a circular path. But since the beam changes its energy every time the particle crosses it, the magnetic field has to be changed in time, i.e. increased, in order to avoid particle losses. The common practice suggested to impose a time dependent law for the magnetic field, and so for the energy gain, and then adjust the RF cavity parameters so that they satisfy the energy condition. When the particle crosses the cavity it gains an amount of energy equal to ΔE_0. Assuming that the RF generator imposes a sinusoidal

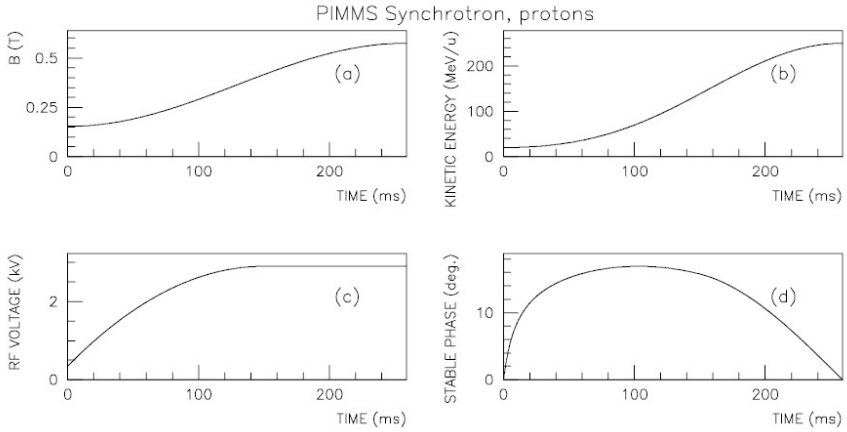

FIGURE 2.25. From left to right in the upper part of the figure you find the time dependent variation of the magnetic field, the kinetic energy increase, in the lower part there is the RV voltage and the phase [16].

potential difference, then it is possible to relate the energy gain with the voltage amplitude and its phase as:

$$\Delta E_0 = eV_{RF}\sin(\Phi) \tag{2.60}$$

The energy gain can be derived from the magnetic field law decided by the designer. The two main parameters are the time dependent magnetic field and the particle momentum:

$$B(t)\rho = \frac{p(t)}{e} \tag{2.61}$$

Being the bending radius ρ constant as well as the charge number (if particle momentum is expressed in terms of eV/c) , then the energy gain, i.e. the kinetic energy relative increase, is proportional to the time dependent law of the magnetic field. The increase of particle energy has to be guaranteed by the RF generator, so the potential difference V_{RF} and the phase Φ have to change in time and, at the same time, they always have to satisfy Equation (2.60). In Figure 2.25 an example of time dependent laws for the PIMMS (Proton-Ion Medical Machine Study) synchrotron. It is possible to observe that the kinetic energy increase (on the top right) has the same sinusoidal shape as the magnetic field (top left) while in the lower part of the figure is represented the time dependent behaviour for the potential difference (on the left) and for the phase (on the right) of the RF cavity.

The description performed till now, implicitly refers to a specific particle that is called the *synchronous particle*, i.e. the one that is exactly synchronized with the RF cavity and so the only one that will gain exactly the energy gain ΔE_0. All the other particles will be accelerated for a lower time, if their energy is slightly below the one of the synchronous particle; or they will be decelerated in the opposite case. The discussion that will follow it is just qualitative but, for

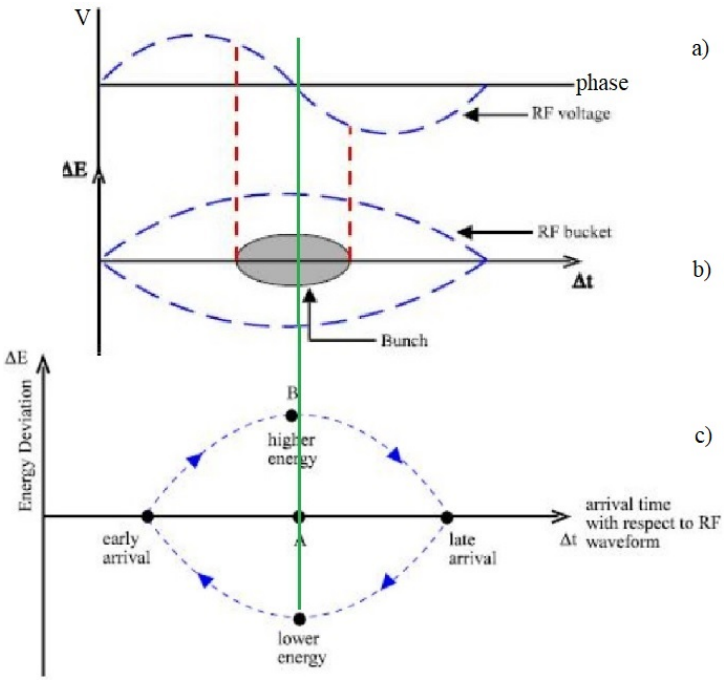

FIGURE 2.26. From top to bottom: sinusoidal waveform in the cavity; Bunch of accelerated particles in the Bucket; motion of non-synchronous particle around the synchronous one. [5].

the sake of completeness, the motion equations in the longitudinal direction for all the particles (the synchronous and all the not-synchronized one) are reported and derived in **Appendix A**. In circular accelerator is common practice give to the synchronous particle a zero phase. Particles on the right-hand side of the green line in Figure 2.26 a) will be decelerated by the negative potential and their phase decreases and it tends to the synchronous phase. On the contrary, particles with lower phase (left-hand side with respect to the green line in Figure 2.26 a) will see a positive potential meaning that they will be accelerated by the RF cavity. As it is accelerated, the particle phase will tend to the zero phase of the synchronous one, and its energy will progressively increase undergoing to the cycle represented in Figure 2.26.c. Here particle A is the synchronous one, while particle B is a generic particle that arrives in the RF cavity at the same time of A but with a higher energy. Both particle will gain the energy ΔE_0 but, as discussed in the previous section, a particle with a higher energy will move on a circumference larger than the one of the reference particle (it will have a revolution frequency slightly lower too). So, at the next turn, particle A will gain again the same amount of energy, while particle B will arrive in the cavity with a certain delay being then decelerated. The deceleration effect will continue until particle B reaches a lower energy than A, so the particle will arrive in the cavity earlier than particle A. In this way it will see a waveform that will increase again its energy (going back to point B in Figure 2.26). This periodic motion is defined as *synchrotron oscillation*. When particles are injected in

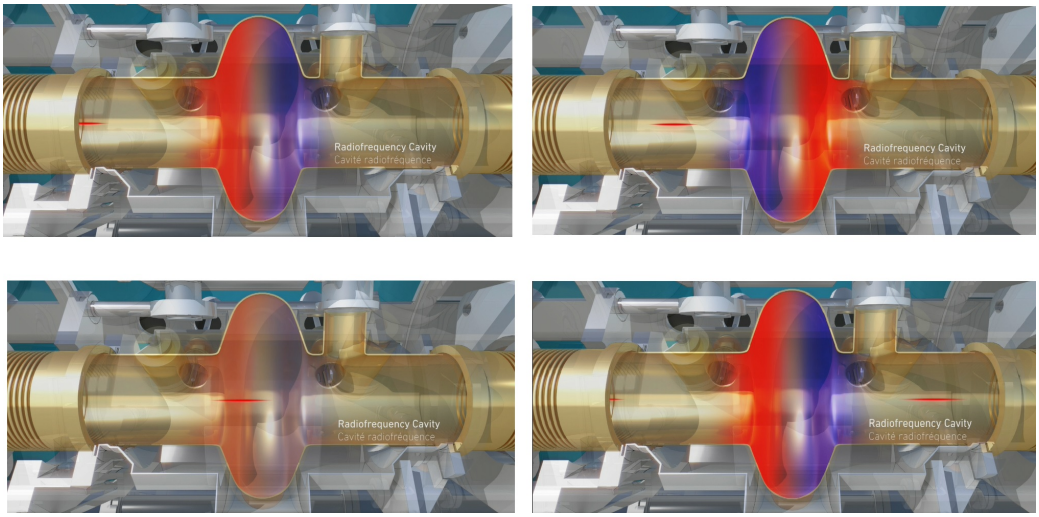

FIGURE 2.27. It is reported the schematic of one of the RF cavity of the LHC at CERN. It is possible to observe the incoming beam and how the electric field in the chamber changes in time (the red and blue color represents the different polarities of the field) [5].

the accelerator, it is possible to assume they occupy a certain space along the circumference of the accelerator. As soon as the acceleration process begins, then particles get “clumped” [5] around the synchronous particles, leading to the formation of bunch of particles that are then accelerated up to the required energy. In Figure 2.27 is reported the acceleration of a bunch of particles highlighting how the electric field in the cavity changes according to the passage of the bunch throughout it. It is also possible to see (in the lower left part of the figure) that particles at the beginning of the bunch are subjected to a decelerating electric field.

CHAPTER 3

BEAM EXTRACTION

Two main approaches could be used to extract particles from an accelerator. A single-turn (fast) extraction and a multi-turn (slow) one. The first one allows the deflection of the beam trajectory into a beam transfer line or, as it is done in big facilities, the transmission of the beam in a bigger accelerator. As the name says, this step is performed in a single turn and since particles travel at a high speed the phenomenon is performed in ms or μs, according to particle mass and accelerator length. It is common practice to adopt the latter technique in medical accelerator for cancer treatment, the reason is that it is of fundamental importance to obtain a beam that lasts some seconds (between 1s and 10s) and which intensity, i.e. the number of particles reaching the patient, is kept constant in time. All these strict requirements are important in order to evaluate the exact dose reaching the patient and making it conformed to the medical requirements. Between the multi-turn extraction, two other categories can be defined: the resonant and the non-resonant one. A non-resonant (slow) extraction is based on beam scattering by internal target, but it is mentioned just for accademic reasons. A resonant multi-turn extraction, briefly called slow extraction, is a technique that allows the withdrawal of a certain number of particles each turn. So, while the core of the beam continues to turn in the accelerator, some other particles are moved towards the extraction line. The different way particles are extracted determines different extraction techniques. Between the different possibilities, just two of these will be analysed:

- Betatron extraction: the beam is extracted by the use of a betatron accelerator;
- Radio Frequency Knock-Out (RFKO) extraction: the beam is extracted by the use of an electrostatic kicker.

3.1 Third-order resonance

From the mathematical description performed in the previous chapter, it is possible to see that under specific conditions the beam optics can be assumed to be linear. In this configuration the machine is made by dipoles and quadrupoles only and the particle trajectory could be found solving the equations presented in Chapter 2. But even in this configuration, their main assumptions that has been performed is that magnets are perfect, so there are no misalignments or imperfections in the strengths of the magnets themselves, moreover the beam is mono-kinetic. When the assumption of mono-energetic beam is removed the concept of dispersion function has been introduced (section 2.4). It is possible compare this beam characteristic with a possible error in the strength of a dipole magnet. In fact, a mono-kinetic beam that undergoes to an imperfect magnetic field (that it is supposed to bend the beam trajectory) would end up moving on a slightly different trajectory because each of its particles have perceived a different intensity of the magnetic field. Under these considerations the particles trajectories can be found from Equation (2.47):

$$D''(s) + K(s)D(s) = \frac{1}{\rho(s)} \tag{3.1}$$

The solution of the Equation (3.1) is:

$$D(s) = \frac{\sqrt{\beta(s)}}{2sin(\pi Q)} \oint \frac{\sqrt{\beta(s')}}{\rho(s')} cos\Big(\Phi(s') - \Phi(s) - \pi Q\Big) ds' \tag{3.2}$$

Where s is larger than s'.

The first condition to be checked is that the denominator does not go to zero, i.e. the tune of the machine has to be chosen so that the dispersion function is not infinite. This condition is attained when:

$$Q \neq n \tag{3.3}$$

Where n is a generic integer number.

So circular accelerators contain in themselves a source of instability. Moreover, a similar rational can be adopted for imperfections in the strength of quadrupoles. Since quadrupoles are responsible for the focusing and defocusing of the beam, their errors mainly affect the amplitude of betatron oscillations. An expression similar to the one in Equation (3.2) can be obtain, the demonstration is avoided but it could be found in [28]. Thus, the change in the betatron oscillations can be evaluated as:

$$\Delta\beta(s) = -\frac{\beta(s)}{2sin(2\pi Q)} \oint \beta(s')\Delta K(s') cos\Big(\Phi(s') - \Phi(s) - 2\pi Q\Big) ds' \tag{3.4}$$

Where s is larger than s'.

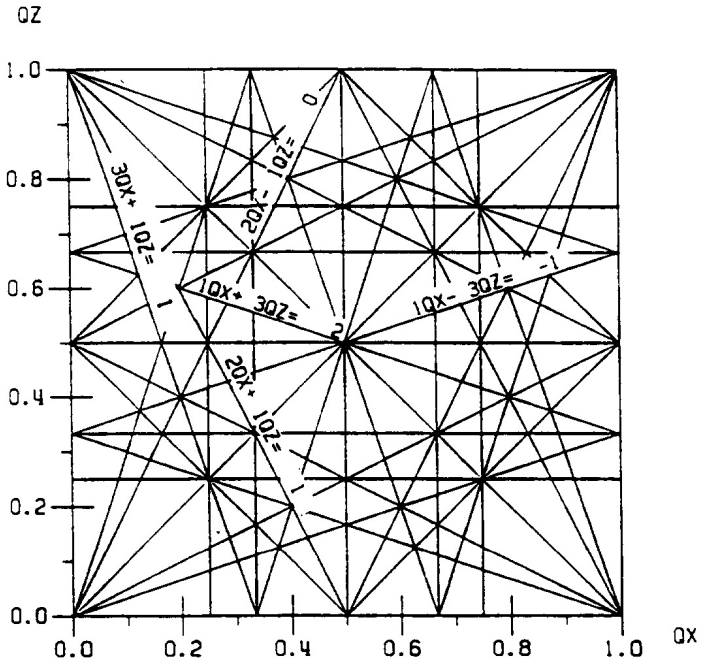

FIGURE 3.1. Tune diagram [28].

Also in this case it is fundamental to check that the denominator does not go to zero otherwise the relative change in the amplitude of betatron oscillations enormously increases. The condition that has to be fullfilled in order to keep limited the amplitude of betatron oscillations is that:

$$Q \neq \frac{n}{2} \tag{3.5}$$

Where n is a generic integer number.

Since quadrupoles focus the beam in one transverse direction and defocus it on the other one it is highly required to avoid a resonant tune on both the transverse directions. Moreover, also the intrinsic instability generated by dipoles has to be prevented. Thus, the combination of Equation (3.2) and Equation (3.5) leads to ask for a tune different from both integers and half-integers values and can be generally resumed in Equation (3.6).

$$mQ_x + nQ_y \neq l \tag{3.6}$$

Where m, n, l are generic integer numbers.

It is quite common to represent Equation (3.6) in a graphic that is known as *tune diagram* reported in Figure 3.1. From the tune diagram it is possible to observe different resonance lines. In order to avoid resonant particle losses, the working point of the accelerator has to be chosen far from the different resonance lines. Considering what has been said so far, dipoles are able to drive first order resonances, as Equation (3.2) and (3.3) show; according to Equation (3.4) and (3.5) quadrupoles drive up to the half-integer resonance, thus it can be expected that sextupoles

induce up to the third-integer resonace. In fact, multipoles are able to drive all the resonances up to the highest order that is defined by the half number of magnet's poles. Even if sextupoles can be present in an accelerator, those responsible for resonances are physically different from those responsible for chromaticity control. In order to study (and exploit) third-order resonance, it is common practice to use the Hamiltonian mathematics, in particular, the Kobayashi simplification. This approach considers sextupoles magnets as a perturbation of the linear optics and it is quite well performing for beam extraction studies.

A general multipole expansion consists in considering magnets which length is larger than the radial dimension of the vacuum chamber so that end fields effect can be neglected. Moreover, the studied region has to be a vacuum space with no electric currents and no iron cores of the magnets included. Under these assumptions the following set of equations can be used:

$$\mathbf{B} = \nabla \times \mathbf{A} \tag{3.7}$$

$$\nabla \cdot \mathbf{B} = 0 \tag{3.8}$$

$$\nabla \times \mathbf{B} = 0 \tag{3.9}$$

$$\mathbf{B} = -\nabla V \tag{3.10}$$

Where A is the magnetic vector potential, the only non-null component is the one along the longitudinal direction A_s due to the trasversality of the magnetic field; while V is the magnetic scalar potential. Using Equation (3.7) and Equation (3.10) it is possible to compute the components of the magnetic field in the transverse direction (x and z) that are reported in Equation (3.11). To avoid confusion, from now on the z coordinate will be replaced by y and the letter z will be used to indicate a general complex number.

$$B_x = \frac{\partial A_s}{\partial y} = -\frac{\partial V}{\partial x} \qquad B_y = -\frac{\partial A_s}{\partial x} = -\frac{\partial V}{\partial y} \tag{3.11}$$

In order to find the analytic form of the two potentials it is useful to define a generic complex potential function:

$$\tilde{A} = A_s(x,y) + iV(x,y) \tag{3.12}$$

If Equation (3.11) is considered again it can be noticed that it expresses the Cauchy-Riemann conditions: it means that both the real and imaginary component of A are holomorfic (i.e., since we are dealing with complex potential function it means they can be expressed in terms of an analytic function) and differentiable. At the same time complex mathematics ensures that the complex potential function can be written as a series that converges for a radius lower than the minimum distance between the origin of the reference system and the closest magnet surface

(i.e., within this radius the Equations (3.7)-(3.10) can be used without violating any assumption made before).

$$\tilde{A} = \sum_n^{\infty} C_n z^n = \sum_n^{\infty} (\lambda_n + i\mu_n)(x+iy)^n, \qquad |z| < r_c; \lambda_n, \mu_n \in R \tag{3.13}$$

If a sextupole has to be studied, then the degree of the sum is reduced to $n = 3$ since it has six poles. Developing the single coefficient part of Equation (3.13) and dividing real and imaginary terms, it is possible to obtain the components of the complex potential function $\tilde{A}$, reported in Equation (3.14) and (3.15).

$$A_s = C_1 x + C_2(x^2 - y^2) + C_3(x^3 - 3xy^2) \tag{3.14}$$

$$iV = i(C_1 y + 2C_2 xy + 3C_3 x^2 y - C_3 y^3) \tag{3.15}$$

So, using Equation (3.11) the transverse components of the magnetic field can be computed.

$$B_x = -6C_3 xy \tag{3.16}$$

$$B_y = -3C_3(x^2 - y^2) \tag{3.17}$$

Comparing the magnetic field components with the Taylor expansion of the magnetic field in the horizontal plane, it is possible to find the coefficient C_3.

$$C_3 = -\frac{1}{6} \frac{d^2 B(x,0)}{dx^2}\bigg|_0 \tag{3.18}$$

For the sake of completeness, the final expression of the magnetic field components is reported in Equation (3.19).

$$B_x = \frac{d^2 B(x,0)}{dx^2}\bigg|_0 xy \qquad B_y = \frac{1}{2} \frac{d^2 B(x,0)}{dx^2}\bigg|_0 (x^2 - y^2) \tag{3.19}$$

In order to find the sextupole strength, as it has been done for dipoles and quadrupoles, it is useful to consider the magnet as a thin lens. A sextupole is used to correct chromatic aberrations, i.e. the enlargement of the focal spot induced by the focusing/defocusing action of quadrupoles on a beam with a non-zero momentum spread. Thus, it is possible to compute the change in divergence induced by a sextupole as the magnetic field B_z the particle perceive along the sextupole length normalized l_s to the magnetic rigidity of the particle itself $B\rho$. Obviously a change in the x-divergence is induced by a vertical field while a change in the z-divergence is induced by a horizontal field. Under the previous assumption of thin lens approximation the change in particle position can be neglected.

$$\Delta x' = \frac{B_z l_s}{|B\rho|} = \frac{1}{2} \frac{l_s}{|B\rho|} \frac{d^2 B(x,0)}{dx^2}\bigg|_0 (x^2 - y^2) \tag{3.20}$$

$$\Delta z' = \frac{B_x l_s}{|B\rho|} = \frac{l_s}{|B\rho|} \frac{d^2B(x,0)}{dx^2}\bigg|_0 xy \tag{3.21}$$

It is common practice two work in the phase-space horizontal x-x' or vertical z-z' where particle position and divergence is displayed. In the same way, a lighter notation can be obtained if a normalized phase-space is considered. Looking to the set of Equation (2.42) it is easy to compute the matrix that allows the conversion from the phase-space to the normalized one and viceversa:

$$M_{x\to X} = \begin{pmatrix} \frac{1}{\sqrt{\beta}} & 0 \\ \frac{\alpha}{\sqrt{\beta}} & \sqrt{\beta} \end{pmatrix} \tag{3.22}$$

$$M_{X\to x} = \begin{pmatrix} \sqrt{\beta} & 0 \\ -\frac{\alpha}{\sqrt{\beta}} & \frac{1}{\sqrt{\beta}} \end{pmatrix} \tag{3.23}$$

So, the particle divergence can be computed as:

$$\Delta X' = \frac{1}{2} \frac{l_s}{|B\rho|} \frac{d^2B(x,0)}{dx^2}\bigg|_0 (\beta_x^{3/2}(X^2 - \frac{\beta_z}{\beta_x} Z^2)) \tag{3.24}$$

$$\Delta Z' = \frac{l_s}{|B\rho|} \frac{d^2B(x,0)}{dx^2}\bigg|_0 (\beta_x^{1/2}\beta_z XZ) \tag{3.25}$$

The sextupole strength can be then defined as:

- Phase-space:
$$\kappa = \frac{1}{|B\rho|} \frac{d^2B(x,0)}{dx^2}\bigg|_0$$
- Normalized phase-space:
$$S = \frac{1}{2}\beta_x^{3/2} l_s \kappa$$

According to the sextupole gradient, the sign of its strength and the presence (or absence) of poles in the median place it is possible to distinguish between normal and skew sextupoles and D-type from F-type. In Figure 3.2 a schematic picture is reported. Normal sextupoles are defined as six poles magnets with no poles on the median plane and are usually the most common in particle accelerators. Between the normal sextupoles it is possible to further distinguish between focusing and defocusing type. If a negatively charged particle is considered, then F-type sextupoles makes the particle with a positive x-coordinate move towards the centre of the vacuum chamber.

According to the matrix formalism adopted in the previous chapter, the general transfer matrix at the n^{th} turn can be written as a function of the tune of the machine since it is the

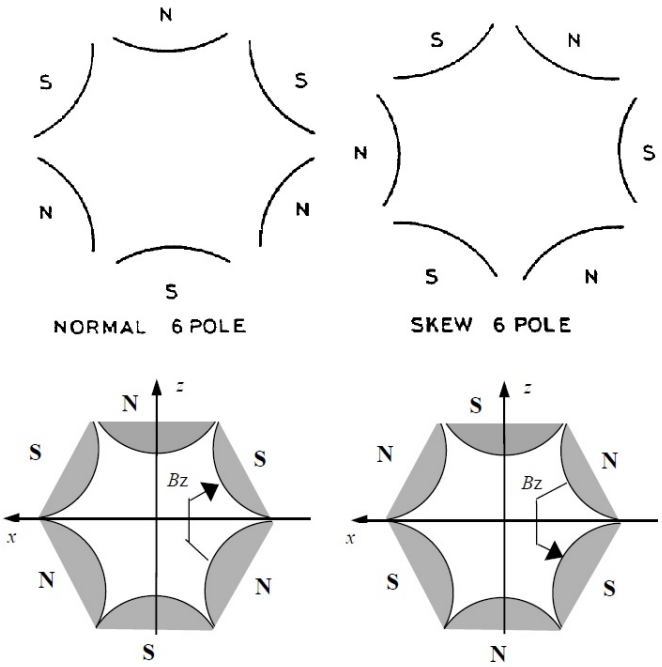

FIGURE 3.2. Normal and skew sextupoles [22, 28].

physical quantity directly connected to betatron oscillations that do not allow a particle to reach the same exact point after a full turn in the machine.

$$M_n = \begin{pmatrix} cos(2\pi(nQ_x)) & sin(2\pi(nQ_x)) \\ -sin(2\pi(nQ_x)) & cos(2\pi(nQ_x)) \end{pmatrix} \tag{3.26}$$

Since the extraction occurs on one of the two transverse planes (x or z), the tune on the direction that host the extraction line has to be brought close to a resonance. The case of an horizontal (x) extraction will be considered. Thus, the tune Q_x must be close to a resonance line, in particular, a third-order one since the aim is to make it reach the resonance with a sextupole that, as said before, is able to excite up to the third-order one. It will be seen that a this type of resonance allows the extraction of particles which amplitude is above an unstable value, thus, all those below this limit are (indefinitely) kept in the accelerator on a stable orbit. Moreover, the control of the unstable amplitude is defined by the extraction technique and by the average momentum beam and momentum spread as well. Thus the characteristics of the spill can be controlled and modified. In order to start the mathematics demonstration for the third-order resonance the Q_x has to be defined accordin to Equation (3.27), where m is a generic integer value.

$$Q_x = m \pm \frac{1}{3} + \delta Q \tag{3.27}$$

Neglecting the effect of sextupoles, beam optics is still linear, so it is possible to evaluate the total transfer matrix with the tune in Equation (3.28), where the term dQ is defined as the particle

tune distance from the resonance:

$$\delta Q = Q_{particle} - Q_{resonance} \tag{3.28}$$

So, the position and divergence of a generic particle can be evaluated as the number of turns increases. If turn 0 is the one at which particle position and divergence is taken as initial conditions, then their new value after one full turn in the machine can be evaluated as:

$$\begin{pmatrix} x \\ x' \end{pmatrix}_1 = \begin{pmatrix} cos\left(2\pi\left(m \pm \frac{1}{3}\right)\right) & sin\left(2\pi\left(m \pm \frac{1}{3}\right)\right) \\ -sin\left(2\pi\left(m \pm \frac{1}{3}\right)\right) & cos\left(2\pi\left(m \pm \frac{1}{3}\right)\right) \end{pmatrix} \begin{pmatrix} x \\ x' \end{pmatrix}_0 = \begin{pmatrix} -1/2 & \pm\sqrt{3}/2 \\ -(\pm\sqrt{3}/2) & -1/2 \end{pmatrix} \begin{pmatrix} x \\ x' \end{pmatrix}_0 \tag{3.29}$$

In the previous equation the effect of the tune distance has been neglected, it means that the particle is on resonance. In the same way the position and divergence can be computed after another turn in the machine (i.e., turns 2):

$$\begin{pmatrix} x \\ x' \end{pmatrix}_2 = M_2 \begin{pmatrix} x \\ x' \end{pmatrix}_0 = \begin{pmatrix} -1/2 & \mp\sqrt{3}/2 \\ -(\mp\sqrt{3}/2) & -1/2 \end{pmatrix} \begin{pmatrix} x \\ x' \end{pmatrix}_0 \tag{3.30}$$

At the third turn the matrix will assume the following form:

$$\begin{pmatrix} x \\ x' \end{pmatrix}_3 = M_3 \begin{pmatrix} x \\ x' \end{pmatrix}_0 = \begin{pmatrix} 1 & sin(6\pi m) \\ -sin(6\pi m) & 1 \end{pmatrix} \begin{pmatrix} x \\ x' \end{pmatrix}_0 = \begin{pmatrix} 1 & 0 \\ 0 & 1 \end{pmatrix} \begin{pmatrix} x \\ x' \end{pmatrix}_0 \tag{3.31}$$

After three turns, a particle with a resonant tune will have the same position and divergence it initially had, i.e. at those of turn 0. But now if a small ($|\delta Q| << 1/3$) tune distance is considered, then its effect can be neglected for the first two turns, but at the third one the transfer matrix will be:

$$\begin{pmatrix} x \\ x' \end{pmatrix}_3 = \begin{pmatrix} 1 & sin(6\pi\delta Q) \\ -sin(6\pi\delta Q) & 1 \end{pmatrix} \begin{pmatrix} x \\ x' \end{pmatrix}_0 = \begin{pmatrix} 1 & 6\pi\delta Q \\ -6\pi\delta Q & 1 \end{pmatrix} \begin{pmatrix} x \\ x' \end{pmatrix}_0 \tag{3.32}$$

Equation (3.32) has been derived under the assumption of small angles. So the particle with a slightly different tune will have a position and divergence slightly different from the initial one. In this configuration (particle not at the resonant tune) a sextupole can be introduced as a perturbation of a linear optic. Three different contributions have to be considered and summed up:

- sextupole is introduced after three turns;
- sextupole introduced after two turns and then a last turn is still performed;
- sextupole introduced after the first turn and then two more turns are performed.

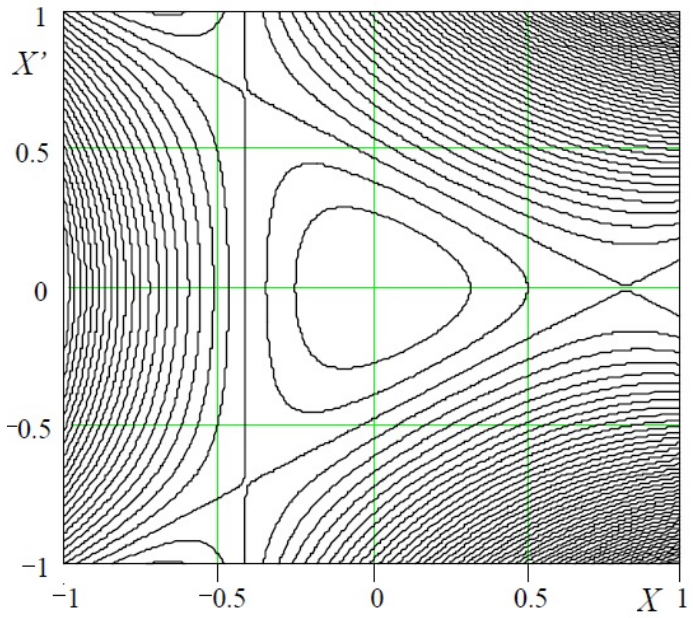

FIGURE 3.3. Stable and unstable particle trajectories [22].

By summing them up it is possible to compute the change of position and divergence after three turns in the machine:

$$\Delta X_3 = \epsilon X_0' + \frac{3}{2} S X_0 X'_0 \tag{3.33}$$

$$\Delta X_3' = -\epsilon X_0 + \frac{3}{4} S (X_0^2 - X_0'^2) \tag{3.34}$$

Equation (3.33) is usually known as spiral step while Equation (3.34) is known as spiral kick. And by their integration it is possible to compute the Kobayashi Hamiltonian:

$$\mathbf{H} = \frac{\epsilon}{2}(X^2 - X'^2) + \frac{S}{4}(3XX'^2 - X^2) \tag{3.35}$$

The Hamiltonian is time independent, so in the *X*-*X*' phase-space it is a constant of the motion, drawing the contours for constant values of the Hamiltonian itself, it is possible to observe the particle trajectories. In particular, from Figure 3.3 three main information can be gathered. At first, when $S = 0$, i.e. non-linear effects induced by sextupoles or higher multipoles are neglected, particles have a circular trajectory. It is quite intuitive to understand it also without looking at Equation (3.35). In fact, without multipoles that lead to non-linear effects, the particle trajectory in the phase-space is an ellipse that turns into a circumference when the normalized phase-space is studied. Then, when non-linear effects are considered (i.e., the second term of Equation (3.35) is added), the circumference is perturbed and it starts looking like a triangle. The lines delimiting the triangle area are called *separatrices*. Within the triangle the particle trajectory is stable,

whereas outside it is unstable and particle trajectories do not close on themselves anymore. Now it is quite intuitive to understand that it is really important to determine the separatrix equations. By their study it is possible to determine particles characteristics in the last three turns before the extraction.

There is a special value of the Hamiltonian that allows the factorization of Equation (3.35) as a product of three terms that represent the separatrix equations:

$$\left(\frac{S}{4}X+\frac{\epsilon}{6}\right)\left(\sqrt{3}X'+X-\frac{4\epsilon}{3S}\right)\left(\sqrt{3}X'-X+\frac{4\epsilon}{3S}\right)=0 \tag{3.36}$$

An important parameter is the area of the triangle that can be evaluated as a function of the apothem h:

$$A_{stable}=3\sqrt{3}h^2 \tag{3.37}$$

By the knowledge of the coordinates of the points where separatrices intersect each other, it is possible to compute the apothem h as:

$$h=h=\frac{4\pi}{S}\delta Q \tag{3.38}$$

Moreover, it is possible to demonstrate that best position where to locate a resonance sextupole is in a free dispersion region in order to avoid change of tune distance that would change the dimensions of the extracted beam.

In order to study and, eventually, modify the characteristics of the extracted beam in the different extraction techniques, it is frequently used the Steinbach diagram that allow the representation of the beam in a tune - (betatron) amplitude diagram, a schematic representation can be found in Figure 3.4. The stopband, i.e. the width of the “V” shape centred at the resonant tune, can be changed. The parameters that affect its shape are found by the comparison between the area of the stable triangle, defined in Equation (3.37) and the *single particle emittance*, i.e. the emittance of the particle in the normalized phase-space. To have a stable particle trajectory, the particle emittance has to be lower or equal to the stable triangle area, in this way the particle trajectory is contained within the triangle:

$$A_{particle}\leq A_{stable}\rightarrow A^2\pi\leq\frac{48\sqrt{3}\pi}{S^2}\delta Q^2\pi \tag{3.39}$$

Substituting Equation (3.28) into Equation (3.39) it is possible to develop an inequality for the particle tune that also defines the width of the "V" shaped unstable region:

$$Q_{res}-\sqrt{\frac{1}{48\sqrt{3}\pi}}|S|A\leq Q_{particle}\leq Q_{res}+\sqrt{\frac{1}{48\sqrt{3}\pi}}|S|A \tag{3.40}$$

This is usually known as stop-band. Once the beam has been positioned on one of the two sides of the resonance, it is possible to extract it by moving the beam into resonance or by moving

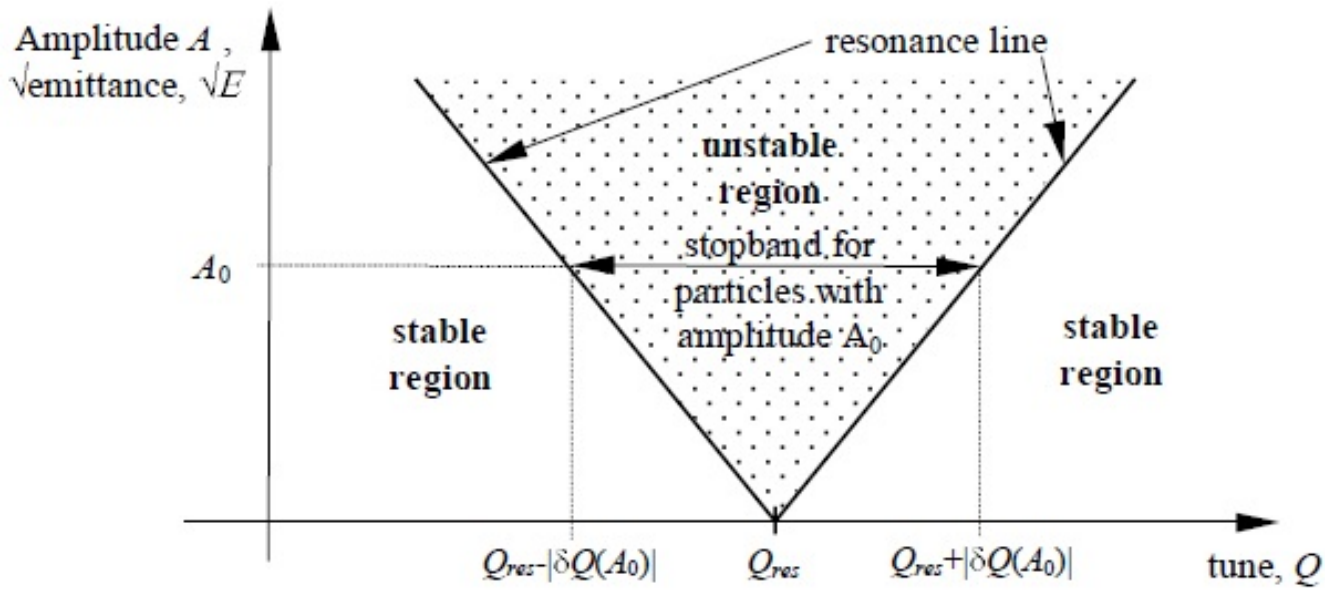

FIGURE 3.4. Steinbach diagram [22].

the resonance towards the beam. To the first type pertains the betatron extraction (also called acceleration-driven) and the RFKO one; while to the latter class the quadrupole-driven and the sextupole-driven are part. In the quadrupole-driven extraction the tune of the machine is changed by changing the quadrupoles strength, i.e. their current, in order to make the resonant tune move towards the beam. In the sextupole-driven extraction the sextupole strength is changed and so the stopband adjusts according to Equation (3.40).

Once the particle enters the unstable region it can be extracted. In particular, from Equations (3.29) till Equation (3.32) the evolution of a particle at resonance has been derived. So, it is possible to draw the related phase-space diagram for the separatrix lines. Now matching the extraction separatrix with the longitudinal position of the electrostatic septum, it is possible to show that after the third turn the particle overcome the septum and can be led to the extraction line. A phase advance of $\Delta\mu = 1.25\pi rad$ is the optimum relative position between the electrostatic septum and the resonant sextupole, it allows the extraction separatrix to cross the septum as reported in Figure 3.6. In this way all the particles contained between the electrostatic septum and the position #3 will be extracted.

Once the particle crosses the electrostatic septum, it receives a kick that increase its divergence and by the positioning of the magnetic septum at phase advance of 0.5π it is possible to separate the circulating beam from the extracted one that is nothing else than a secondary beam then directed in the extraction line. A schematic representation of the extraction is given in Figure 3.7. After the magnetic septum there will be a sequence of magnets that drives the

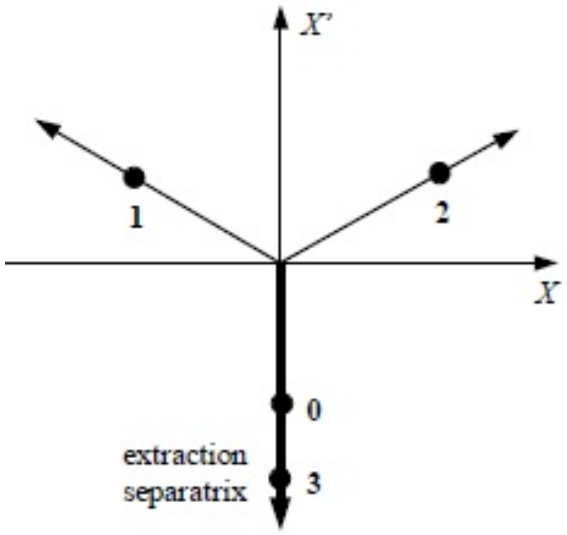

FIGURE 3.5. Evolution of a particle at resonant on the separatrices for the longitudinal position corresponding to the resenant sextupole [22].

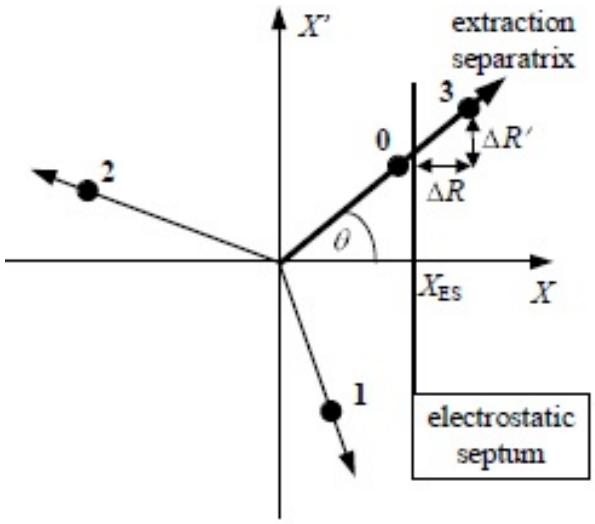

FIGURE 3.6. Evolution of a particle at resonant on the separatrices for the longitudinal position corresponding to the resonant sextupole [22].

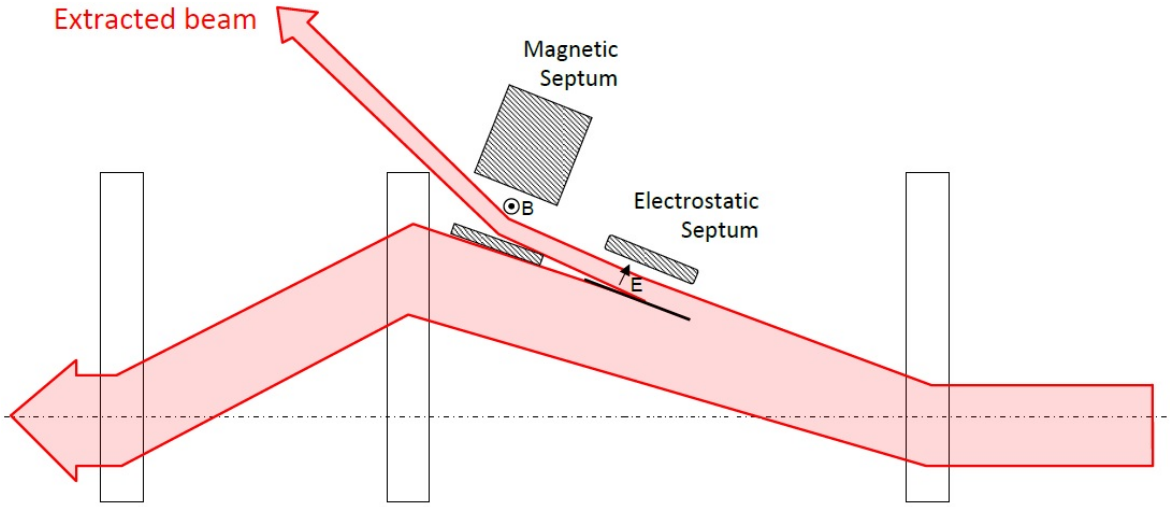

FIGURE 3.7. Beam trasnfer between electrostatic and magnetic septum [15].

beam towards the treatment rooms or to the experimental points. This sequence is usually called extraction line.

3.2 Betatron slow extraction

A betatron core is a circular magnetic circuit and the beam passes trough it. With a coil is possible to change the magnetic flux inside the magnetic circuit. Varying the magnetic flux an electric field directed along the axis of the betatron core is induced and it is responsible for the beam acceleration towards the resonance. The betatron core accelerates the beam gradually and the beam goes in the unstable region. It is possible to observe the shape of the beam in the Steinbach diagram in Figure 3.8. Once the particles have reached the resonance line (i.e., one of the two lines that enclose the "V" shaped unstable region) it enters the unstable region and it can be extracted. The extraction process follows the mathematical description performed before, i.e., once the particle achieves an unstable betatron amplitude oscillation, it jumps from one separatrix to the other until it crosses the electrostatic septum where it receives a kick. It is then transformed in a position difference with respect to the circulating beam as the particle moves from the electrostatic to the magnetic septum. The main characteristic of such an extraction is the continuously varying momentum of the beam remaining in the machine. While as far as the extracted beam is concerned it has a constant amplitude, small momentum spread and a constant momentum. The only negative remark of such process is that it doesn't have a fast response, i.e., it cannot be switch on and off in order to synchronize with the patient breath. Thus an on-off system on the extraction line has to be used.

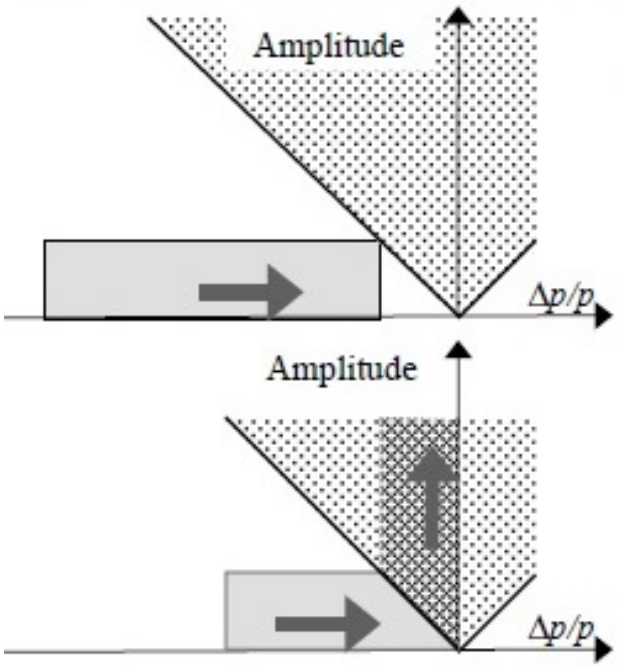

FIGURE 3.8. Beam evolution for a betatron extraction in Steinbach diagram [22].

3.3 RFKO technique

Apart from the beam energy and the extracted beam has to be uniform in time, i.e. the number of extracted particles as the beam turns in the machine has to be kept constant in time. In this way it is possible to ensure that the number of particles reaching the tumour accomplish the medical requirements. Since the number of particles to be extracted depends on the dose that has to be delivered to a tumour slice, it is common to still have a circulating beam in the acceleration after the treatment of a single tumour slice. At present CNAO performs a betatron extraction. This technique needs the beam to be de-bunched in order to allow its acceleration up to the resonance. Thus, the acceleration of the non-extracted beam to the new treatment energy requires to turn on again the RF cavity. Unfortunately, the bunching and de-bunching process is not efficient, it requires the increase of the RF cavity potential so that the longitudinal acceptance is matched with the longitudinal emittance of the beam. If the two quantities are not compatible particles do not get trapped in the bucket, and so they are not accelerated. The process is highly inefficient since the trapping of particles within the bucket would lead to lose half of the non-extracted beam. On the contrary, if the extraction could be performed with a bunched beam then the change of the beam energy would be feasible since it won't lead to significant particle losses (RF cavity switched on also during the extraction time). A technique that allows the extraction of a bunched beam is the RF Knock-Out (RFKO). After the RF cavity brings the beam to the required energy (acceleration step), it imposes a zero potential to the synchronous particle. Thus,

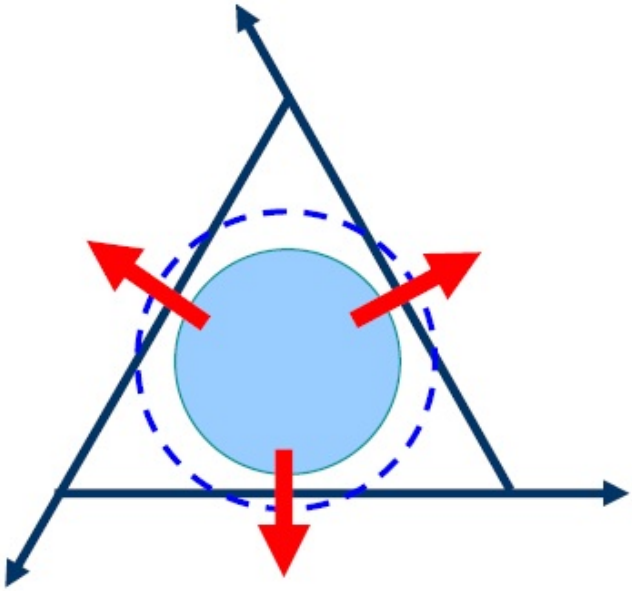

FIGURE 3.9. Schematic representation of RFKO beam extraction in the phase-space [20].

the beam turn in the accelerator with the desired energy and performs betatron oscillations on both the transverse planes and synchrotron oscillation in the longitudinal direction. In order to bring the beam close to a resonance the machine parameters are changed: x and y tunes assume different values in order to move the beam towards one of the third-order resonance line in the tune diagram; moreover x and y chromaticities are changed to avoid chromatic aberrations. With this new setup the extraction procedure can start. The RFKO extraction consists in perturbing the beam transversely with a noise whose frequency and amplitude evolve in time. The change of the frequency is needed in order to hit all the particles; thus a study of their betatron frequency is needed: frequency modulation (FM). The study of the noise amplitude induce changes in the time profile of the extracted particles: amplitude modulation (AM). It is fundamental to understand which type of noise performs the best action. From a theoretical point of view a white noise is the best type of solution that could be provided to the beam since it is characterized by the absence of periodicity in time. In practice it is no possible to generate a purely random noise over an infinite frequency range. So, a white noise cut on the desired frequency range could be used as well. At present, the configuration that has been chosen is a sweep in frequency. It is still far from being a random noise but it allows the particle extraction. The introduction of a noise, or a controlled perturbation, allows the diffusion of particles from the beam core to the stable triangle, as shown in Figure 3.9. The frequency sweep ensures to kick all the particles within the beam and thus start the diffusive process. The general effect of such an extraction is the progressively increase of the transverse beam emittance. Another strong difference with respect to other extraction techniques (apart from the bunched beam) is that the stable triangle is fixed in phase-space. In

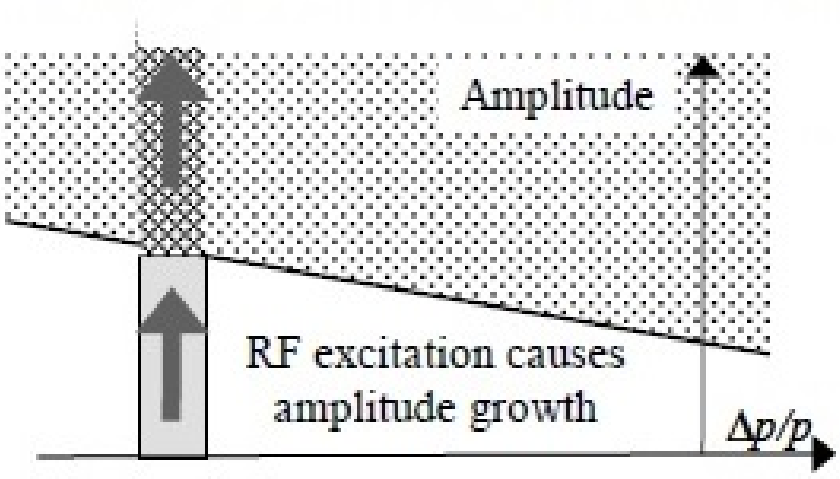

FIGURE 3.10. Beam evolution for a RFKO extraction in Steinbach diagram [22].

fact, it is the diffusion of particles towards the separatrix that enables their extraction; otherwise particle extraction occurs because the stable triangle progressively closes on the beam.

In Figure 3.10 the beam and the extracted particles are shown in the Steinbach diagram. The non-extracted beam as well as the extracted one have a constant momentum and a constant momentum spread. In order to have a small momentum spread of the spill the beam core has to have a small one too, unlike to what happens in a betatron extraction. It leads to adjust the voltage of the RF cavity that keeps the beam bunched in the longitudinal direction.

3.3.1 FM - mathematical description

As far as the study of the frequency range is concerned it is important to determine how to perform the frequency sweep as the beam turns in the accelerator. In particular the frequency of betatron oscillation is computed for the generic particle p that will be called $f_{RES,p}$, i.e. resonance frequency for the particle p, its expression is reported in Equation (3.41).

$$f_{RES,p} = f_p(n \pm q_p) \tag{3.41}$$

Where f_p is the revolution frequency and q_p is the decimal part of the particle tune. The first term can be written in terms of the revolution frequency of the synchronous particle using the definition of the slip factor, defined previously in Equation (2.48), as reported in Equation (3.42); while the latter quantity can be written in terms of the decimal part of the tune of the synchronous particle q_0, the chromaticity ξ and the relative momentum deviation with respect to the nominal value dp/p, as shown in Equation (4.43).

$$\frac{f_p - f_0}{f_0} = \eta \frac{dp}{p} \quad \rightarrow \quad f_p = f_0\left(\eta \frac{dp}{p} + 1\right) \tag{3.42}$$

(3.43) $$q_p = q_0 + \xi \frac{dp}{p}$$

By the substitution of Equation (3.42) and (3.43) into Equation (3.41), it is possible to obtain a mathematical expression for the resonance frequency of the particle p, in Equation (3.44). A simplification has been performed since the second power of dp/p is negligible with respect to the other terms.

(3.44) $$f_{RES,p} \approx f_0 \left[(n \pm q_0) + \frac{dp}{p} \left(\xi + \eta (n \pm q_0) \right) \right]$$

In order to define the frequency range for the sweep, i.e. frequency modulation, the maximum and minimum relative momentum deviation has to be evaluated. Its value depends on two contributions, which expression can be found in Equation (3.45). The first term is the average momentum of the beam and it is computed as the ratio between position and dispersion, as can be retrieved from Equation (2.44). In order to consider the real transverse position of the beam within the vacuum chamber, it is necessary to add the the magnets misalignment and beam bumps (both considered in the $x_{max.disp.}$ term) to the transverse position of the synchronous particle x_{closed} (i.e. the "theoretical" particle that should pass at the centre of the vacuum chamber all over the accelerator). Then, the momentum spread has to be added and subtracted to the average momentum of the beam in order to obtain the maximum and minimum value at the beam tail. The coefficient in front of the momentum spread term in Equation (3.45) is due to the fact that it is retrieved from experimental measurements that gave the maximum full width of the momentum beam distribution. From a practical point of view the measurement is performed by the passage of the RF bucket across the beam, thus a time distribution of the average beam momentum can be obtained.

(3.45) $$\frac{dp}{p} = < \frac{\Delta p}{p} > \pm \frac{1}{2} \frac{dp}{p}\Big|_{tot} = \frac{x_{closed} + x_{max.disp.}}{D_{max}} \pm \frac{1}{2} \frac{dp}{p}\Big|_{tot}$$

By the substitution of Equation (3.45) into Equation (3.4) it is possible to find the boundaries for the frequency range. The maximum and the minimum value is reported in Equation (3.46) and (3.47) respectively and their difference gives the frequency range for the sweep in frequency δf.

(3.46) $$f_{RES,max} \approx f_0 \left[(n \pm q_0) + \left(< \frac{\Delta p}{p} > + \frac{1}{2} \frac{dp}{p} \right) \left(\xi + \eta (n \pm q_0) \right) \right]$$

(3.47) $$f_{RES,min} \approx f_0 \left[(n \pm q_0) + \left(< \frac{\Delta p}{p} > - \frac{1}{2} \frac{dp}{p} \right) \left(\xi + \eta (n \pm q_0) \right) \right]$$

$$\delta f_{RES} = f_{RES,max} - f_{RES,min}$$

Physical quantity	Unit	Meaning
θ	μrad	kick given by the electric field
$\frac{\|V_x\|}{d}$	V/m	electric field imposed at the kicker plates
l_{eff}	m	effective length of the kicker
p	eV/c	momentum of the beam
β	-	relativistic Lorentz factor

Table 3.1: Units and meaning of the physical quantities involved in the evaluation of the kick

Physical quantity	Value
$\frac{\|V_x\|}{d}$	2676 V/m
l_{eff}	37 cm

Table 3.2: Units and meaning of the physical quantities involved in the evaluation of the kick

3.3.2 AM - mathematical description

The amplitude modulation is also required in order to have a constant profile of the extracted beam over the extraction time. From a practical point of view, particles move towards the separatrix if they receive a kick that changes their divergence. In this way, their orbit is perturbed and if the kick is randomly distributed between particles (thanks to the sweep in frequency) after some turns it will be possible to observe a diffusion of particles towards the outermost region of the stable triangle. From here the need to evaluate the kick intensity. By the imposition of an horizontal electric field in a specific longitudinal position, the extraction process can be initiated. The deflection due to an electric field is computed as [15]:

$$\theta_x = tan^{-1}\left(\frac{|V_x| \cdot l_{eff}}{d \cdot p \cdot \beta}\right) \tag{3.48}$$

The meaning and the units of the different quantities in Equation (3.48) are reported in Table 3.1. At CNAO the kicker has the characteristics defined in Table 3.2 .

CHAPTER 4

HARDWARE STUDIES

This chapter will deal with hardware studies. At first it will be presented the electronic instrumentation in detail. A schematic representation of the electronic line will be reported so that it will be possible to follow the path of the signal and how it is modified when it undergoes to the action of the considered component. Then, there will be the presentation of test bench measures and check in the field one. Different analysis have been performed, at first the optimization of the connections between components, i.e. where to locate them (either in the electronic room or in the synchrotron one), and then the assessment of impedance match. Under the same rationale, the Fourier analysis will be described; it has been performed to understand which the dominant harmonics are when the voltage of the inlet signal is changed. In these case too test bench and in field measures have been done. Later, softwares will be considered.

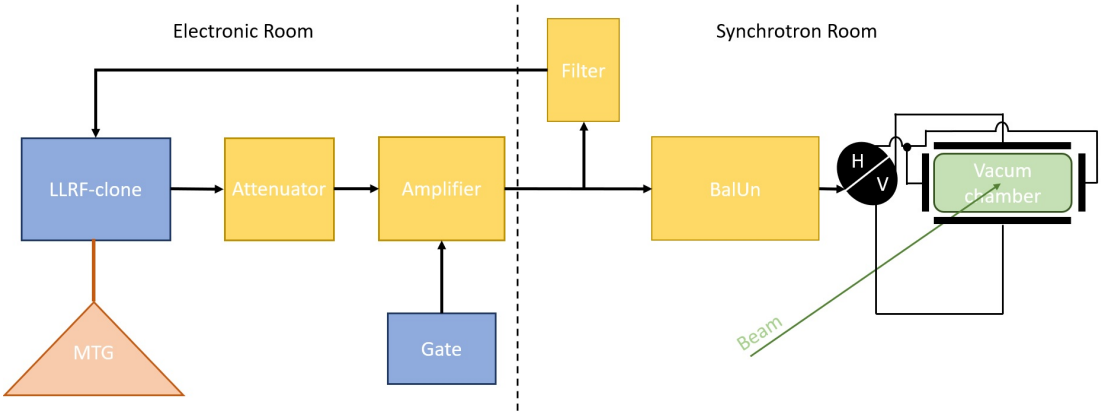

width=8cm

FIGURE 4.1. Schematic representation of the components needed to perform a RFKO extraction.

4.1 Introduction

In order to attain the beam extraction with the RFKO method, the amplitude of betatron oscillations has to be perturbed in order to make them move to the closest separatrix (as explained in detailed in the previous chapter). From a practical point of view, this action is performed by the sequence of components reported in Figure 4.1. The MTG generates the trigger event that enables the RF signal generation performed by the LLRF-clone. Thus, the signal undergoes to components that change its intensity. The attenuator performs a reduction in order to mach the signal with the amplifier requirements. Then the increase of the signal amplitude is performed in two steps: by the amplifier and by the BalUn. The quality of the signal can be checked after the first amplification by the filter and, if needed, the signal parameters can be adjust to accomplish the user requirements. Moreover, it is possible to generate the signal and not deliver it to the circulating beam, this action is performed by the gate that can enable (or not) the amplifier. It could be useful to work in this configuration when tests on the signal have to be performed.

4.2 Master Timing Generator (MTG)

The Master Timing Generator (MTG) is a device that generates and distributes, via optic fibre, the trigger events to all the elements in the accelerator in order to synchronize them. It can receive a signal from the API or the treatment code and, once it has been processed, the MTG generate a signal that contains all the fundamental information on the beam to be generated and delivered to the patient. Between all of them the most important are the beam energy and the type of particle (protons or carbon ions), additional information are the ramps of the magnets in order to achieve the required energy.

FIGURE 4.2. The LLRF-clone can be observed. In particular, the different connections are visible as well as the screen that shows the correct status of the component.

4.3 Low Level Radio Frequency (LLRF)

LLRF-clone is an acronym that stands for Low Level Radio Frequency and "clone" is added to distinguish it from the one daily used for clinical treatments. It has the same architecture of the one used for the RF cavity but it has been adapted for the RFKO extraction objectives. In Figure 4.2 it is possible to observe the LLRF-clone and from left to right the different connections:

- *GAP-IN* is the cable that comes back from the synchrotron room where there is a filter, as shown in Figure 4.1, that withdrawn part of the signal and send it to the LLRF to check that it corresponds to the user requirements;
- *POS1-IN* is used in the control of the RF cavity, in particular it is connected to a DCT, a transformer located in the synchrotron that allows the indirect computation of the number of particles in the beam by the measure of the electric current intensity generated by the passage of the beam through the transformer;
- *RF-0* is the outgoing cable brings the signal generated inside the LLRF to the attenuator, as reported in Figure 4.1;
- *RF-MON* is a possible outlet, the signal in this door is an exact copy of the one in the RF-0;
- *RF-180* is a possible outlet, the signal in this door is 180° phase shifted;

There is just one way in which it is possible to communicate with the LLRF: the ethernet connection (SLC door), that could also allows the connection with other systems on the internet. It

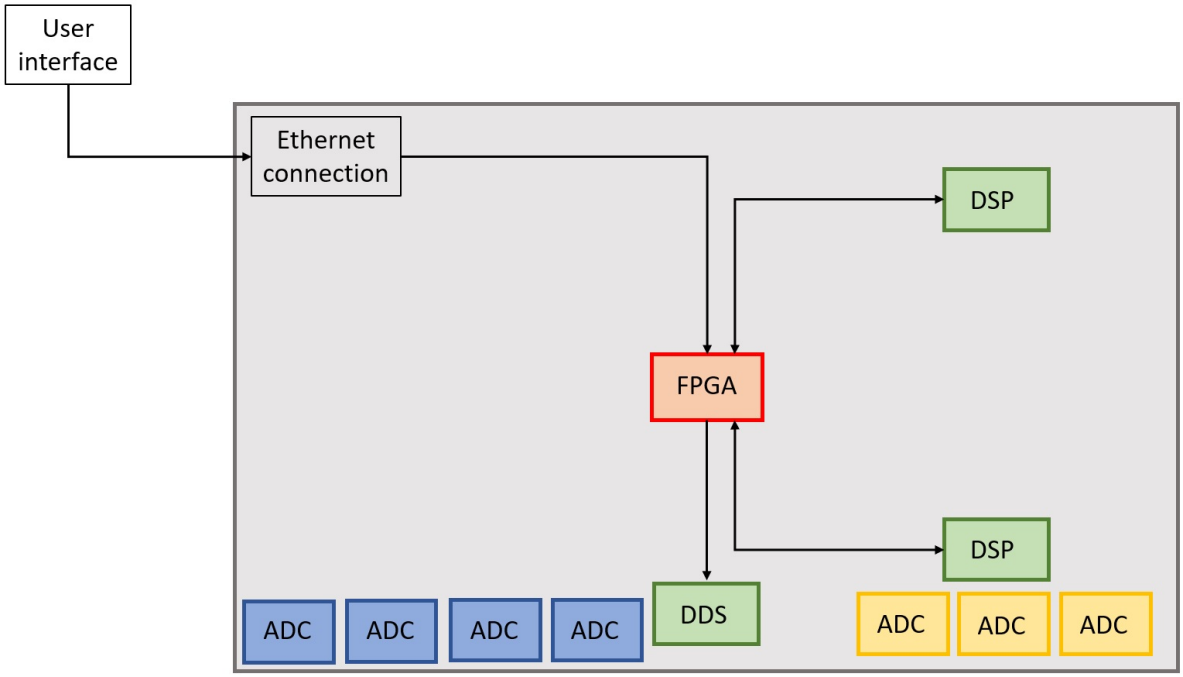

FIGURE 4.3. LLRF architecture

is used to communicate all the fundamental information from the user graphical interface to the FPGA. By the use of the interface is possible to type the user requirements for the beam. The architecture of the LLRF can be found in Figure 4.3. From the electronic point of view, the main component is the FPGA (Field Programmable Gate Array); through the ethernet processor it receives the parameters (defined by the user in the interface) needed to build the RF signal. Then it sends some of them to the Digital Signal Processor (DSP) that is able to perform complex algebraic operation; between all the outputs it gives the amplitude of the RF signal that has to be generated. The FPGA sends the frequency of the RF signal to the Direct Digital Synthesiser (DDS) that, once it receives the amplitude of the signal from the DSP, it generates the required RF signal that goes out from the component from the RF-0 door. There is no direct communication between the electronic boards, the exchange of information is performed by the FPGA. Other boards like the ADC, are used to control and adjust the signal itself. In this case these functions are performed in a closed voltage loop. Thanks to the filter that withdrawn part of the signal and send it to one of the ADC fast doors (“*GAP-IN*”), it is possible to check the peak-to-peak amplitude and adjust it according to user requirements. This control is performed by one of the DSP that makes a Proportional-Integral check, it communicates to the FPGA the how much the amplitude of the signal has to be modified and so the DDS provides the correct signal. In order to conclude this description, it could be of interest to highlight that the distinction between slow (blue components in Figure 4.3) and fast ADC (yellow ones in the same figure) is due to the

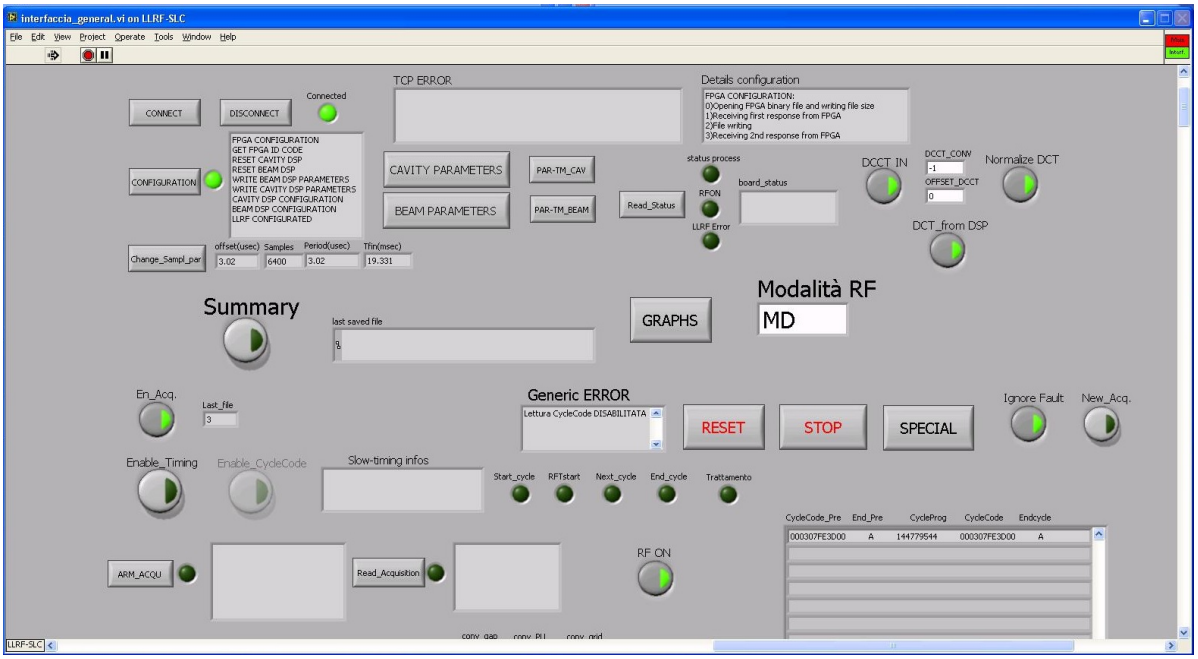

FIGURE 4.4. LLRF user interface.

maximum frequency at which they can work. Four of them are slow, i.e. they use signals up to some kHz frequencies, the others are said to be fast and the frequency limit is of some MHz.

The user interface is shown in Figure 4.4. On the top part it is possible to observe that the LLRF has been switched on correctly, in fact the green dot near "*connected*", the absence of errors and details of the FPGA configuration in the "*Details configuration*" ensures that the component is ready to work and has been correctly configured. The parameters can be changed going either in the "*Cavity parameter*" section (in Figure 4.5) or in the "*Beam parameter*" one (in Figure 4.6). In the cavity parameter section just few quantities can be changed.

- *voltageLoop (0; 1)*: as written in the identifying name, the magnitude can only take two values. In particular, 0 refers to the open loop work configuration in which the supplied voltage has a logarithmic trend with the value set by the user in Volt (pp) EmptyBuck. (This trend can be observed by looking at the data collected in the Excel file called $Data\_LLRF\_Vpp.xlsx$). The configuration in which the parameter assumes a unit value will be used after the end of the interface modification process. The aim is to put a limit on the RF voltage value that can be generated (this is achieved by imposing a limit on the Volt (pp) EmptyBuck parameter in order not to exceed 0.6Vpp, to make the amplifier work in conditions of safety and not in compression.

- *FreqRFKO*: this is the frequency at which the RF signal is generated. The tests were done

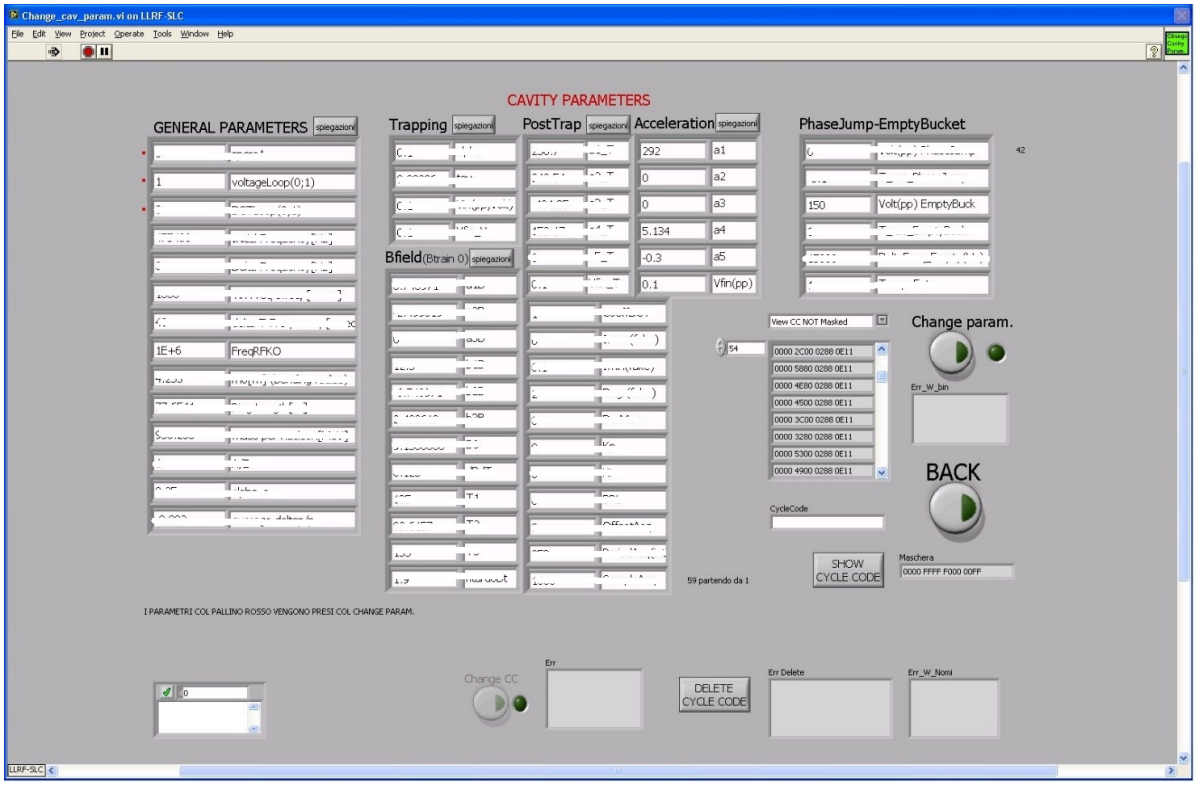

FIGURE 4.5. LLRF user interface - Cavity parameters. The obscured lines are not of interest for the purpouse of this work, that is the reason why just few lines can be read.

for the following frequencies: 0.5MHz, 1MHz, 2MHz, 3MHz, 4MHz, 5MHz, 6MHz.

- characteristic parameters of data acquisition as:
  - *OffsetAcq*: quantifies how much the offset should be;
  - *PeriodAcq (nt)*: length of the acquisition period in ns;
  - *SampleAcq*: number of samples to be acquired.
- characteristic column of the acceleration called *Acceleration*: five coefficients (a1, a2, a3, a4, a5) characteristic of the 4th degree polynomial to change the amplitude of the signal, to avoid that the amplitude changes in this way it is sufficient to impose 0.1 at the last cell , called Vfin (pp).

Also in the Beam Parameter section, only few parameters can be changed and they are:

- *ESB algorithm*: defines how the frequency must change during sweep. For each numerical value a different form is associated. In particular the user can choose between four different shapes:

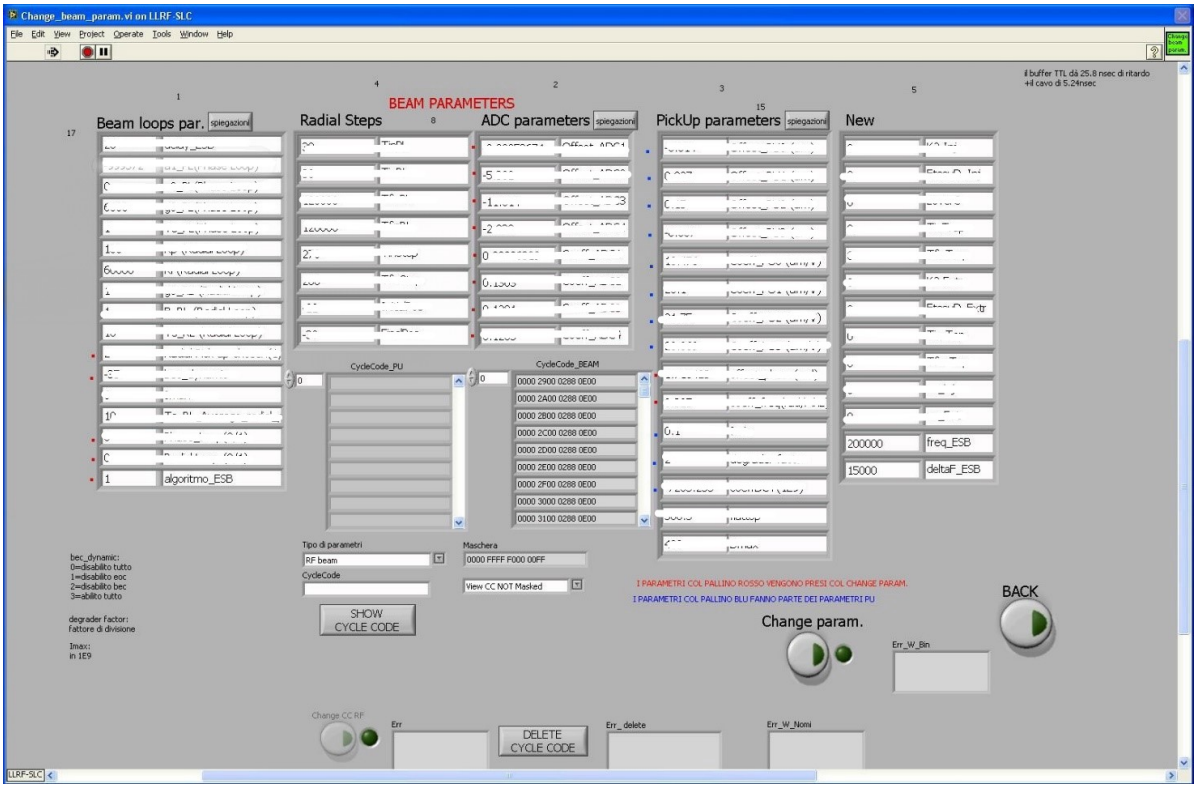

FIGURE 4.6. LLRF user interface - Beam parameters. The obscured lines are not of interest for the purpose of this work, that is the reason why just few lines can be read.

  - *1*: saw tooth;
  - *2*: the next value of frequency is randomly generated between in a range defined by $deltaF\_ESB$, defined here below;
  - *3*: saw tooth decreasing and vertically increasing;
  - *4*: saw tooth increasing and vertically decreasing. For the sake of completeness these frequency sweep are reported in Figure 4.6.

- $freq\_ESB$: is a numerical value that multiplied by 5e-6s quantifies how often the frequency of the signal has to be changed;
- $deltaF\_ESB$: defines instead how much the frequency should be changed;

During the first tests with the LLRF, a problem has been detected. The component is able to generate a RF signal up to $4MHz$. In order to overcome this limit it is necessary to modify its code, this action is planned to be performed in the next future.

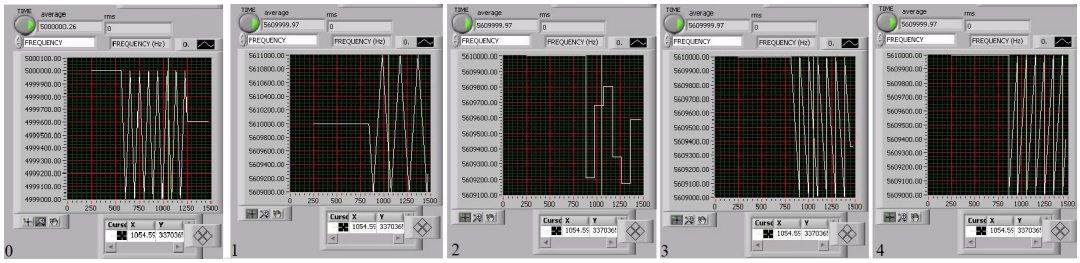

FIGURE 4.7. Sweep in frequency, possible shapes.

4.4 Electronic line

The electronic line is composed by several elements, it starts from the attenuator and it ends with the BalUn. In the following it will be presented the line itself with, where necessary, a brief description of the considered element. The different operational configuration tried will be shown too so that at the end it will be clear why just one of those has been chosen. Frequency calibration and response as well as Fourier analysis will be part of this section. The first component to be study is the BalUn for two main reasons, it is the most important and it has been designed for the exact purpose of this thesis.

BalUn is an acronym that stands for Balanced to Unbalanced line, and a schematic can be found in Figure 4.9. It can be considered as a particular type of transformer that makes floating the ground of the incoming line thanks to the fact that the signal propagates in the magnetic field generated by the passage of the signal itself in the twelve wires around the ferritic cores. This is an interesting application when the studied line has a slightly different ground level than the one of the other components, and it is subjected to an intense electric current or potential difference. In this condition a normal transformer could induce voltage loops between the two ground levels which strongly decrease its effect, i.e. the increase or reduction of the signal amplitude between its ends. In fact, at the beginning of the work the BalUn was not a component of the line, there was just a normal transformer; then the project of the BalUn has started due to the detection of voltage loops and to the extremely high feasibility of building “in loco” a balanced to unbalanced transformer. Dr. Mauro Paoluzzi from CERN provided a scheme of the BalUn knowing that it has to operate between 0.3MHz and 10MHz and that it has to increase by a factor of two the potential difference of the incoming signal. Requirements and characteristics of the line are reported in Table 4.1.

The amplifier is an instrument that can generate up to 500W power on a line with impedance equal to 50Ω, this is a fundamental requirement to make the component work properly. The other ways that could bring it to failure are due to an excessively high mismatch in the impedances of the lines or because the lines try to draw over current from the supply, in this latter case the amplifier try to protect itself by reducing voltage and current outputs. In Figure 4.5 a red light near “MISMATCH” will stand for the first type of fault; while a red light near “REF LIM” in

Electronic line	
Attenuator	-17dB
Impedance of the line outgoing the amplifier	50Ω
Maximum power generated by the amplifier	500W
Filter (or divider)	56 [-]
Capacity of the kicker	40pF
Frequency range	0.3-10 MHz

Table 4.1: Specifications of the electronic line

FIGURE 4.8. Real picture of the amplifier used, it is located in the electronic room.

case the second fault occurs. For further details look to the user manual [500W CW RF amplifier Model BT00500-ALPHAS _ CW].
The impedance of the kickers plates has been measured with a Network Analyser and its value can be found in Table 4.1. The frequency range has been determined in a preliminary study on the possible extraction frequencies with the RFKO technique: the lower value is slightly slower than the minimum frequency required to extract a proton beam at the minimum energy (30mm Bragg-peak position); while the upper limit has been arbitrarily chosen to allow the extraction of all the beams for every possible energy of interest, but usually it won't even exceed 8MHz. A resuming table with the BalUn characteristics, Table 4.2, and a real picture of the component, Figure 4.10, will follow.

In Figure 4.9 is reported a schematic of the electric circuit of the BalUn. Looking to the picture from left to right it is possible to follow the signal path. As all the RF signal it propagates in a co-axial cable, and once it enters in the metallic enclose it is split in two. In the upper line the metallic shield is at ground level and so the signal propagates just in the copper core, while in the lower line the opposite occurs. In fact, the copper core is at ground level while the signal propagates in the metallic shield (for graphical reasons the metallic shield and the plastic jacket are drawn as coincident). The ferritic ensures the generation of a magnetic field when the signal passes in the twelve wires wounded around the ferritic core. Then, in order to have a signal in the desired frequency range, a band-pass filter is added before the kicker's plates. The filter is

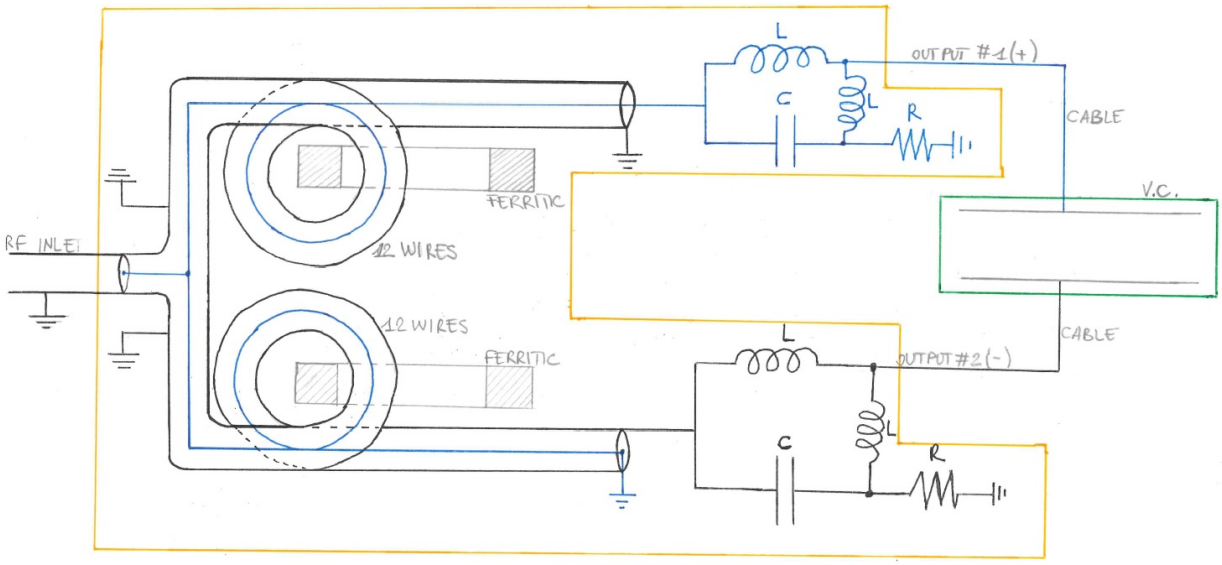

FIGURE 4.9. Electric circuit of the BalUn.

Component	Characteristic
RF inlet signal	-
Ferritic element	12 wires with 95Ω cable
L	0.6μH
C	30pF
R	100Ω
cable	40cm* 50Ω
Kicker plate	40pF

Table 4.2: Design parameters of the BalUn. * In the following pages it will be explained how the cable length has been chosen.

made by a combination of capacitors and inductors which values and electrical connections have been determined in order to have a RF signal in the frequency range defined in Table 4.1 and whose characteristics are reported in Table 4.2. At the end the signal sees a parallel between the resistance of the two lines that ensures a 50Ω impedance of the line and one of the kicker's plates. On one of the plates the signal arrives with a positive sign, i.e. with the same amplitude of the generated signal; on the other one it arrives with an opposite sign. So, the difference of the two leads to a signal which intensity is twice the original one.
In Figure 4.10 it is possible to see the Balun itself. On the top left of the figure, it is possible to observe the band-pass filter. In the same picture there is the view from the top of the metallic structure. It is a static heat sink, the black elements at the ends are two fans that make the air

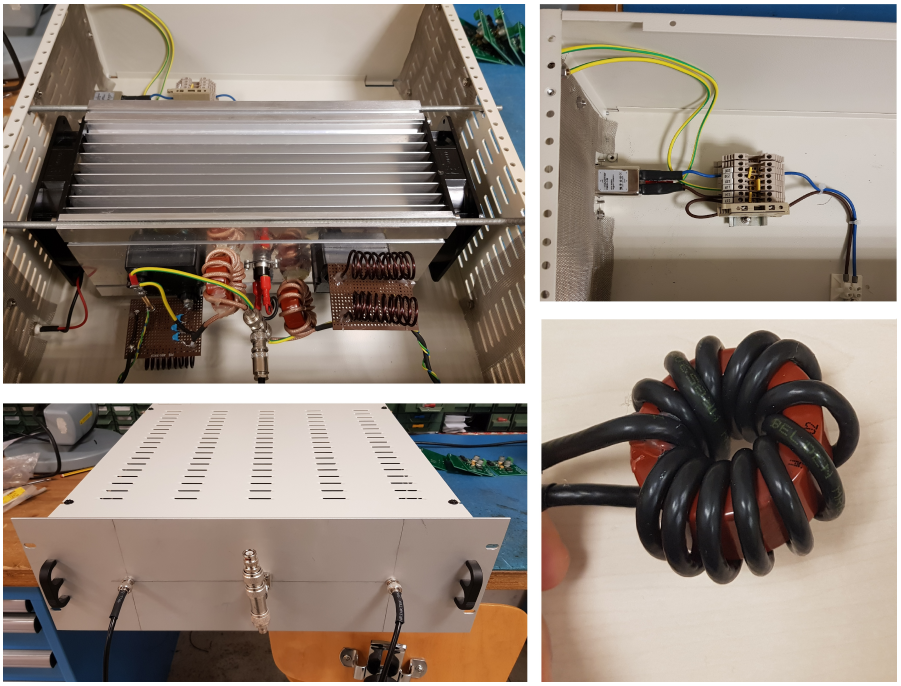

FIGURE 4.10. Picture of the different elements that compose the BalUn.

flow through the metallic structure in order to ensure heat removal. The rationale behind the choice of having two reduntant fans is due to ensure always a minimum heat removal. In addition, as a further emergency system there is a temperature probe (on the top right of Figure 4.10) that when the heat sink reaches the 100°C it removes the “enable” signal in the amplifier that then stops working. On the bottom right of Figure 4.10 it is possible to observe the toroidal ferritic element with the twelve wires, while on the bottom left the whole component is enclosed. On the front part there are tree connections, the central one is where the signal enters, in particular the "T" connection allows a double inlet or outlet of the signal. One of the two gate is used to withdrawn of part of the inlet signal that is sent back to electronic room in order to check that the signal perturbing the beam is matched with the user will. While the other one is where the cable coming from the electronic room brings the signal from the amplifier to the BalUn. Once the signal is split in two and its amplitude is increased (as explained before), it is sent on the two outgoing cables that then are directly connected to the kicker plates as shown in Figure 4.9.

From Figure 4.11 and 4.12 it is possible to see the location of the BalUn in the synchrotron and the cable connections that will be described in the next section.

4.5 Optimization of connections in the electronic line

One of the first measures performed was to check the good accordance between impedances of different components. Once the frequency range of interest was defined, the BalUn was the first

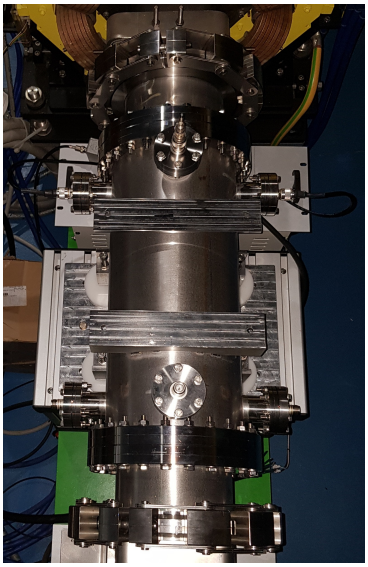

FIGURE 4.11. Picture of the BalUn in the synchrotron room. It is possible to observe the connection from the BalUn to the kicker's plates.

FIGURE 4.12. Picture of the BalUn in the synchrotron room. Observe the cable bringing the signal, the filter and one of the two connections to the kicker's plates.

Configuration	Length	Impedance
Long cable low impedance	92m	75Ω
Short cable low impedance	1.5m	75Ω
Long cable high impedance	92m	95Ω
Short cable high impedance	1.5m	95Ω

Table 4.3: Relative position between amplifier and BalUn

component to be studied. In particular the following parameters have been changed checking that the impedance at the end of the transmission line, i.e. inlet of the BalUn, was 50 Ω for the whole frequency range:

- length of the cable bringing the signal from the electronic room to the inlet of the BalUn;
- length of the cables connecting the output of the BalUn with the kicker's plates.

At the beginning different configurations have been studied at test bench and the capacity of the kicker plates has been simulated with two capacitors connected at the end of the cables (which length, as said before, was one of the parameters that could be changed).

4.5.1 Impedance BalUn cable

As a first case study, it has been chosen to study the impedance of the cable to be used to wrap the ferromagnetic elements of the BalUn and the length of the cable bringing the signal from the amplifier to the BalUn, i.e. where to locate the two components. The aim being to assess if there were differences between a short and a long cable (few meters versus 92 meters) and also if different impedances of the cable wrapped around the ferritic element (75 Ω or 95 Ω) could lead to significant modifications of the signal.

From Figure 4.13 it is possible to observe that the long cable connection is characterized by an oscillation behaviour. This peculiarity is further highlighted in Figure 4.14 where it is reported the Smith diagram, i.e. how impedance of the line (Balun + cable) changes as a function of the frequency range defined in Table 4.1. The reason why a long cable connection has this characteristic can be explained by the comparison of the cable length and the wavelength of the signal. In the frequency range of interest (0.3MHz – 10MHz) the wavelength of the signal changes from 600m to 30m; so, with a short cable connection the signal, considered as an electromagnetic wave, does not succeed in performing a full oscillation. The contrary occurs for a long cable connection because it is longer than the wavelength of the signal itself. So, looking at a given position in time, a conductor does not feature the same signal level at all its points. Nevertheless, the long cable connection has been preferred to the short one in order to have the amplifier and the BalUn located in the Electronic Room and the Synchrotron one respectively, in addition it also ensures an average impedance of 50 Ω. As far as the impedance of the cable wrapped around

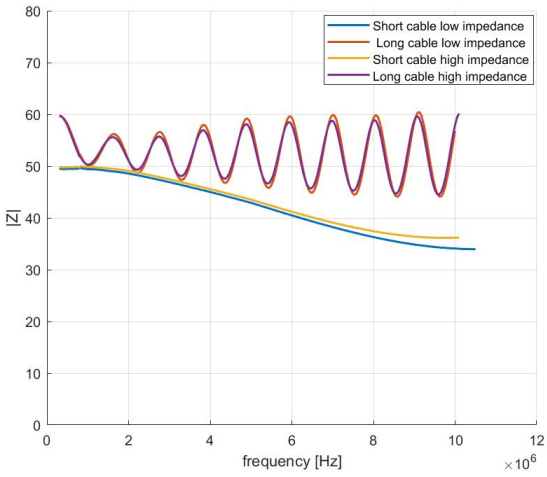

FIGURE 4.13. Output of the frequency response when a long/short cable is connected at the inlet of the BalUn. Used to simulate the relative positioning between amplifier and BalUn in the electronic and synchrotron room respectively.

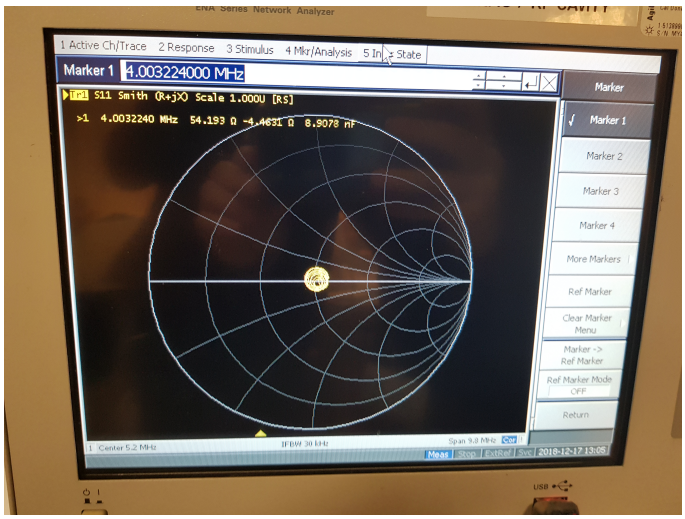

FIGURE 4.14. Picture of the Network Analyzer output for the third configuration described in Table 4.2

Configuration	Location N.A.	Location BalUn	Presence of Filter
N.A. in E.R. w/o Filter	Electronic Room	Synchrotron Room	No
N.A. in E.R. w. Filter	Electronic Room	Synchrotron Room	Yes
N.A. in Sync w/o Filter	Synchrotron Room	Synchrotron Room	No
N.A. in Sync w. Filter	Synchrotron Room	Synchrotron Room	Yes

Table 4.4: Possible configurations and tests to check if a filter used to withdrawn part of the signal changes the impedance of the system.

the ferritic elements are concerned, the 95 Ω cable was chosen to build the BalUn because it shows lower peak-to-peak impedance variations, as reported in Figure 4.13.

4.5.2 BalUn positioning

Then the BalUn has been brought in the Synchrotron and the long cable has been deployed between the Electronic room and the Synchrotron one. In this new configuration the ends of the BalUn have been connected to the kicker's plates but, as the previous case study. This setup doesn't affect the result of the measures since the signal is studied before it passes by the BalUn itself. Now the aim is to assess that the impedance of the line (BalUn + cable) has the same trend as the one determined in the test bench and, in addition, to check if the presence of a divider (i.e., the filter used to withdraw part of the signal) could induce changes in the impedance of the studied system. The set of measures consists in evaluating the impedance without divider by measuring with a Network Analyzer (N.A.) at the beginning of the chain (i.e. in the electronic room) and at the end of the same (i.e. in the synchrotron room). Then the filter has been added (as explained in the previous section) and the same set of measure has been performed again. These configurations have been resumed in Table 4.4.

From the analysis, which results are resumed in Figure 4.15, it is possible to observe two main features: when the measure is performed in the electronic room the oscillating trend is still present while it disappears when the Network Analyser is moved in the synchrotron room, due to the fact that in this last configuration the long cable is excluded from the analysis. Moreover, the presence of the filter improves the response of the system at high frequencies because it adds a small resistive charge parallel connected to the line. Thus, in the final configuration the filter will be part of the line since it does not affect the characteristic of the line itself. Furthermore, it will be used to have a close voltage loop control in the LLRF-clone to check (and eventualy modify) the voltage between the kicker's plates.

4.5.3 Length cables to the kicker

The last configuration that has been considered concerned the determination of the best configuration for the length of the cables connecting the exit of the BalUn to the kicker's plates. The two

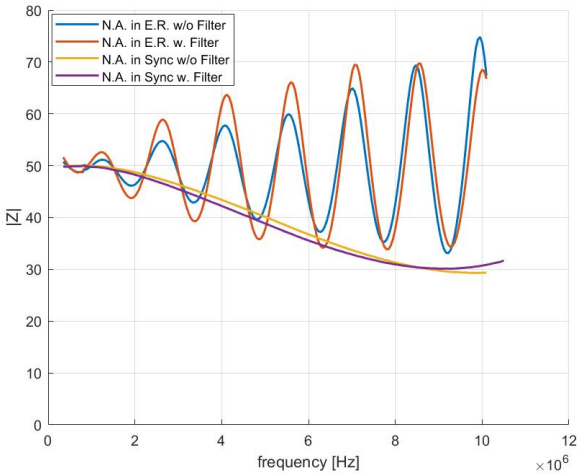

FIGURE 4.15. Output of the frequency response when a filter is added as a component of the line trough a T connection.

Configuration	Length	Presence of Filter
Long cable w. Filter	80cm	Yes
Short cable w/o Filter	40cm	No
Long cable w/o Filter	80cm	No
Short cable w. Filter	40cm	Yes

Table 4.5: Possible configurations to optimize the connection between the BalUn and the Kicker

possible setups are reported in Table 4.5.

From the MatLab output, reported in Figure 4.16, it is quite obvious that the configuration with short cables (40cm) is better than the one with longer one (80cm) and that the presence of the filter does not change the behaviour of the system, as was previously assessed too. This is a fundamental achievement since it allows to have a feedback of the signal injected in the system without perturbing the response of the system and the signal itself. From the Smith diagram reported in Figure 4.17, the impedance of the system as a function of the frequency can be observed. It is almost constant all over the frequency range and it is also confirmed by the diagram in Figure 4.16. So, at the end of this measure it was decided that the best way to connect the BalUn to the kicker was with short cables (40cm).

4.5.4 Final checks

The last check performed was to assess the impedance of the whole system: BalUn with 95 Ω impedance of the cables wrapped around the ferritic elements, long cable from output amplifier to inlet BalUn, “T” connection to allow a filter extract part of the incoming signal, short cable

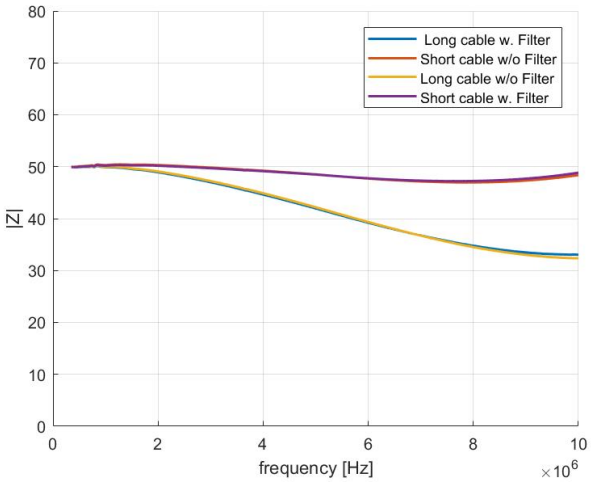

FIGURE 4.16. Output of the frequency response when the BalUn is connected to the kicker with cables of different lengths.

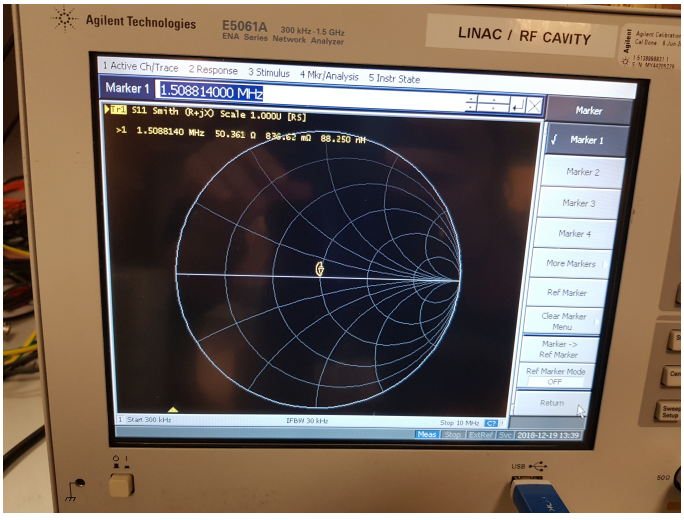

FIGURE 4.17. Picture of the Network Analyzer output for the fourth configuration described in Table 4.4

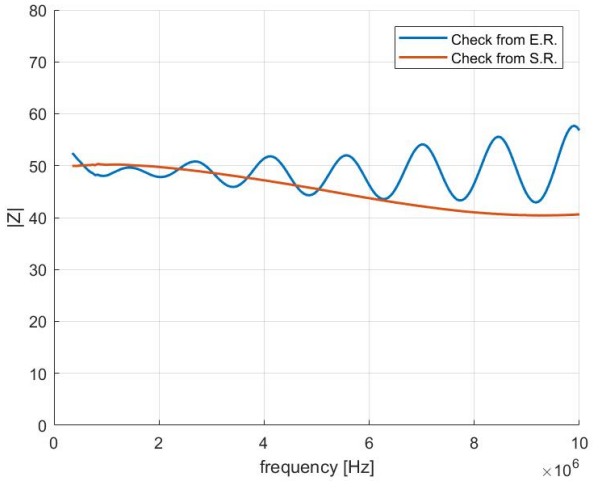

FIGURE 4.18. Final check of the system impedance. Measures performed at the beginning (from the Electronic room) and at the end of the line (in the Synchrotron room).

from output BalUn to kicker plates. The measures have been performed at the beginning of the line in the electronic room and in the synchrotron one, the results are reported in Figure 4.18. The oscillating behaviour due to the long cable connection is quite visible when the measure is performed from the electronic room (blue line), while it is absent when the same check is performed in the synchrotron. Moreover it is possible to see that changing the frequency of the signal the whole electronic line has an average impedance of 50Ω, as strongly request by the amplifier.

4.6 Fourier analysis of the electronic line

The Fourier analysis has been performed on part of the electronic line: from the attenuator till the inlet of the BalUn. This last component was substituted by a fictitious load resr of 50 Ω. Moreover, instead of connecting the LLRF-clone, a standard function generator was preferred due to the easiness in changing frequency and amplitude of the signal generated. Then, in order to assess the behaviour and the quality of the signal at the input and output of the components, different "T" connections where installed and the signal was sent to an oscilloscope where the amplitude was read. The test bench built for these measures is reported in Figure 4.20. From the right to the left there is the function generator, the oscilloscope, the amplifier and above it there are the attenuator near the right corner and the gate that has on its top the filter, behind the oscilloscope there is the 50Ω resistor. To have a better understanding of the signal path, a schematic representation is reported in figure 4.19. Four different signals have been obtained:

- Output of the function generator, amplitude and frequency of the signal generated in order

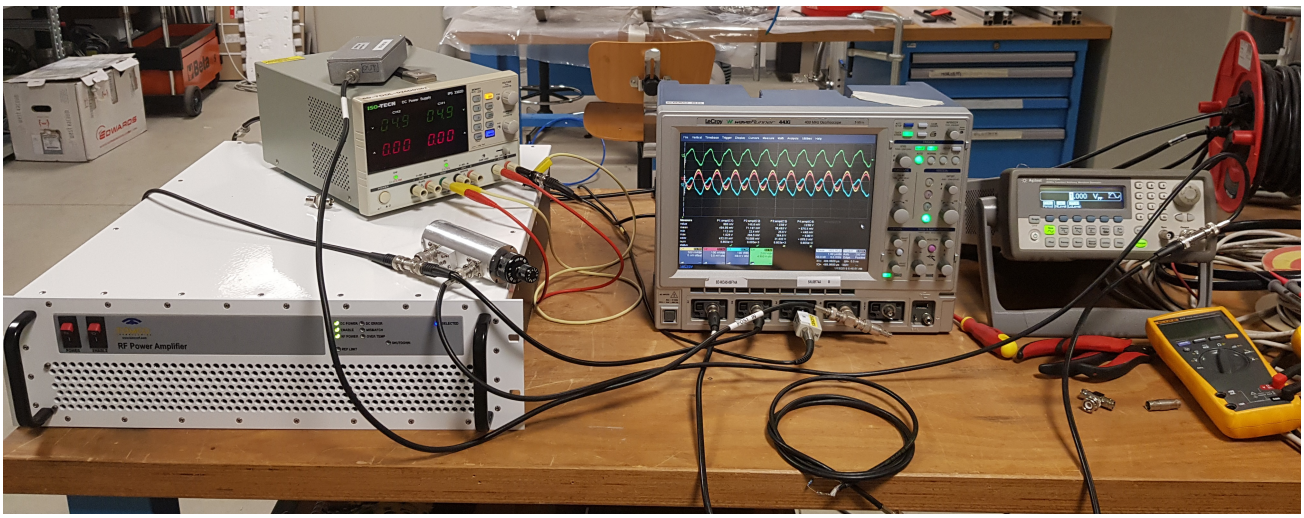

FIGURE 4.19. Picture of the test bench built for the Fourier analysis.

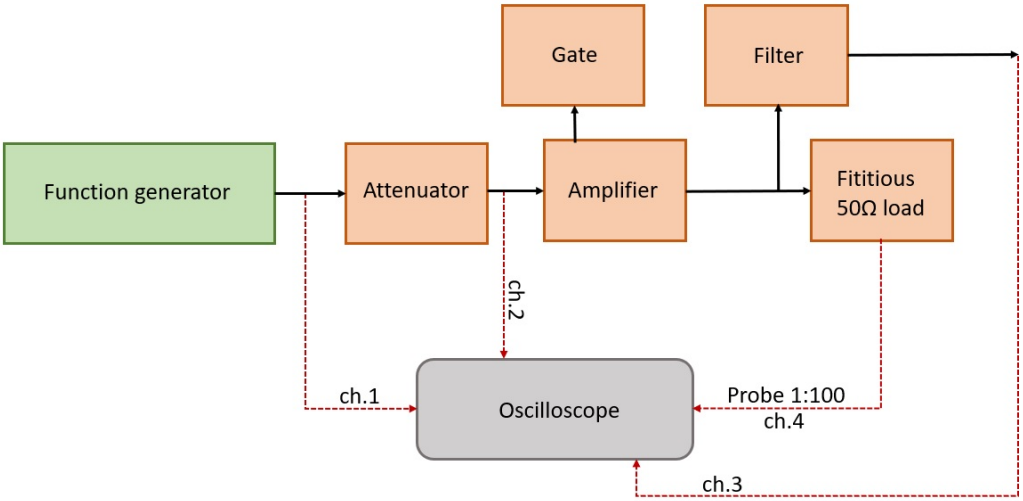

FIGURE 4.20. Schematic representation of the Fourier test bench.

Impedance	**0.3MHz - 10MHz**		**0.5MHz - 6MHz**	
	Measure from E.R.	Measure from S.R.	Measure from E.R.	Measure from S.R.
Min |Z|	42.9177	40.4164	44.3053	43.6931
Max |Z|	57.6904	50.3383	52.9964	50.3383

Table 4.6: Maximum, minimum and average impedance in the final configuration for the total and restricted range of frequency.

to check its accordance with user requirements

- Output of the attenuator;
- Intensity of the signal withdrawn by the filter or divider;
- Voltage on the fictitious load.

The objective was to check that the attenuation coefficient of the attenuator was the one required by the user, compute the gain and the power of the amplifier as a function of the frequency and compare the results with the specifications in the user manual, check the fraction of the signal taken by the filter and evaluate the voltage on the resistor.

The impedance of the line in the final configuration is reported in Figure 4.18, so the frequency range initially defined in Table 4.1 has been changed, i.e. reduced, from 0.5MHz up to 6MHz where the impedance of the system changes slightly, as reported in Table 4.6.

In the restricted range of frequency, the maximum and minimum impedance is closer to the required 50Ω than the one for the whole frequency range.

The frequencies chosen to perform the Fourier analysis were 0.5MHz and from 1MHz to 6MHz with a step of 1MHz. The values read on the oscilloscope have been written on an Excel file then used to perform the following calculations:

- Attenuation coefficient:

$$20Log\left(\frac{V_{out}}{V_{in}}\right) = 20Log\left(\frac{V_2}{V_1}\right) \tag{4.1}$$

- Filter withdrawn

$$\frac{V_{probe}}{V_{out,filter}} = \frac{V_4}{V_3} \tag{4.2}$$

- Gain of the amplifier:

$$20Log\left(\frac{V_{out}}{V_{in}}\right) = 20Log\left(\frac{V_3}{V_2}\right) \tag{4.3}$$

Frequency [MHz]	Average attenuation [dB]	Average gain amplifier [dB]	Filter [-]
0.5	-16.675	60.577	51.7
1	-16.606	59.990	51.9
2	-16.616	58.506	50.7
3	-16.681	57.462	49.6
4	-16.730	56.856	47.9
5	-16.231	57.705	49.1
6	-15.184	56.147	48.9
Average	-16.402	-	50.0

Table 4.7: Attenutator, amplifier and filter characteristics as a function of the signal frequency.

- Power of the signal leaving the amplifier:

$$P_{RMS} = \frac{1}{2}\frac{V_p^2}{R} = \frac{1}{2R}\left(\frac{V_{pp}}{2}\right)^2 \tag{4.4}$$

Having a closer look to the shape of the waveform in Figure 4.19, it is possible to notice that it does not look like a sinusoidal wave even if the one imposed by the generator is sinusoidal. This is due to imperfections of the amplifier that induces bigger distortions in the waveform as the frequency and the intensity of the incoming signal is increased. Moreover, when the Fourier transform of the signal is performed with the function already implemented on MatLab, then an additional multiplication factor must be added and Equation (4.4) becomes:

$$P_{RMS} = \frac{1}{2R}(2\overline{V}_{pp})^2 \tag{4.5}$$

This is due to the different way the Fast Fourier Transform is defined. On MatLab the algorithm implemented is:

$$X_k = \sum_{j=1}^{n} x_j e^{\frac{-i2\pi}{n}(j-1)(k-1)} \tag{4.6}$$

While the mathematical definition of the FTT is:

$$X_k = \sum_{n=0}^{N-1} x_n e^{-i2\pi\frac{kn}{N}} \tag{4.7}$$

For each frequency the voltage on the generated signal was varied four times in order to attain more data and so assess the previous characteristics with more confidence. The average gain of the amplifier and of the attenuator has been computed as the mathematical average of the values computed for each voltage so that it was possible to have an average value characteristic for a certain frequency. The results obtained from these calculations are reported in Table 4.7. As far as the amplifier is concerned, it is better to give a graphical representation of its behaviour

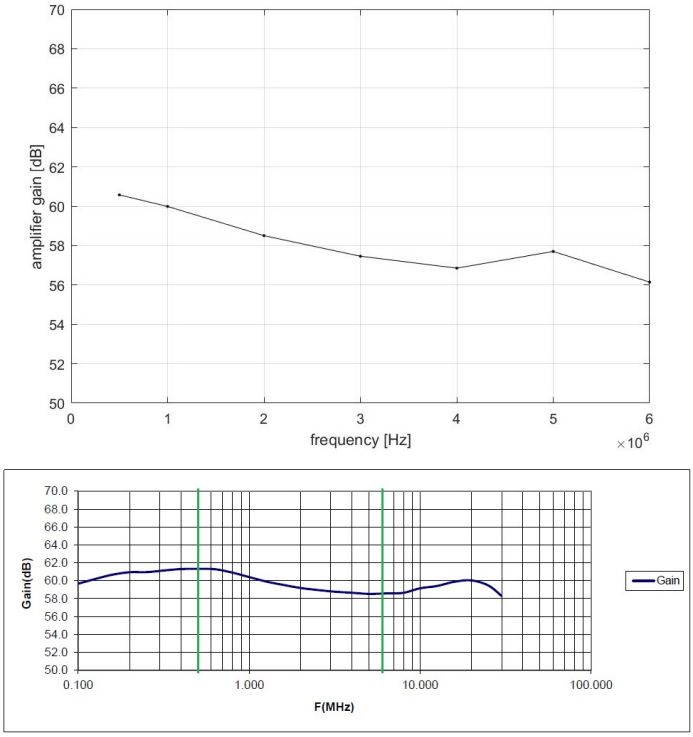

FIGURE 4.21. Comparison between the amplifier gain measured at the test bench (in the upper part) and the user manual, in which the frequency range of interest is highlighted.

Component	Test bench measure	Long cable connection
Filter	51.2	56

Table 4.8: Final filter characteristics.

rather than a simple numerical value, so that a comparison with the characteristics defined in the user manual could be performed. In the upper part of Figure 4.21 there is the gain of the amplifier measured at the test bench while in the bottom part there is the gain as a function of the frequency taken by the user manual. It is highlighted the frequency range of interest and it is possible to observe that the trend is almost the same while the numerical values are a bit different. There is a main reason that could explain this difference: the user manual does not refer exactly to the amplifier used and tested. On the 8th January 2019, the BalUn has been brought in the synchrotron and it has been connected to the kicker plates with the final configuration described in Table 4.5; while the filter was added on the 25th of January and its final characteristics are reported in Table 4.8. The one used and tested at the test bench was not the one brought in the Synchrotron since there was already one dedicated for the purpose of this work. It has been brought in the Synchrotron when the long cable has been deployed and then

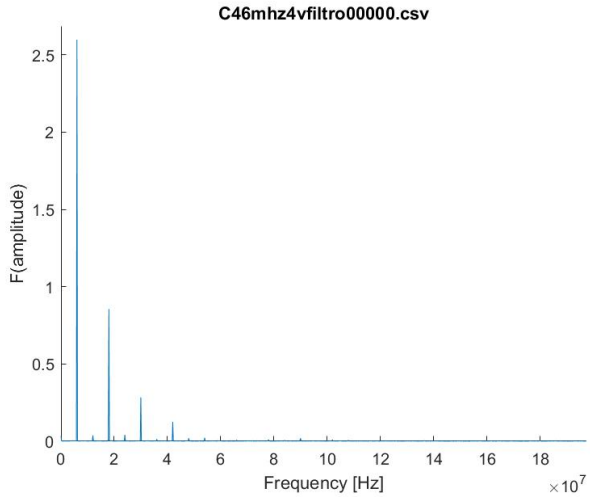

FIGURE 4.22. Example output file of the Fourier analysis performed with MatLab.

it has been left there, measures and tests have been performed with another similar filter, as can be seen comparing the Table 4.7 and 4.8. So, in Table 4.8 are reported the characteristics of the filter that will be used from now on to perform additional experimental measures. From the same table it is possible to observe that the test bench measures gave a certain value of the filter withdrawal capacity, the presence of the long cable connection (that brings the signal from the electronic room to the synchrotron one) modifies its behaviour due to the resistance added by the cable itself, for this reason it is this last value that must be considered in further analysis.
During the measures, for each frequency of the signal generated three waveforms have been acquired: one at the maximum voltage and the other two for two lower values. This allows to study which are the main harmonics at the maximum power and also if and how they change when the intensity of the signal is reduced. So, the Fourier analysis has been performed. A MatLab code has been developed and it takes the Excel file acquired from the oscilloscope, it does the Fourier transform of the signal (using the Fast Fourier algorithm implement in the environment) and for each measure, i.e. for each Excel file analysed, the code looks for the frequency at which the amplitude of the Fast Fourier transform is maximum, identifying in this way the nominal or fundamental frequency and then it also looks for the three successive values, identifying other three harmonics. So, at the end it is possible to check that the fundamental frequency of the signal is equal to the one imposed by the function generator and that the signal itself is not “pure” but it has some noise which can be characterized by the frequency and amplitude (referred as percentage with respect to the amplitude of the fundamental amplitude). In Figure 4.22 it is shown an example of the output obtained from the previous analysis. The title of the picture as to be interpreted as “Channel 4, 6MHz 4Vpp signal outgoing from the filter”. In order to have a better representation of the frequency that characterize the signal, only a part of the frequency range has been reported. In addition, the MatLab program writes (for each waveform analysed)

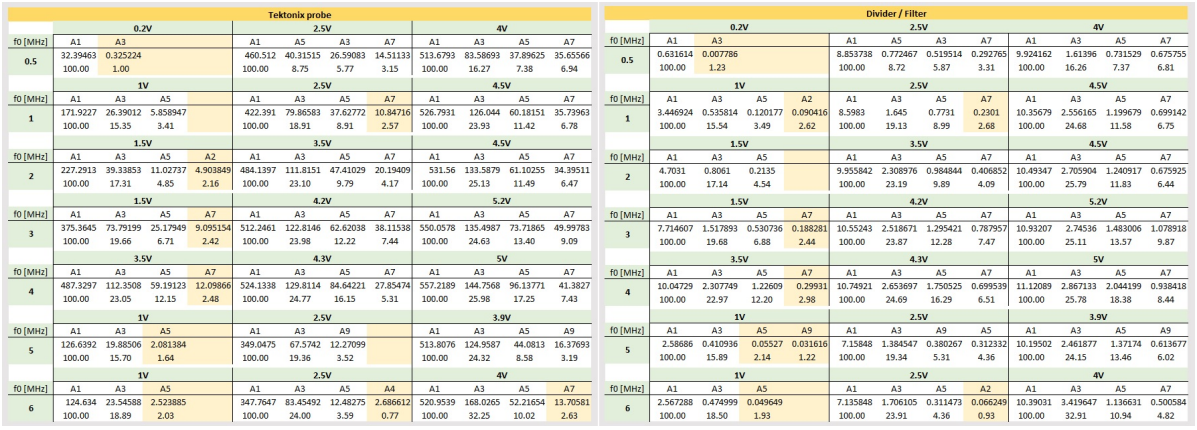

Tektonix probe

f0 [MHz]	0.2V				2.5V				4V			
	A1	A3			A1	A5	A3	A7	A1	A3	A5	A7
0.5	32.39463	0.325224			460.512	40.31515	26.59083	14.51133	513.6793	83.58693	37.89625	35.65566
	100.00	1.00			100.00	8.75	5.77	3.15	100.00	16.27	7.38	6.94
f0 [MHz]	1V				2.5V				4.5V			
	A1	A3	A5		A1	A3	A5	A7	A1	A3	A5	A7
1	171.9227	26.39012	5.858947		422.391	79.86583	37.62772	10.84716	526.7931	126.044	60.18151	35.73963
	100.00	15.35	3.41		100.00	18.91	8.91	2.57	100.00	23.93	11.42	6.78
f0 [MHz]	1.5V				3.5V				4.5V			
	A1	A3	A5	A2	A1	A3	A5	A7	A1	A3	A5	A7
2	227.2913	39.33853	11.02737	4.903849	484.1397	111.8151	47.41029	20.19409	531.56	133.5879	61.10255	34.39511
	100.00	17.31	4.85	2.16	100.00	23.10	9.79	4.17	100.00	25.13	11.49	6.47
f0 [MHz]	1.5V				4.2V				5.2V			
	A1	A3	A5	A7	A1	A3	A5	A7	A1	A3	A5	A7
3	375.3645	73.79199	25.17949	9.095154	512.2461	122.8146	62.62038	38.11538	550.0578	135.4987	73.71865	49.99783
	100.00	19.66	6.71	2.42	100.00	23.98	12.22	7.44	100.00	24.63	13.40	9.09
f0 [MHz]	3.5V				4.3V				5V			
	A1	A3	A5	A7	A1	A3	A5	A7	A1	A3	A5	A7
4	487.3297	112.3508	59.19123	12.09866	524.1338	129.8114	84.64221	27.85474	557.2189	144.7568	96.13771	41.3827
	100.00	23.05	12.15	2.48	100.00	24.77	16.15	5.31	100.00	25.98	17.25	7.43
f0 [MHz]	1V				2.5V				3.9V			
	A1	A3	A5		A1	A3	A9		A1	A3	A5	A9
5	126.6392	19.88506	2.081384		349.0475	67.5742	12.27099		513.8076	124.9587	44.0813	16.37693
	100.00	15.70	1.64		100.00	19.36	3.52		100.00	24.32	8.58	3.19
f0 [MHz]	1V				2.5V				4V			
	A1	A3	A5		A1	A3	A5	A4	A1	A3	A5	A7
6	124.634	23.54588	2.523885		347.7647	83.45492	12.48275	2.686612	520.9539	168.0265	52.21654	13.70581
	100.00	18.89	2.03		100.00	24.00	3.59	0.77	100.00	32.25	10.02	2.63

Divider / Filter

f0 [MHz]	0.2V				2.5V				4V			
	A1	A3			A1	A5	A3	A7	A1	A3	A5	A7
0.5	0.631614	0.007786			8.853738	0.772467	0.519514	0.292765	9.924162	1.61396	0.731529	0.675755
	100.00	1.23			100.00	8.72	5.87	3.31	100.00	16.26	7.37	6.81
f0 [MHz]	1V				2.5V				4.5V			
	A1	A3	A5	A2	A1	A3	A5	A7	A1	A3	A5	A7
1	3.446924	0.535814	0.120177	0.090416	8.5983	1.645	0.7731	0.2301	10.35679	2.556165	1.199679	0.699142
	100.00	15.54	3.49	2.62	100.00	19.13	8.99	2.68	100.00	24.68	11.58	6.75
f0 [MHz]	1.5V				3.5V				4.5V			
	A1	A3	A5		A1	A3	A5	A7	A1	A3	A5	A7
2	4.7031	0.8061	0.2135		9.955842	2.308976	0.984844	0.406852	10.49347	2.705904	1.240917	0.675925
	100.00	17.14	4.54		100.00	23.19	9.89	4.09	100.00	25.79	11.83	6.44
f0 [MHz]	1.5V				4.2V				5.2V			
	A1	A3	A5	A7	A1	A3	A5	A7	A1	A3	A5	A7
3	7.714607	1.517893	0.530736	0.188281	10.55243	2.518671	1.295421	0.787957	10.93207	2.74536	1.483006	1.078918
	100.00	19.68	6.88	2.44	100.00	23.87	12.28	7.47	100.00	25.11	13.57	9.87
f0 [MHz]	3.5V				4.3V				5V			
	A1	A3	A5	A7	A1	A3	A5	A7	A1	A3	A5	A7
4	10.04729	2.307749	1.22609	0.29931	10.74921	2.653697	1.750525	0.699539	11.12089	2.867133	2.044199	0.938418
	100.00	22.97	12.20	2.98	100.00	24.69	16.29	6.51	100.00	25.78	18.38	8.44
f0 [MHz]	1V				2.5V				3.9V			
	A1	A3	A5	A9	A1	A3	A9	A5	A1	A3	A5	A9
5	2.58686	0.410936	0.05527	0.031616	7.15848	1.384547	0.380267	0.312332	10.19502	2.461877	1.37174	0.613677
	100.00	15.89	2.14	1.22	100.00	19.34	5.31	4.36	100.00	24.15	13.46	6.02
f0 [MHz]	1V				2.5V				4V			
	A1	A3	A5		A1	A3	A5	A2	A1	A3	A5	A7
6	2.567288	0.474999	0.049649		7.135848	1.706105	0.311473	0.066249	10.39031	3.419647	1.136631	0.500584
	100.00	18.50	1.93		100.00	23.91	4.36	0.93	100.00	32.91	10.94	4.82

FIGURE 4.23. Fourier analysis of the signal waveforms on the fititious charge and outgoing from the filter (or divider). The light yellow of some cell represents those configurations where the percentage value of the harmonic was lower than the 3%.

the value of frequency and amplitude of the four highest harmonics in an Excel file. Then all the data have been collected and ordered. The final results are reported in Figure 4.23. It is possible to notice that if the value of the nominal frequency is fixed while the peak-to-peak amplitude is progressively increased, then the signal amplitude is strongly dominated by the fundamental one and the percentage of further harmonics progressively increase. In fact, at low signal amplitude most of further harmonics can be neglected either because their percentage value is lower than the 3% or because the harmonic is larger or equal to the ninth. At the maximum voltage it is extremely unusual to have a signal strongly dominated by the fundamental harmonic only, in fact the relative percentage of the third harmonic is always larger than the 15% and it arrives up to the 33%.

For the waveforms acquired at the maximum voltage a further study has been performed. It was interesting to study the evolution of the power, so its value has been computed for each one of the four harmonics and then the value of the last three has been compared to the one of the fundamental harmonics in order to quantify the relative contribution (expressed as a percentage) to the total power of the signal (computed as the sum of the power of all the considered harmonics). As usual the analysis has been performed for the signal outgoing the filter and for the one at the inlet of the fictitious load. The results are reported in Figure 4.24.

At the maximum amplitude the signal is dominated by even harmonics only. On the row of the table reported in Figure 4.24 there is the value of the frequency of the signal (dark green) expressed in MHz, the value of the peak-to-peak amplitude for each considered harmonic and the value of the power associated to each harmonic. In particular, the value of the power for all the harmonics (except the fundamental) is expressed as a percentage with respect to the fundamental one, while the amplitude is the real value of each harmonic, i.e. it is not a percentage of the

	Tektronix probe				Divider 1/50			
	Fundamental Frequency [MHz]	Third Harmonic [MHz]	Fifth Harmonic [MHz]	Seventh Harmonic [MHz]	Fundamental Frequency [MHz]	Third Harmonic [MHz]	Fifth Harmonic [MHz]	Seventh Harmonic [MHz]
	0.49998	1.49994	2.49999	3.49986	0.49998	1.49994	2.49999	3.49986
p.p Amplitude	513.68	16.27	7.38	6.94	9.92	16.26	7.37	6.81
Power	659.67	17.47	3.59	3.18	615.56	16.28	3.34	2.85
	0.99992	2.99976	4.99960	6.99944	0.99992	2.99976	4.99960	6.99944
p.p Amplitude	526.79	23.93	11.42	6.78	10.36	24.68	11.58	6.75
Power	693.78	39.72	9.05	3.19	670.39	40.84	89.95	3.05
	1.99984	5.99952	9.99920	13.99888	1.99984	5.99952	9.99920	13.99888
p.p Amplitude	531.56	25.13	11.49	6.47	10.49	25.79	11.83	10.28
Power	706.39	44.61	9.33	2.96	688.21	45.76	9.62	2.86
	2.99976	8.99928	14.99880	20.99832	3.00	9.00	15.00	21.00
p.p Amplitude	550.06	24.63	13.40	9.09	10.93	25.11	13.57	9.87
Power	756.41	45.90	13.59	6.25	746.94	47.11	13.75	7.28
	3.99968	11.99904	19.99840	27.99776	4.00	12.00	20.00	28.00
p.p Amplitude	557.22	25.98	17.25	7.43	11.12	25.78	18.38	8.44
Power	776.23	52.39	23.11	4.28	772.96	51.38	26.12	5.50
	4.99960	14.99880	24.99800	44.99640	5.00	15.00	25.00	45.00
p.p Amplitude	513.81	24.32	8.58	3.19	10.20	24.15	13.46	6.02
Power	660.00	39.04	4.86	0.67	649.61	37.88	11.76	2.35
	5.99952	17.99856	29.99760	41.99664	6.00	18.00	30.00	42.00
p.p Amplitude	520.95	32.25	10.02	2.63	10.39	32.91	10.94	4.82
Power	678.48	70.58	6.82	0.47	674.74	73.09	8.07	1.57

FIGURE 4.24. Signal power and amplitude for the first four harmonics at the maximum power

fundamental frequency amplitude. It is possible to notice that increasing the frequency the power of the harmonics increases, in particular for the third one. As far as the amplitudes are concerned, the main difference is in the magnitude of the signal going to the probe and the one withdrawn by the filter. Obviously the one of the filter is much smaller than the one of the probe since it withdrawn almost 1/50 of the incoming signal, and for both the measurements it is possible to observe a reduction in the amplitude as further harmonics are considered.

CHAPTER 5

SOFTWARE ANALYSIS

Before giving a detailed description of the rationale behind the codes studied and developed it could be useful a brief introduction on the different programming languages and software used. The main codes used for particle generation, tracking in the accelerator and between septa has been developed using:

- FORTRAN 77: FORTRAN codes have been developed for the generation of particles, for the ramp-up of the resonance sextupole and for the random kick generation. In particular, the last two codes have been written in MatLab because there was the need to change parameters in order to optimize the extraction of the particles;
- MAD-X (Methodical Accelerator Design): is a scripting language developed at CERN and used to describe accelerators, their optical functions, and to simulate and optimize beam optics and dynamics;
- MatLab is a numerical computing environment optimized for matrix and data manipulation, and for algorithms implementation.

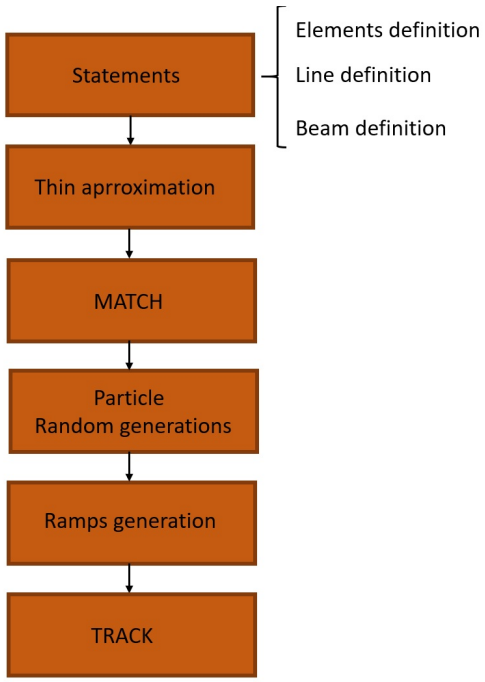

FIGURE 5.1. Rationale of the codes used for particle tracking

5.1 Codes description

Figure 5.1 there is a generic explanation of the main code procedure. It is written in MAD-X except for the particle random generation and ramps generations that has been written in FORTRAN 77 first and on MatLab later in order to study the effect of different kicker ramp-up on the spill. Figure 5.2 shows a more detailed explanation of the previous routine. The order in which different codes had to be run, the data saving in sub-directories, creation, copy and removal of files is managed by "*.bat*" files. Thus, just by running one of these .bat files the whole set of codes can be run, and the beam extraction can be simulated.

From the command prompt the code *supergo.bat* can be launched. It is the code where the user can define how many and which average beam momenta have to be simulated, then the code creates the sub-directories for each one of the momenta. Moreover, all the files needed for further simulations are copied in the sub-directories and an additional sub-directory for the output is created for each momentum too. At the end of this step the code runs the first MAD-X file: *extraction_makethin_v3.madx*. This is the main code in which CNAO synchrotron is defined as a "line" of elements which properties (e.g., physical dimensions of the magnets, quadrupoles and sextupoles strength, ...) are loaded and read from another file (that, eventually, can be modified by the user). Before any other operation is performed, the quadrupoles and sextupoles strengths are modified in order to accomplish the user requirements using the *match* command. It is important to do this step because the working point of the accelerator has to be moved from

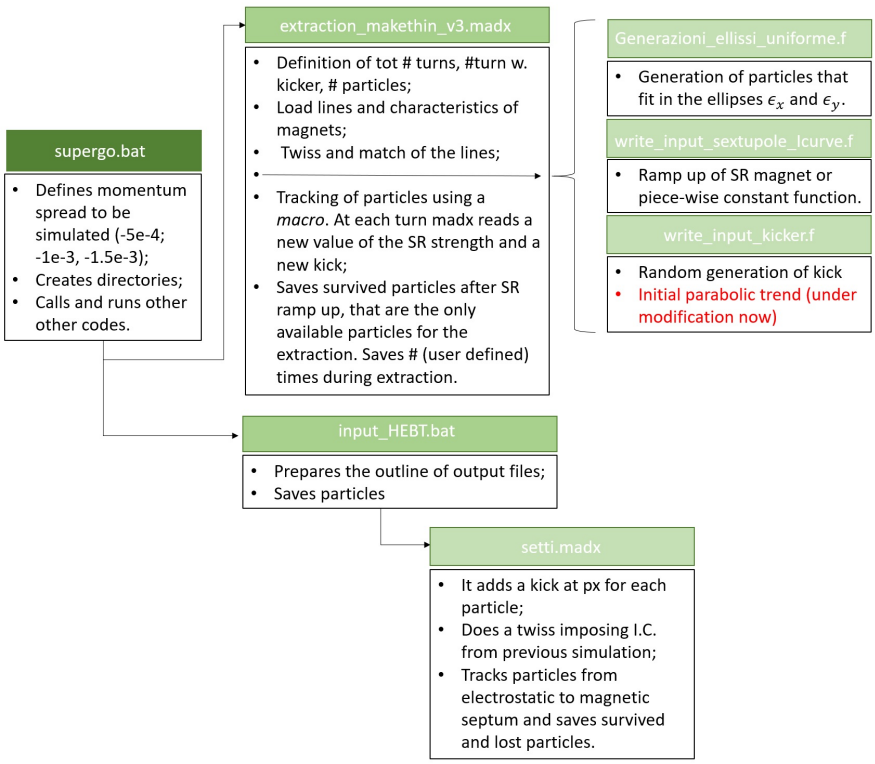

FIGURE 5.2. Detailed description of the codes used for particle tracking

the normal conditions, after the beam has been accelerated, to the extraction configuration, i.e. the shape of the beam in the phase-space is changed (according to the extraction technique that it is used) and the working point of the machine is brought closer to a resonance. Then, before tracking the particles it is necessary to transform the accelerator elements because the tracking module can work only on "thin" elements. So, the *makethin* command is executed and specific characteristics (i.e., the number and type of slices in which the component has to be cut) are defined for each class of elements (dipoles, quadrupoles). Thus, another match is done to check that nothing has changed. Now, it is possible to generate the particle distribution and to start their tracking in the machine. At this point different external codes are called, at first the one for the particle generation, then the one for the sextupole and kicker ramp-up. At present, only the code for particle generation has been left unchanged. The sextupoles and kicker ramp-up has been written on MatLab and, at present, the user has to copy the *.txt* output files in the subdirectories for the average beam momenta simulated. The main reason of this choice is that the modification of the kicker ramp is one of the key parameters to be used to improve particle extraction. Then MAD-X reads the *.txt* files and it memorizes the values in tables. So, it starts the tracking of particles, in particular at each turn it reads the value of the resonance sextupole strength and of the kick from the table and checks that all the particles are within the apertures otherwise it considers the particle as lost. Among all the turns simulated (1e6), some of them are

used for the ramp-up of the sextupole (6e3) that then is kept constant at the nominal value, all the others are used to simulate the extraction, i.e., the kick assumes a different value at each turn.

5.2 Post-processing code: outputs

In order to understand how a selected configuration leads to modifications in the number of extracted particles, different output files can be studied:

- Particles still available in the machine, the check is performed before the kicker is switched on and five times (the value can be changed by the user) during the kicker operations (so it is expected to observe a reduction in the number of particles available for the extraction);
- Particles lost during the sextupole ramp-up: some particles already close to the resonance are immediately lost as the SR is switched on, so they are removed before further analysis are removed;
- Particles available after sextupole ramp-up (i.e., ready to undergo to RFKO extraction);
- Particle lost during the kicker ramp-up (i.e., considered as extracted). As indirect measure, those not extracted could be (theoretically) extracted if the number of turns is further increased. This is why the percentage of extracted particles will be considered in the study of the quality of a simulation rather than the real number that is meaningless.

To all the particles is associated the longitudinal position at which they are lost, their momenta and transverse position.So, the particles lost during the kicker operations are then the input particles for the track module between the electrostatic and magnetic septa. To all the particles is added the kick of the electrostatic septum making them have a larger x-momentum and then the magnetic septum allows a physical separation between the remaining circulating beam and the one that is extracted. Also in this case, particles that are lost in the line can be saved on a file, otherwise all the extracted particles with their momenta and position are saved on another file.

On the basis of the code described above a MatLab code for the post processing of the results has been developed and it is possible to find it in **Appendix B**. Its aim is to give a graphical representation of the results obtained from the MAD-X simulations. The interesting outcomes are:

- x-x' phase-space representation of the particles still not extracted, in particular the picture is saved as a *.gif* so that the turn evolution can be observed;
- histogram of the particles lost during the extraction in order to see if there are unexpected longitudinal positions where losses occur, apart from the electrostatic septum and how many particles are lost (not reported in Figure 5.3);

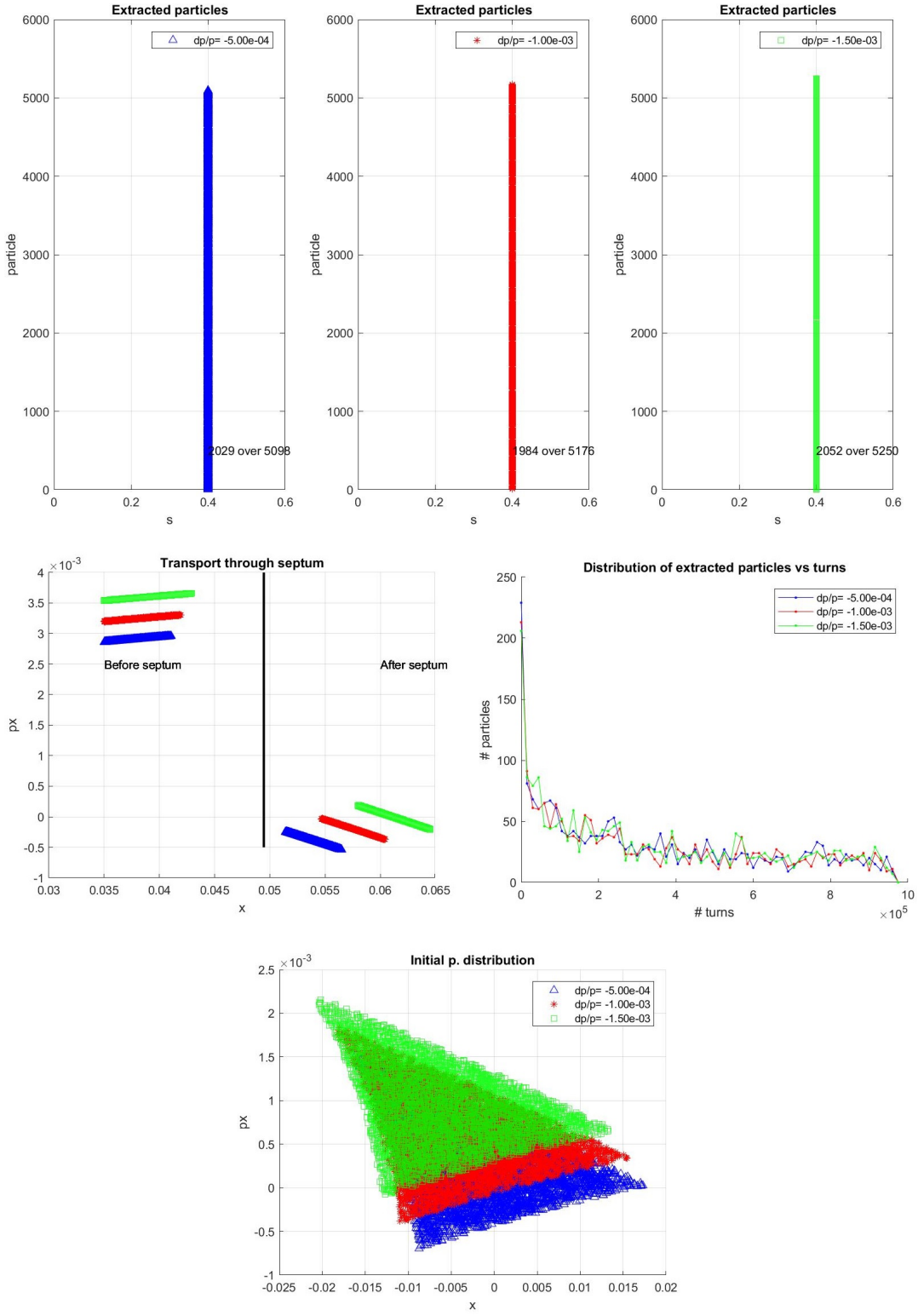

FIGURE 5.3. Example of the possible results from the post-processing code

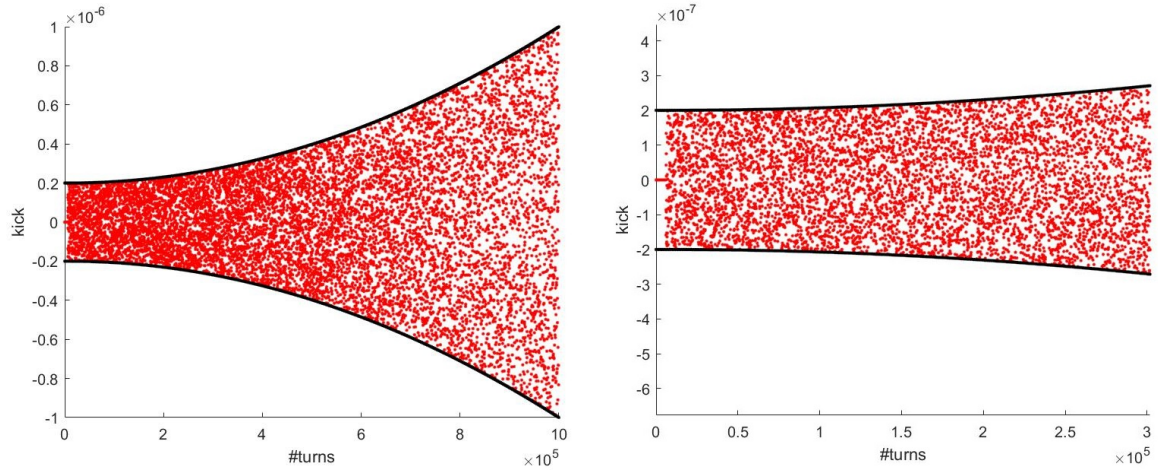

FIGURE 5.4. Example of parabolic ramp for the kicker

- transport between septa: particles that have reached the electrostatic septum are represented in x-x' phase-space just before they receive the kick from the septum itself and the same particles are reported after the magnetic septum has transformed their divergence in a physical separation from the circulating beam;
- the evolution of the spill as a function of the number of turns;
- the shape of the beam in the x-x' phase-space once the resonant sextupole has been switched on and it has reached the nominal strength.

In Figure 5.3 there are the graphical results of the post-processing code. The figures have to be considered as an example to understand which kind of outputs can be obtained from the code, an additional possible outcome is the histogram of the particle losses during the sextupole ramp.

5.3 Kicker ramp-up code

As far as the kicker ramp-up is concerned another Matlab code has been developed and it can be found in **Appendix C**. In Figure 5.4 it is possible to observe an example of the parabolic ramp-up provided by the code. Moreover, a zoom on the first turns has been performed in order to highlight that at the beginning of the track the kicker is switch off in order to allow the SR ramp.

The code has been developed in order to allow the used to choose the type of ramp. At present, there are just three possible functions:

- Constant: the random generation is performed between ± constant value;
- Parabolic: the random generation is performed within a symmetric parabolic shape which initial and final value can be chosen by the user (as shown in Figure 5.4);

- Exponential: it is analogous to the parabolic ramp, but there is the exponential function instead of a second order polynomial.

An index is associated to each type of function, so by the definition of its value it is possible to obtain the required trend. Thus, the user defined the initial and final value and then the coefficients associated at each function are computed. Since it is necessary to generate a number of kicks equal to the number of turns the beam performes in the machine, the value can be either defined by the user or can be automatically read from the *.madx* code. According to the description performed before, the first $6e3$ turns are performed with the kicker switched off, so the random generation starts just after that number is overcome. Thus, the exponential function and the parabola assume the minimum required value at $6e3 + 1$ in order to start the kick generation between the values defined by the user. Even if the number of turns with the kicker switched off is changed, the kicker code adapts in order to move the minimum of the function where the kicker is turned on. Moreover, at the end of the random generation two *.txt* files are generated: in the first one there is the kick for the first $6e3$ turns, while in the other there are the kicks for the remaining turns. By their substitution in the proper folder it is possible to run the next simulation with the new kicker ramp-up.

CHAPTER 6

RESULTS

The results of the numerical simulation will be presented. As described in Chapter 5, each simulation studies three different beam momentum offsets with respect to the resonance ($dp/p = -0.0005; -0.0010; -0.0015$) so there will be three lines in the diagrams that will be described, one for each dp/p. At first the present configuration (betatron extraction) and the starting point will be described. Thus the interesting features of the results will be highlighted in order to understand which characteristics can be optimized, which one have to be avoided or just modified. The optimization procedure has been performed on both the machine parameters (tune and chromaticity) and the kicker. The reason for this choice is due to the fact that those physical quantities affect the quality and quantity of the extracted beam. The different configurations will be explained and it will be shown why some setups have been abandoned and why others have been further analysed. After the definition of the "best" kicker ramp-up, a sensitivity analysis on the machine parameters has been carried on; as well as a study on additional beam momentum offsets. At the end it will be given a description of the parameters to be computed before the planning of experimental measurements. Moreover, an Excel file developed for the aim of this work will be presented: it gives to the user a tool to retrieve data for FM and AM modulation.

6.1 Present configuration and starting point

At present CNAO performs the beam extraction with a betatron, as described in Chapter 3. From experimental measurements the machine parameters that allow such an extraction are reported in Table 6.1. Calling back the tune diagram in Figure 3.1, it could be intuitive why a change of tune has to be performed (the beam has to be brought close to a third-order resonance) while a change of chromaticity could be less intuitive. Equation (6.1) recalls the definition of the chromaticity and shows another way to define the same quantity:

$$\xi = \frac{\delta Q/Q}{\delta p/p} \qquad\qquad Q' = \frac{\delta Q}{\delta p/p} \tag{6.1}$$

Changing its value would mean changing the momentum spread of the beam, if the tune distance from resonance is kept constant; or viceversa. Moreover, as Equation (3.39) and (3.40) shows, the shape of the Steinbach diagram (amplitude vs. dp/p) would change up to the limit of an horizontal line, i.e. constant amplitude of extraction, if the chromaticity approaches to zero. Thus, a change in chromaticity has to be carefully handled. The starting point for the optimization of the RFKO

Machine parameter	**Value**
Q'_x	-4.1
Q'_y	0.05
Q_x	1.669
Q_y	1.785

Table 6.1: Chromaticity and tune for a betatron extraction

extraction has been fixed to the results obtained by previous beam simulation studies performed by Dr. Marco Pullia and Simone Savazzi. The results of those simulations can be resumed looking at the machine parameters (tune and chromaticity) reported in Table 6.2.

Machine parameter	**Value**
Q'_x	-0.2
Q'_y	-1
Q_x	1.672
Q_y	1.74

Table 6.2: Chromaticity and tune at the starting point of RFKO extraction

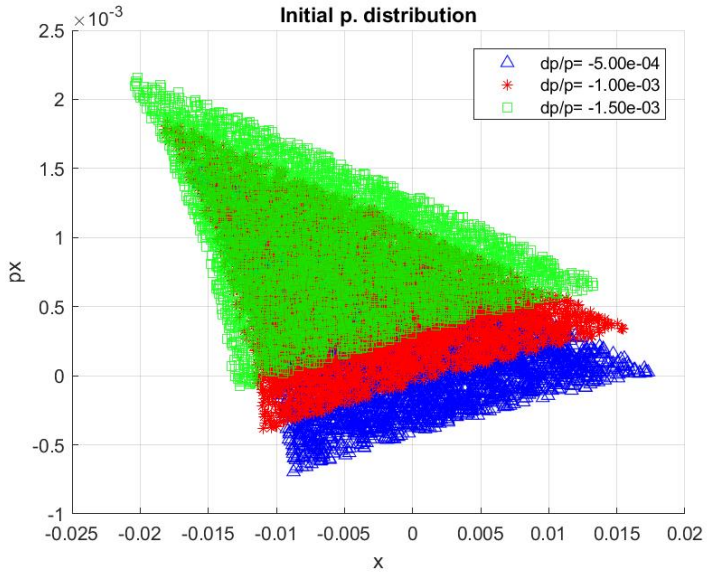

FIGURE 6.1. Phase-space representation for a constant kick

6.2 Kick studies

All the studies on the possible random kick generation will be performed with the machine parameters defined in Table 6.2.

6.2.1 Constant kick

Extraction studies start after the ramp of the resonant sextupoles. Therefore, the phase-space distribution of the beam is not anymore circular (or ellipse shaped) but triangular, as reported in Figure 6.1. Being the sextupole ramp always the same there is no difference in the shape and/or dimensions of the triangles. The only difference will be due to how (and how fast) particles are extracted from the stable area. At the beginning, a random generation between a positive and negative constant kick has been chosen due to its simplicity. In this way it has been possible to check the basic characteristics of the extracted beam. The maximum and minimum kicks have the same value but opposite sign, in Figure 6.2 it is possible to observe two configurations. On the left hand side of the picture it is possible to see a random generation of the kick between $\pm 0.5 \mu rad$ while on the right hand side the limit has been doubled. In both cases not all the kicks have been shown otherwise it would have not be possible to distinguish one point from the other in the diagram; thus in the figure there is just one kick every 200 generated. Furthermore, it is not possible to see that the first 6000 turns are performed without the kicker in order to allow the ramp-up of the resonant sextupole. So, in Figure 6.3 is reported a zoom on the first 10000 turns. The first feature to be analysed concerns the spill. At first there is the need to check if the extraction is achieved and then the time (or turn) profile of the extracted particles. Thus

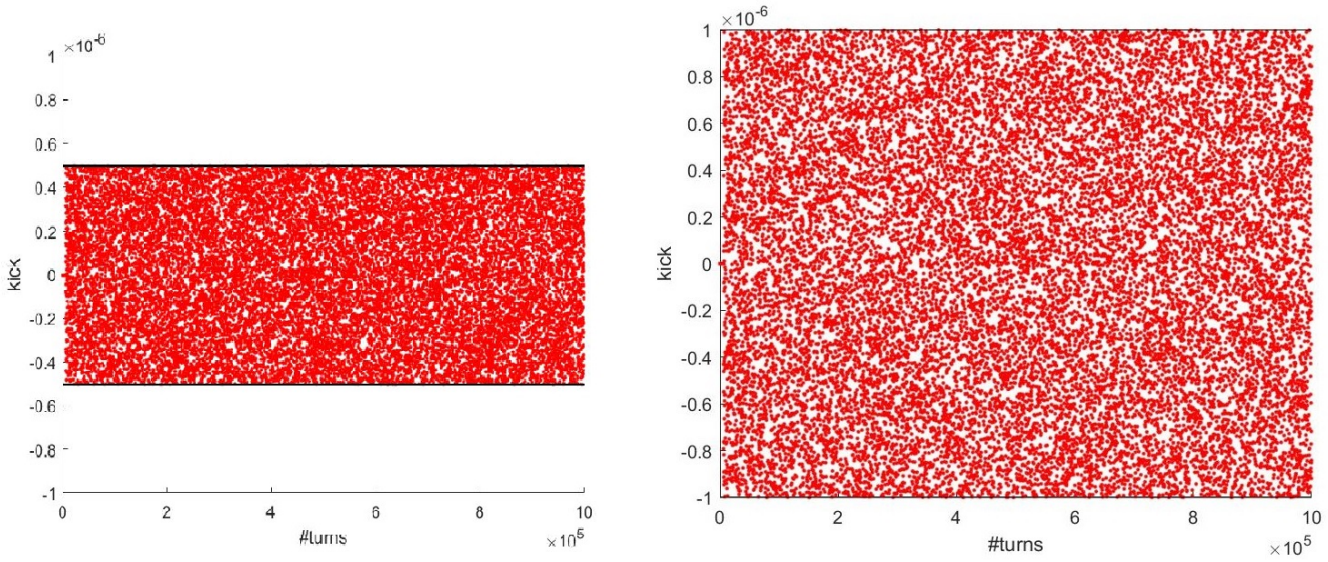

FIGURE 6.2. Kick random generation between $\pm 0.5\mu$rad (on the left side) and $\pm 1\mu$rad kick (on the right one)

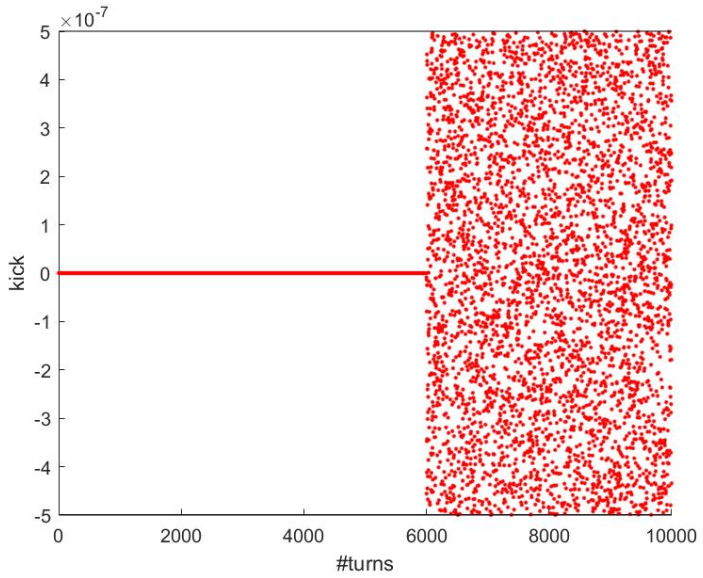

FIGURE 6.3. Zoom on the first 10000 turns for the random generation of the kick

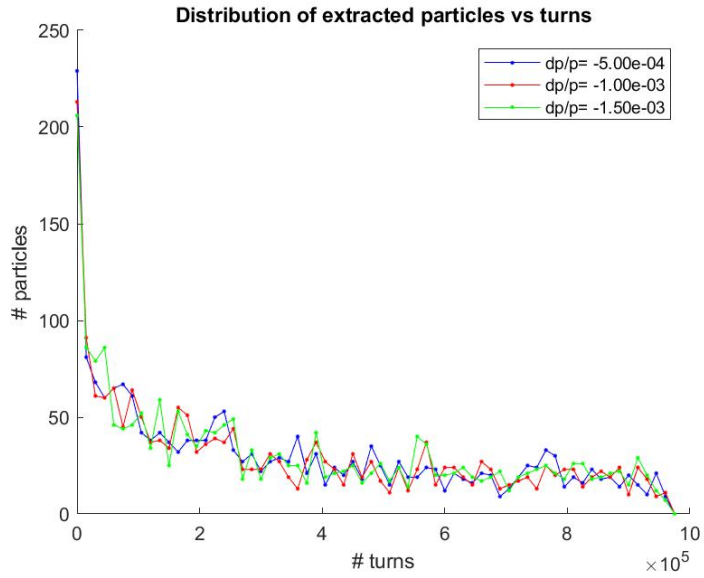

FIGURE 6.4. Spill profile for $\pm 0.5 \mu rad$ kick random generation

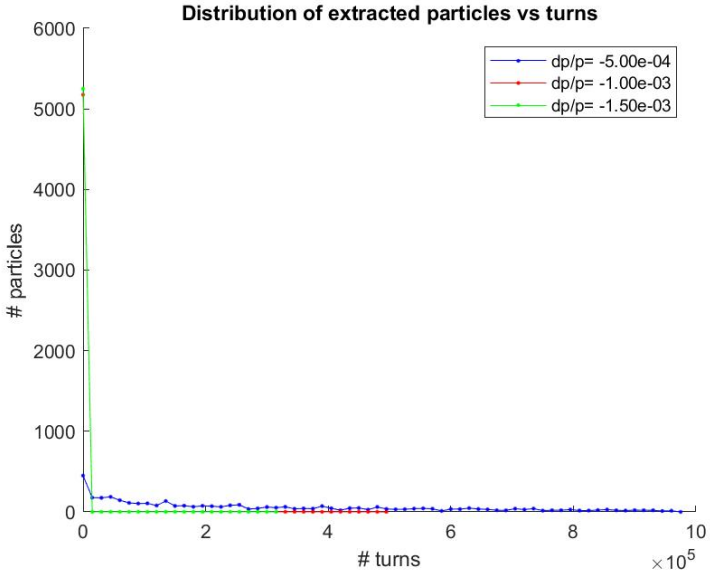

FIGURE 6.5. Spill profile for $\pm 1 \mu rad$ kick random generation

Figure 6.4 shows the turn spill profile for a random generation between $\pm 0.5 \mu rad$ while Figure 6.5 shows the same profile in the case of $\pm 1 \mu rad$. From the comparison of the two figures it is possible to notice that a $\pm 0.5 \mu rad$ allows the beam extraction while the other one seems to not achieve it. Moreover, the profile of the spill is exponentially decreasing. Table 6.3 collect the percentage of the extracted particles over $1e6$ turn in the accelerator, thus if this number is

increased it is expected to obtain more extracted particles. The configuration with $\pm 1 \mu rad$ seems

	dp/p	**% extracted**
$\pm 0.5 \mu rad$	-0.0005	39.8%
	-0.0010	28.3%
	-0.0015	39.1%
$\pm 1 \mu rad$	-0.0005	71.2%
	-0.0010	55.4%
	-0.0015	45.1%

Table 6.3: Percentage of extracted particles over $1e6$ turns for a constant kick

to ensure an higher percentage of extracted particles but it is also in contrast with the spill profile (Figure 6.5). The reason of this discrepancy is due to the characteristics (spiral step and spiral kick) with which particle arrive to the electrostatic septum. Thus, they aren't really extracted but just lost due to collisions with the septum itself. Moreover, this configuration induces lost of particles all over the accelerator length. The combination of these features doesn't allow the beam extraction with the machine parameters defined in Table 6.2.

As far as the $\pm 0.5 \mu rad$ is concerned, it shows a lower percentage of extracted particles but it is expected to give a better results if the spill profile (Figure 6.3) is considered too. In fact, as the beam turns in the accelerator the spill profile is exponentially decreasing at the beginning and then it assumes a uniform shape. In order to further study the extracted beam, it is useful to look to particle transport between the electrostatic and magnetic septum: Figure 6.6.

On the left hand side of the figure the particles that have crossed the electrostatic septum are represented just after they've received the kick from the septum itself. Then, the same group of particles is shown after the 0.3π phase-advance has (partially) transformed the kick into a position difference with respect to the circulating beam. Those particle will then be subjected to the magnetic field of the magnetic field and reach the extraction line.

After all these considerations it is possible to list pro and cons and start the optimization procedure.

- The spill profile does not match with the usage of the beam itself. In fact it is strictly required a beam with almost the same number of particles as a function of time in order to accomplish the physical dose. Moreover, there are characteristics of the spill to be strongly avoided while other that can be kept. So, looking at Figure 6.6:
  - the initial exponential decay has to be strongly avoided;
  - the almost constant trend that can be observed from turn #$5e5$ till the end can be improved.

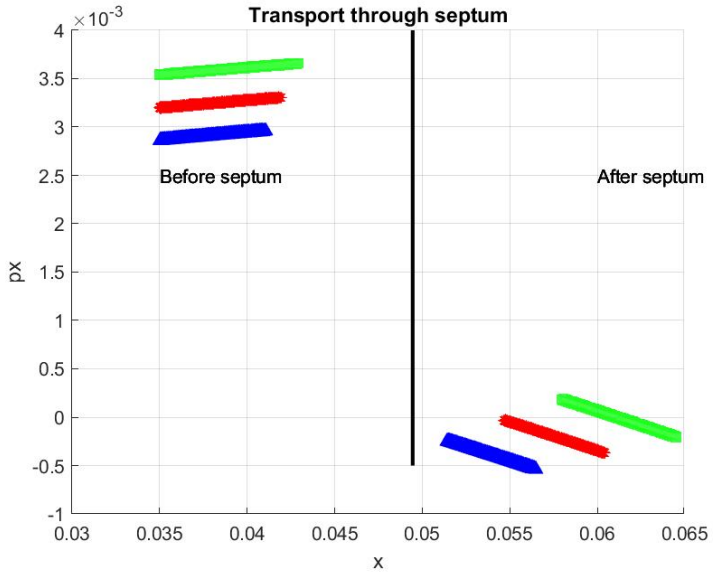

FIGURE 6.6. Transport of particles between the electrostatic and magnetic septa for $\pm 0.5 \mu rad$

Ramp-up	Type	Initial and Final values
Figure 5.9 left	parabolic	$\pm 0.5 \mu rad \div \pm 1 \mu rad$
Figure 5.9 centre	parabolic	$\pm 0.2 \mu rad \div \pm 1 \mu rad$
Figure 5.9 left	parabolic	$\pm 0.1 \mu rad \div \pm 0.8 \mu rad$

Table 6.4: Type of kicker ramp and their features

6.2.2 Parabolic ramp

The first requirement that has to be fulfilled is the spill uniformity. Therefore, in order to avoid the exponential decay in the number of extracted particles the kicker has to be raised to the maximum value in a different way. Moreover, it is expected that the initial and final values of the ramp could influence the spill profile thus, different possibilities have been tried. In fact, if at the beginning of the extraction a low kick is given to the beam it is expected to let particle diffuse towards the outermost region of the triangle with a lower speed. Being the number of particles available for the extraction higher at the beginning of the extraction phenomenon a lower diffusion velocity is needed. On the contrary, at the end of the phenomenon, where a lower number of particles is available in the accelerator, it is necessary to increase the kick and thus the diffusion velocity in order to keep constant in time the number of extracted particles.

Three different configurations are shown in Figure 6.7 and their characteristics are resumed in Table 6.4. Following the picture from left to right and the table from up to down, the first parabolic ramp has been chosen in order to try to mitigate the effects of the random generation of

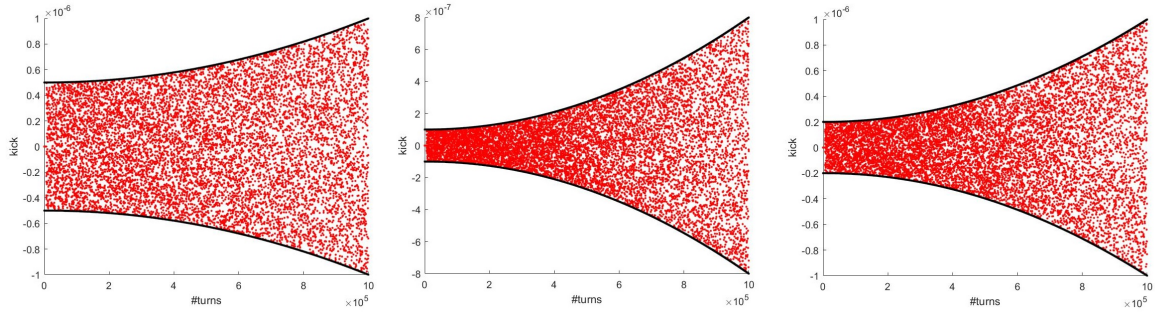

FIGURE 6.7. Study to optimize the kicker ramp-up

	dp/p	**% extracted**
$\pm 0.5\mu rad \div \pm 1\mu rad$	-0.0005	55.2%
	-0.0010	53.0%
	-0.0015	54.4%
$\pm 0.2\mu rad \div \pm 1\mu rad$	-0.0005	42.7%
	-0.0010	41.7%
	-0.0015	39.8%
$\pm 0.1\mu rad \div \pm 0.8\mu rad$	-0.0005	32.5%
	-0.0010	31.4%
	-0.0015	30.8%

Table 6.5: Percentage of extracted particles for three parabolic ramps

the $\pm 1\mu rad$ setup. While the other two setups have the aim of reducing the initial peak in the turn spill profile. From Table 6.5 it is possible to observe the percentage of extracted particles over $1e6$ turns. Also in this case it is expected to achieve higher values if the beams performs more turns. As far as the spill profile is concerned, it is reported in Figure 6.10. It is possible to observe that the first type of parabolic growth has the same trend as the one of the random generation between $\pm 0.5\mu rad$ as well as the same magnitude of the initial peak (as expected since the range for the random kick generation at the beginning the two simulations is the same). But it also shows an almost constant spill over a larger number of turn, actually it starts at $3e5$ instead of $5e5$. Reducing the magnitude of the initial spike and making smoother the spill profile are the features to be improved in this simulation. On the contrary, the other two simulations show a strong reduction of the initial peak but also a growing trend in the number of extracted particles that has to be avoided. So, it could be interesting to study a new setup where:

- The initial value of the parabola has to be closer to $0.2\mu rad$ rather than $0.5\mu rad$ in order to reduce the magnitude of the initial peak;

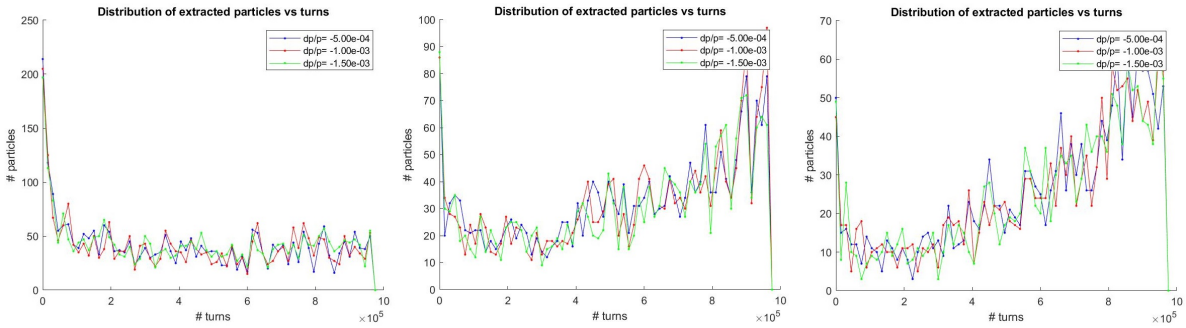

FIGURE 6.8. Evolution of the spill with three different ramp-up of the kicker

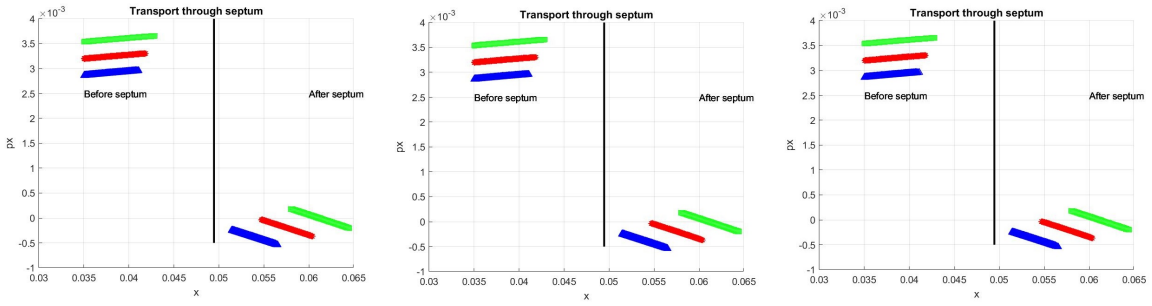

FIGURE 6.9. Spill evolution from the electrostatic to the magnetic septum for three parabolic kicker ramps

- The difference between the initial and final value of the peak has to be close to $0.5\mu rad$ (as the first type of parabolic ramp-up) in order to have a uniform spill rather than a growing trend;

As it can be observed by the comparison of Table 6.3 (excluding the $\pm 1\mu rad$ case study) and Table 6.5, a general increase in the percentage of the extracted particles can be assessed. Thus, the choice of having a smother ramp-up of the kicker was good. For the sake of completeness, Figure 6.9 shows the x-x' phase-space for the particles that compose the spill studied above. As it was expected a parabolic ramp of the kick doesn't affect the characteristics of the extracted beam in phase-space since it just induces variation in the "velocity" at which particles are extracted, i.e. the diffusion speed towards the separatrices.

Type	Initial and Final values	Δ kick
parabolic	$\pm 0.3 \mu rad \div \pm 0.9 \mu rad$	$0.6 \mu rad$

Table 6.6: New setup with optimized initial and final values

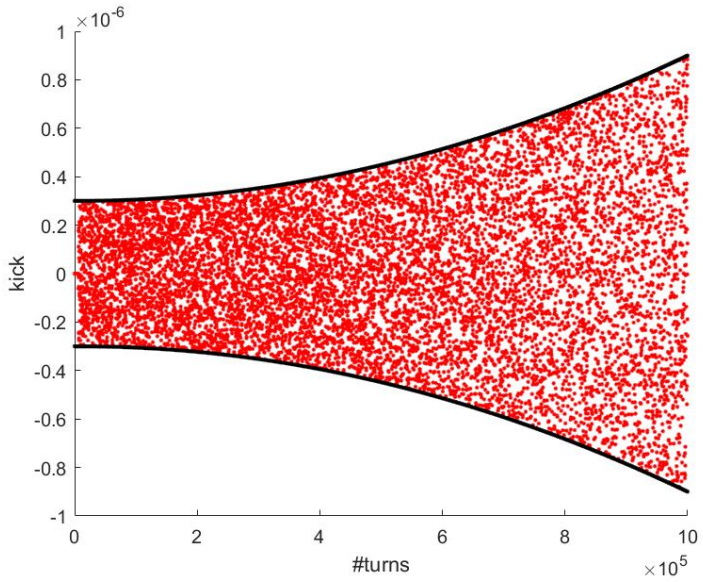

FIGURE 6.10. Parabolic ramp of the kicker between $\pm 0.3 \mu rad$ and $\pm 0.9 \mu rad$

6.2.3 Optimum parabola

According to the information retrieved till now a new setup has been considered. The characteristics of its parabolic ramp can be found in Table 6.6 while the kicker ramp-up can be found in Figure 6.10. As usual, the first $6e3$ turns are performed with the kicker switched off in order to let the beam assume the characteristic triangular shape by the use of the resonant sextupole. As far as the spill profile is concerned it is possible to find it in Figure 6.11. With respect to previous simulations the magnitude of the peak has been reduce. In this new setup a value between those described above is obtained thanks to the reduction of the initial value of the kicker ramp. Moreover, the evolution is almost constant as the beam turns in the accelerator, and it matches the conditions of an almost uniform spill profile.In particular, it is possible to identify which one between the three momenta gives better results with respect to the others. In fact, with a $dp/p = -0.0010$ the spill profile is more uniform than the other two. A further confirmation is given in Table 6.7 where the percentage of extracted particles over $1e6$ turns is reported. Even if a $dp/p = -0.0005$ shows an higher value, its high initial peak still leads to prefer the $dp/p = -0.0010$. For the sake of completeness the phase-space distribution of the beam after the resonance sextupole ramp is reported in Figure 6.12. It can be observed that the change

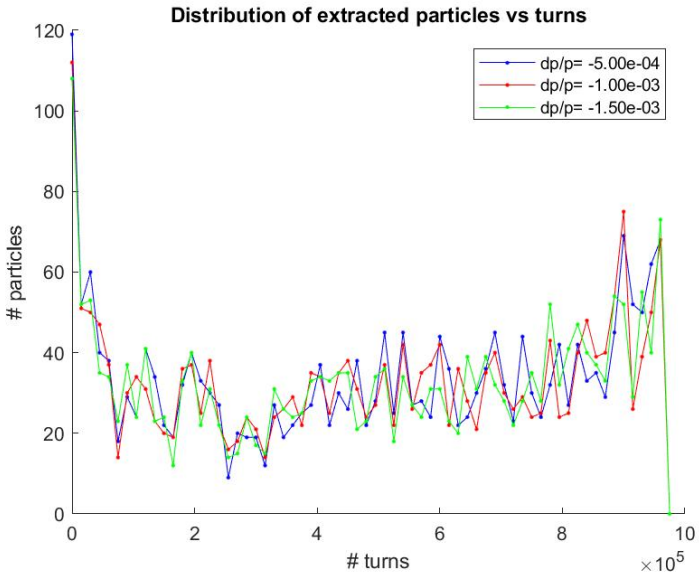

FIGURE 6.11. Spill profile for the parabolic ramp of the kicker between $\pm 0.3 \mu rad$ and $\pm 0.9 \mu rad$

dp/p	**% extracted particles**
-0.0005	43.8%
-0.0010	42.7%
-0.0015	41.2%

Table 6.7: Percentage of extracted particles for parabolic ramp $\pm 0.3 \div \pm 0.9 \mu rad$

in the random generation of the kick doesn't affect the beam configuration as the extraction process is activated.

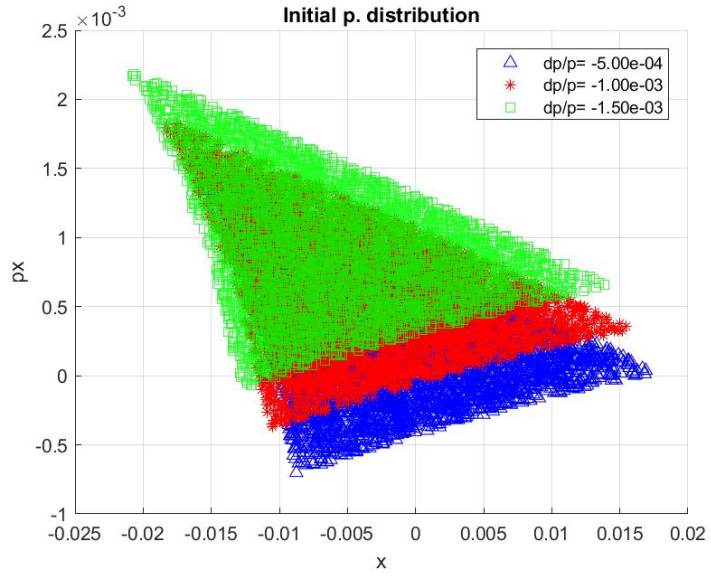

FIGURE 6.12. Phase-space representation for the optimum parabola setup

6.3 Change in chromaticity and tune

Since in the previous section an optimum parabolic ramp for the kick has been found. It is of interest to investigate which machine parameter (or which ones) mostly affect the extraction process. Between all the possibilities, tune and chromaticity are the selected ones. Tune has been chosen since it is one of the first parameters to be changed when a beam has to be brought close to a resonance (tune diagram in Figure 3.1). Chromaticity induce changes in both the beam momentum and tune (Equation (6.1)) as well as in the width of the unstable region in the Stainbach diagram. Due to the computational time needed for each simulation (2 days) not all the average beam momentum could be simulated. Therefore, considering the result obtained in the previous section an additional check on the intermediate momentum offset has been performed. It has been verified if it has almost the same trend for the different configurations tried till now. In Figure 6.13, it is possible to see how the spill profile changes in each setup for the $dp/p = -0.0010$. Then sensitivity analysis on the machine parameters has started. The analysis as been performed by changing one parameter each time and studying how it affects the spill profile, the transport between septa, the number of extracted particles, ... In Table 6.8 it is possible to find which parameters have been changed and, moreover, their initial value (i.e. the one considered in the previous simulations) and final one (i.e. the one under investigation). It can be observed that the vertical tune is not included in the analysis. There are multiple reasons but, above all, the fact that the extraction occurs on the horizontal plane. The same cannot be said for the y chromaticity since sextupoles non-linearities make not obvious its independence from the extraction process. It is expected to have a strong dependence on the x-chromaticity while the other two parameters

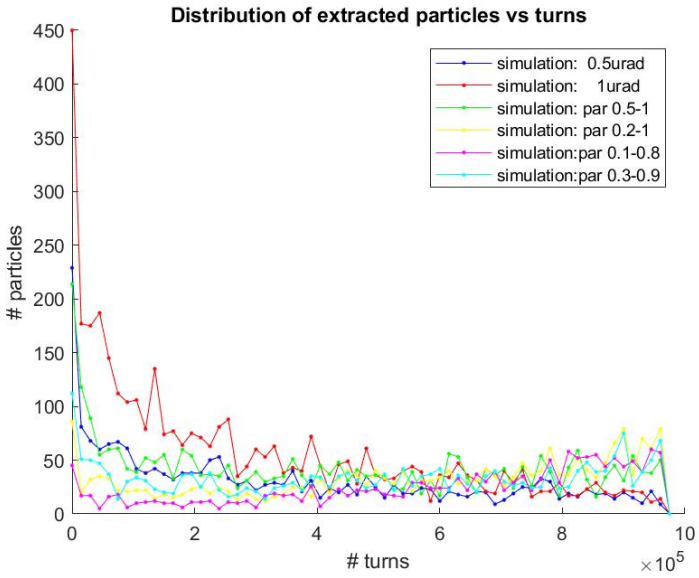

FIGURE 6.13. Spill profile for the different setup studied till now

Parameter	Initial value	Studied value
Q'_x	-0.2	-2
Q'_y	-1	-0.1
Q_x	1.74	1.87

Table 6.8: Parameters' change in sensitivity analysis

should induce just some modifications. This assumptions is assessed in Figure 6.14. As foreseen, the x-chromaticity strongly changes the shape of the spill and, above all, it allows the extraction of a uniform beam. The other two parameters do not affect the results in a significant way, in fact, it is possible to recognize the exponential decay widely seen in the previous simulations. This is the reason why, the vertical tune as well as the y-chromaticity will be changed. It is expected that their change won't induce modifications in the spill profile. The optimization will be reduced to check if the new values of machine parameters with the optimum parabola of the previous section will improve the beam extraction.

Another feature of the extracted beam that changes is the phase-space representation, as shown in Figure 6.15. The position and divergence of the spill is not significantly affected by the change of the vertical tune and chromaticity. It still has a divergence between $3mrad$ and $3.5mrad$ at a radial position between $0.035m$ and $0.04m$ before it receives the kick from the electrostatic septum. This values are almost the same of those obtained from the previous simulations if the intermediate momentum-0.0010 is observed. By the observation of the blue spill in Figure 6.18 a great change can be detected. The spill dimension has been strongly reduced

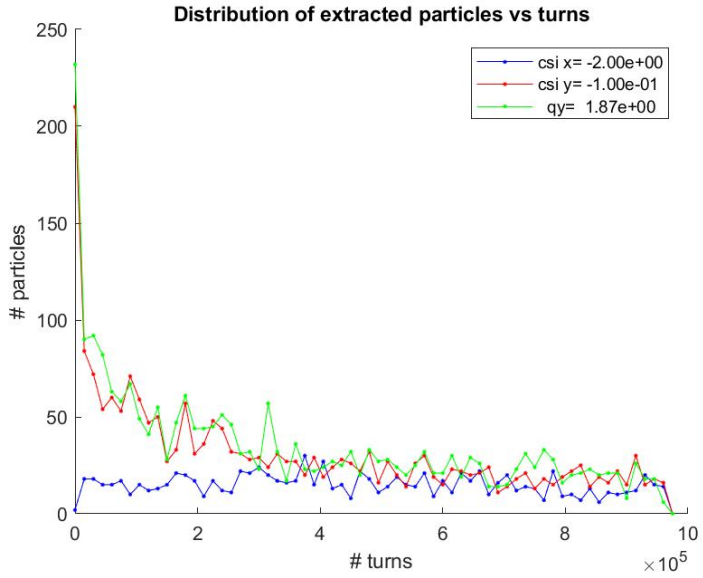

FIGURE 6.14. Spill profile for the sensitivity analysis

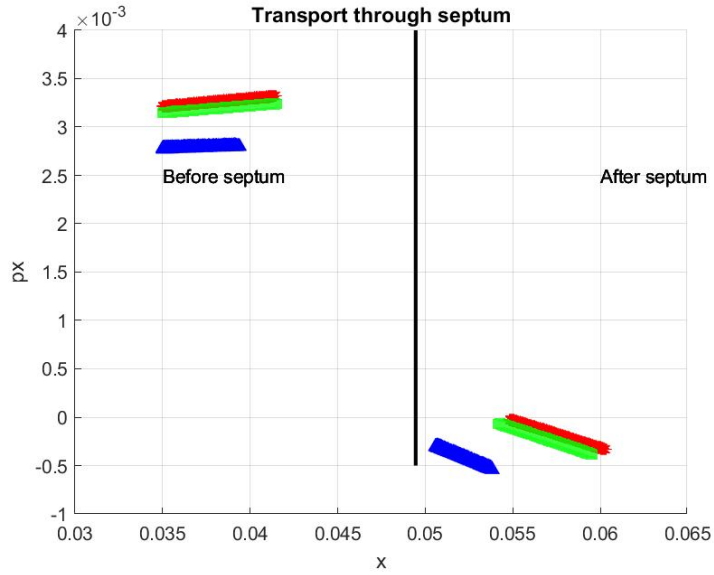

FIGURE 6.15. Spill transport between septa in the sensitivity analysis

	Septa	$\xi_x = -0.2$	$\xi_x = -2$
	Before ES	0.007 m	0.005 m
Δ position	After MS	0.0065 m	0.004 m
	Before ES	0.25 mrad	≃0 mrad
Δ divergence	After MS	-0.3 mrad	-0.3 mrad

Table 6.9: Change of spill dimensions due to x-chromaticity changes

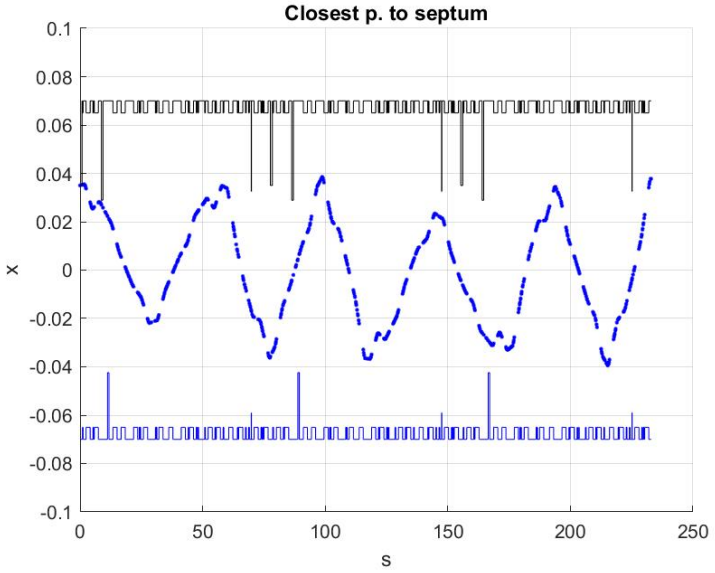

FIGURE 6.16. Detailed transport between septa of the closest particle to electrostatic septum

as it is highlighted in Table 6.9. The reduction of the radial position after the magnetic septum reduces the risk to lose particles due to collisions with other elements of the extraction line (the vacuum chamber has always a maximum radial dimension equal to 0.07 m) but increases the probability to lose it due to collisions within the vacuum chamber. A drawback of this setup is the closeness of the last extracted particles to the magnetic septum. The particle studied is the blue one on the far left on the left hand side of Figure 6.18, i.e. in the *Before septum* region before it receives the kick from the electrostatic septum. Then it is kicked and tracked for three turns before the magnetic septum is able to convert the particle divergence into a position difference with respect to the circulating beam. Thus, since it is the closest to the physical clearances of the accelerator it is the particle with the highest probability to be lost. The MAD-X code developed for the purpose of this analysis is reported in **Appendix D** while the one used to post-process the results and produce Figure 6.19 can be found in **Appendix E**. In Figure 6.19 the x transverse position is represented as a function of three times the accelerator length and the blue and black contours represent the physical clearances in the machine. The transverse clearances are not

Parameter	Value
Q'_x	-2
Q'_y	-0.02
Q_x	1.67
Q_y	1.87

Table 6.10: Optimized machine parameters for an optimized kicker ramp-up

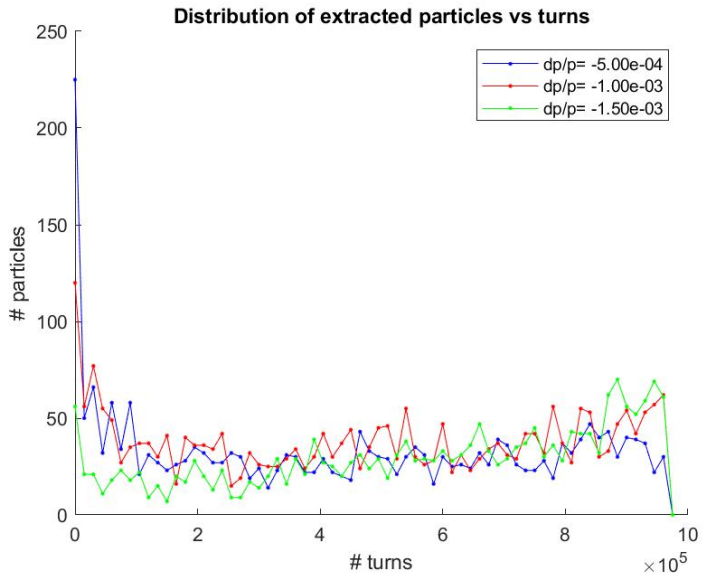

FIGURE 6.17. Spill profile for the investigated optimized configuration

symmetric, the black one refers to those on the outer part of the ring (where the magnetic and electrostatic extraction septa are located) while the blue one to the inner one (where there is the electrostatic injection septum).

6.4 Investigation on optimized configuration

According to the results of the sensitivity analysis and the studies performed on the kicker ramp, a new setup has been built the aim being to understand how much the machine parameters affect the results from a quantitative point of view. Thus, since the last parabolic ramp-up of the kicker seemed to be optimized, it is considered again and the machine parameters are changed according to the analysis of the previous section. Hopefully an higher value of extracted particles is expected. The vertical chromaticity has been further changed in order to check if it could influence the spill profile. The reason of this choice will be explained at the end of this chapter. The very first result to be checked is the spill profile, that is reported in Figure 6.17. The combination of machine parameters changes and kicker ramp lead to a uniform beam over a large number of turns (from

dp/p	**% extracted particles**
-0.0005	58.2%
-0.0010	46.8%
-0.0015	31.8%

Table 6.11: Percentage of extracted particles for parabolic ramp $\pm 0.3 \div \pm 0.9 \mu rad$ with optimized machine parameters

$\approx 1e6$ till the end). Also in this case it is interesting to perform a more detailed analysis for the three different momenta offset. The only setup where the initial spike is not negligible is for a momentum of -0.0015 whereas the other two ($dp/p = -0.0005$ and $dp/p = -0.0010$) have a low intensity peak, almost negligible. Moreover, between the three momenta the central one (-0.0010) seems to be the best (and it further confirms the initial hypothesis) since it has an uniform spill profile. Moreover, the percentage of extracted particles over $1e6$ is higher than the one obtained with the previous machine parameters. Even if the lower momentum offset shows an higher percentage in the extracted particles the profile of its spill still leads to prefer the intermediate momentum offset.

6.4.1 Momenta offset study

To further study how a change in the machine parameters could influence the extracted spill, they have been changed as reported in Table 6.12. All the parameters have been left unchanged with respect to the starting point, the only difference has been performed in the x chromaticity. In this way it will be possible to compare if changes in the spill profile can be attributed just to changes in the x chromaticity or if they are due to changes of all the machine parameters (as performed in the previous section). The momentum offset with respect to the resonance has been studied on

Parameter	**Value**
Q'_x	-2
Q'_y	-1
Q_x	1.67
Q_y	1.74

Table 6.12: Optimized machine parameters for an optimized kicker ramp-up

a limited range, i.e. simulating three different values determined by previous studies ($dp/p = -0.0005; -0.0010; -0.0015$). A check on a wider range could then be performed. In particular, being the actual betatron extraction performed with a momentum between $-0.003 \div -0.002$, two additional values have been considered. In Figure 6.18 it is possible to observe the trend of the extracted spill. The additional momenta added do not allow beam extraction. In the Steinbach

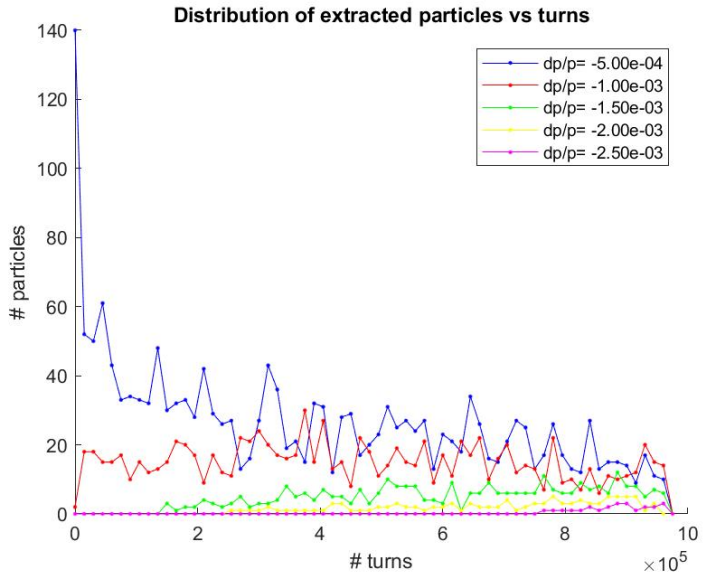

FIGURE 6.18. Spill profile for momenta offset study

diagram, these momenta are too far from resonance and their extraction is so slow that can be almost neglected compared to the other momenta. In order to achieve the beam extraction with these momenta and the machine parameters defined above, it could be necessary to "wait" more until the beam reaches the unstable region. By the comparison of this spill profile with the one of the previous sections it is possible to notice that the characteristic exponential decay is a feature of the lowest momentum offset, it can be explained considering the fact the $dp/p = -0.0005$ is the closest to the resonance, thus the feature could be improved by studying another kicker ramp. This step won't be performed since it is sufficient to find a single momentum offset that satisfied the requirements. It is the case of $dp/p = -0.0010$ since it allows the extraction of a uniform extracted beam.

6.5 Towards experimental measures

In order to have an experimental verification, it is important to define the frequency range for the sweep and the amplitude range for the kicker ramp. Thus, an Excel file has been built. The file contains all the fundamental information and calculations for protons and carbon ions both. For each value of energy (protons: 60MeV - 240 MeV; carbon ions: 120MeV/u - 400MeV/u) the following physical quantities have been computed:

- Momentum $p[Mev/c^2]$ from the relativistic triangle:

(6.2)
$$\begin{cases} E^2 = (m_0c^2)^2 + (pc)^2 \\ E = E_k + m_0c^2 \end{cases}$$

Where E_k is the kinetic energy of the beam; m_0c^2 is the rest energy and E is the total energy.

- Lorentz factors γ and β [1] :

(6.3)
$$\gamma = \frac{E_k + E_0}{E_0} \qquad \beta = \sqrt{\frac{\gamma^2 - 1}{\gamma^2}}$$

- Momentum compation factor η[1]:

(6.4)
$$\eta = \frac{1}{\gamma^2} - \alpha_c$$

Where α_c is defined as the change of relative change in the orbit length due to a momentum spread.

- From experimental measures the following quantities have been retrieved:
  - RF frequency: it is the frequency imposed by the RF cavity;
  - Tune;
  - Maximum dispersion;
  - Closed orbit distortion: it quantifies how much the beam is moved with respect to the centre of the vacuum chamber due to magnets misalignments or dumps;
  - Magnetic rigidity;

From this set of data it is possible to compute the betatron frequency range that has to be excited using Equation (3.46) and Equation (3.47). Moreover, since there is a direct dependence on $n \pm q_0$ the Excel file allows the modification of the tune and thus of the frequencies. Once the beam energy has been chosen, the amplitude of the frequency sweep is fixed, i.e. the FM modulation can be performed. As far as the AM modulation is concerned, there is an additional column in the file that allows the calculation of the differential potential to be imposed between the kicker plates in order to obtain the required kick (the user can easily modify this value in the data box of the file). Thus, assuming to perform a parabolic kick ramp-up between $\pm 0.3 \mu rad$ and $\pm 0.9 \mu rad$, then the user has to insert the values in the provided space and look for the corresponding voltage, computed from Equation (3.48). Figure 6.19 shows the required data in order to plan FM and AM experimental sessions. Some of them can be modified by the user,

Data			
Tune	Qx [-]	1.672	Req. Input
	qx [-]	0.672	
Frequency limit		4.00E+06	Req. Input
Chromaticity		-2.00	Req. Input
Kicker lenght		3.70E-01	
pos s4_11 [m]		-2.50E-02	Req. Input
Kick		2.99E-06	Req. Input (rad!!!)

FIGURE 6.19. Required input data for planning FM and AM experimental sessions

BEAM Bragg-Peak position RESEARCH GATE

Bragg-Peak position		Frequency [Hz]	0.328			0.672			Kick
			f_1	f_2	δf	f_1	f_2	δf	V_pp
User value	Closest lower value 30	1347166.97	445970.88	453121.92	7151.04	908883.78	915140.90	6257.12	159.91
30	Closest upper value 31	1357109.15	449064.59	456724.33	7659.74	915420.05	922125.26	6705.22	162.43

FIGURE 6.20. Betatron frequencies and kicker voltage for FM and AM

e.g. tune Q_x (the decimal part of the tune is automatically computed, thus there is no need to directly modify it), chromaticity, kick and position of the beam within the vacuum chamber at the maximum dispersion region ($pos\ s4\_11$) while others are fixed like the kicker length. The frequency limitation cell has been added after the studies on the hardware in order to highlight which is the maximum generation frequency of the RF signal due to a limitation (that can be solved) of the LLRF component. Figure 6.20 shows the research gate that the user can handle in order to look for a particular beam. Since at CNAO the beam is used for patient treatments it is preferred to look for the Bragg-peak position rather than the beam energy. As output the user can see the closest lower and upper value available. Then of each $n \pm q_0$ under investigation it is possible to observe the maximum and minimum betatron frequencies and their difference. As an example just the values for $1 - q_0$ and q_0 are shown in Figure 6.24. The last column shows the peak-to-peak voltage of the signal that has to be provided to the kicker's plates.

The great limitation of the set of simulation that has been described and performed is that the RF cavity is not part of the analysis. The RF cavity has to be switched on all over the extraction process because the beam is longitudinally bunched in order to allow the re-acceleration of the non extracted particles. Therefore, particles see an electric field (or a sinusoidal voltage) while the synchronous one sees a zero potential difference that keep constant its revolution frequency. All the other one with a slightly bigger or smaller energy oscillate around the synchronous one,

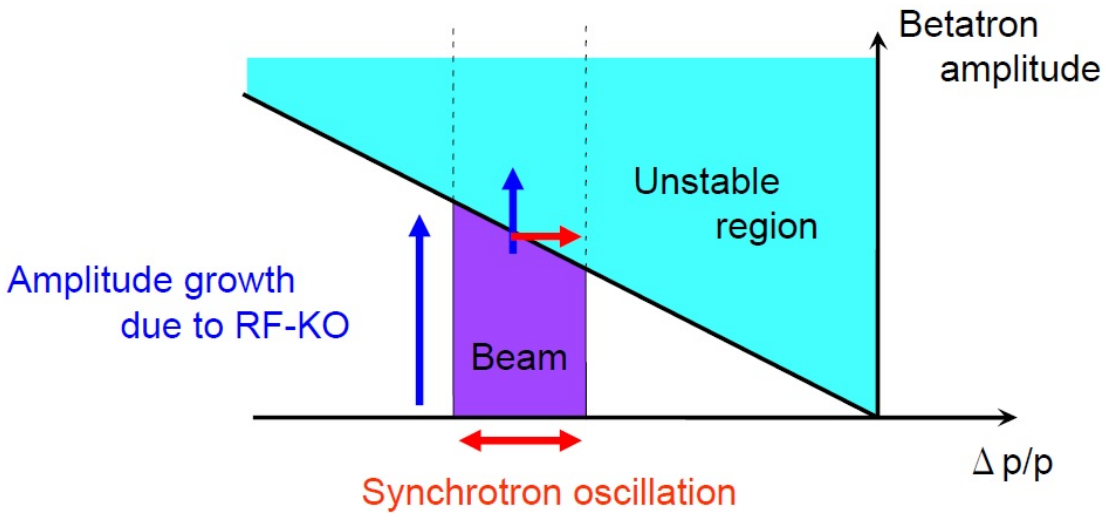

FIGURE 6.21. Amplitude growth and synchrotron oscillations

the frequency of these oscillations is called *synchrotron frequency*. During a RFKO extraction the beam enters the unstable region by the growth of betatron oscillations amplitude. But it also happens that particles enter the unstable region because synchrotron oscillations make them move towards it, as shown in Figure 6.25. The problem directly connected to such a secondary and unwanted extraction is due to the frequency of these particles. It is of the order of some $\simeq kHz$ and thus it is not matched with the frequency range for medical treatments. The solution could be to work with an almost zero chromaticity in order to make the relative variation of the tune linearly independent from the momentum spread.

CHAPTER 7

CONCLUSIONS

At the beginning of this work preliminary studies to assess the feasibility of a RFKO extraction had been performed. Now it is possible to say that the hardware implementation has been completed while the simulation part needs to be compared with experimental results, thus at present, it is not possible to say if more simulations will be needed.

As far as the hardware implementation is concerned, it has been tested and verified over a large frequency and voltage range. Moreover, during the in field tests it worked properly. As reported in Chapter 4, the LLRF-clone shows an important limitation in the maximum frequency of the RF signal it can generate. Thus it can be useful to re-code it and allow the noise generation in wider frequency range.

From the set of simulations presented in Chapter 6, it is possible to conclude that good results have been obtained for a $dp/p = -0.0010$ with a parabolic ramp-up between $\pm 0.3 \mu rad \div \pm 0.9 \mu rad$ and with the machine parameters reported in Table 6.12. For sure additional studies on the chromaticity have to be performed as well as planning experimental measurements. In fact, even if a zero chromaticity seems to be better since it should avoid the extraction of particles at the synchrotron frequency, it is not sure it can be practically reached. Moreover, it could be interesting to develop a code that evaluates the maximum decrease of the RF voltage in the cavity that allows the extraction of a small dp/p of the beam. It requires the evaluation of intermediate quantities that influence each other and thus the need of an iterative procedure. In addition, it could be useful to add the extraction of particles at the synchrotron frequency in the MAD-X code in order to have a code that simulates all the fundamental features of the phenomenon. Another modification could be on the *.bat* file in order to allow the automatic copy of the kicker ramp in the

required sub-directories (now this step is performed by the user before running each simulation). Moreover, in order to allow the use of the Excel file, developed to plan experimental measures, on a wider range it could be possible to add another research gate where energy selection of the beam is performed instead of the Bragg-peak position. I will work on this topic for two months more and I hope to find the experimental verification of the work performed and improve the code cited before.

APPENDIX A

APPENDIX A: DERIVATION OF THE MOTION EQUATIONS IN THE LONGITUDINAL DIRECTION

In order to compute the motion equation in the longitudinal direction, at first the energy gain per unit path is computed for the synchronous particle and for those with delay or in advance:

$$\frac{dW_s}{dz} = \frac{1}{dz}\left(\frac{1}{2}mv_s^2\right) = \frac{1}{dt}\left(mv_s\right) = qE_s sin(\Phi_s) \tag{A.1}$$

Where at the second last passage the following expression has been substituted:

$$\frac{d}{dt} = \frac{dz}{dt}\frac{1}{dz} = v\frac{1}{dz} \tag{A.2}$$

The energy gain of a generic particle is expressed as:

$$\frac{d\Delta E}{dz} = qE_s\Big(sin(\Phi_s + \varphi) - sin(\Phi_s)\Big) = \frac{dw}{dz} \tag{A.3}$$

Where w is just the difference between the energy of the particle W and the one of the synchronous one W_s.

$$\frac{d\varphi}{dz} = \omega\left(\frac{dt}{dz} - \frac{dt_s}{dz}\right) = \omega_{RF}\left(\frac{1}{v} - \frac{1}{v_s}\right) \tag{A.4}$$

Being φ the difference between the phase of a particle and the one of the synchronous one. It is useful to write the explicit form for w:

$$w = \frac{1}{2}m(v^2 - v_s^2) = \frac{1}{2}m(v + v_s)(v - v_s) \approx \frac{1}{2}m2v_s(v - v_s) = mv_s(v - v_s) \tag{A.5}$$

So Equation (A.4) can be written as follows using Equation (A.5):

$$\frac{d\varphi}{dz} = \omega\frac{v_s - v}{v \cdot v_s} \tag{A.6}$$

But

$$v \cdot v_s = \frac{w + mv_s^2}{m}$$

So at the end it is possible to obtain:

$$\frac{d\varphi}{dz} = -\frac{\omega \cdot w}{mv_s^3} \tag{A.7}$$

Performing the difference between the sinusoidal functions in Equation (A.3):

$$sin(\Phi_s + \varphi) - sin(\Phi_s) = 2cos\left(\frac{\Phi_s + \varphi + \Phi_s}{2}\right) \cdot sin\left(\frac{\Phi_s + \varphi - \Phi_s}{2}\right) = 2cos\left(\Phi_s \frac{\varphi}{2}\right) \cdot \frac{\varphi}{2} \tag{A.8}$$

Being φ defined as:

$$\varphi = \Phi - \Phi_s$$

Then $\varphi << \Phi_s$ and Equation (A.8) can be simplified as:

$$sin(\Phi_s + \varphi) - sin(\Phi_s) = 2cos\left(\Phi_s \frac{\varphi}{2}\right) \cdot \frac{\varphi}{2} \approx \varphi cos(\Phi_s) \tag{A.9}$$

A simplified version of Equation (A.3) can be then obtained:

$$\frac{dw}{dt} = qE_s \varphi cos(\Phi_s) \tag{A.10}$$

By the derivation of Equations (A.6) and it combination with Equation (A.10), it is possible to obtain:

$$\frac{d^2\varphi}{dz^2} + \frac{\omega}{mv_s^3}\Big(qE_s cos(\Phi_s)\Big)\varphi = 0 \tag{A.11}$$

Equation (A.11) can be also written as:

$$\frac{d^2\varphi}{dz^2} + \Omega^2 \varphi = 0 \quad where \quad \Omega^2 = \frac{\omega}{mv_s^3}\Big(qE_s cos(\Phi_s)\Big) \tag{A.12}$$

Equation (A.12) has the same form of an harmonic oscillator. In order to find physical solution, a real solution has to be found, i.e. the coefficient multiplying φ has to be positive.

$$\Omega^2 = \frac{\omega}{mv_s^3}\Big(qE_s cos(\Phi_s)\Big) > 0 \rightarrow cos(\Phi_s) > 0 \tag{A.13}$$

Giving a graphical representation of the energy gain ΔE versus the phase difference φ it is possible to obtain a circumference that has the synchronous particle at the centre of the reference system and those with delay or in advance move around it on a circular path. But when the assumption of $\varphi << \Phi_s$ is removed then the circumference is deformed and the well known bucket shape is obtained. As the non linearity induced by sextupoles, it is still possible to see the circular path near the center of the reference system while moving towards the non linear effects get more and more important.

APPENDIX B

APPENDIX B: POST-PROCESSING CODE ON MATLAB FOR MAD-X RESULTS

```
clearvars
close all
clc

%% CHANGE THE DIRECTORY!
cd ..
cd ..
cd('1-0.5urad');
mkdir 'RESULTS'%makes dir where saves figures
%% Insert the momentum value of momenta simulated on MAD-X
momenta=[-0.0005,-0.0010,-0.0015];%[-2,-0.1,1.87];
names=['dp/p=';'dp/p=';'dp/p='];%['csi x=';'csi y=';' qy= '];
%% Definition variables and tables TO NOT DELETE
cextr=zeros(length(momenta),1); %# particles lost @ EL septum, i.e. extracted
clost=zeros(length(momenta),1); %# particles lost somewhere else
closts R=zeros(length(momenta),1); %# particles lost in SR ramp-up at EL septum
celseSR=zeros(length(momenta),1); %# particles lost in SR ramp-up somewhere else
cIn=zeros(length(momenta),1); % initial # of particles generated
cSR=zeros(length(momenta),1); %particles alive after SR ramp-up
%% Colours to be used in the plot
col=['^b';'*r';'sg';'xy';'om']; %all other plots
coltt=['.-b';'.-r';'.-g';'.-y';'.-m']; %for the BIN plot
%next line for the plot evolution of available particles
col1=[[1 0 0];[0 1 0];[1 1 1];[0 0 1];[1 1 0];[0 1 1];[1 0 1];[1 0.4 0.6];[123/255
    104/255 238/255];[1 140/255 0];[128/255 0 0]];
```

```
%% START OF THE ROUTINE (it will be done a #of times = # momenta simulated)
for ii=1:length(momenta)
    %Go in the subdirectories, furhter specification needed for -0.0010
    if (ii==2 || ii==4)
        cd(strcat('deltap_',num2str(momenta(ii)),'0'));%('csi_y@',num2str(momenta(ii)))
    else
        cd(strcat('deltap_',num2str(momenta(ii))));
%     elseif ii==1
%         cd(strcat('csi_x@',num2str(momenta(ii))))
%     elseif ii==3
%         cd(strcat('qy@',num2str(momenta(ii))))
    end

    %1-INITIAL DISTRIBUTION OF PARTICLES -> part_input_coord.txt
    ff=fopen('part_input_coord.txt');
    line=0;
    j=1;
    PartIn=zeros(j,6);
    while line~=-1
        line=fgetl(ff);
        if line~=-1
            char=['s','t','a','r','x','y','p',';','='];
            for k=1:length(char)
                line=erase(line,char(k));
            end
            PartIn(j,:)=str2double(strsplit(line(2:end),','));
            j=j+1;
        end
    end
    cIn(ii)=length(PartIn);
    fclose(ff);
    clear ff line j k char

    %2-PARTICLES AVAILABLE 4 EXTRACTION AFTER SR RAMP-UP
    %'tracksumm1.txt' copied into 'part_input_coord1.txt'
    ff=fopen('part_input_coord1.txt');
    line=0;
    j=1;
    PartSR=zeros(j,6);
    while line~=-1
        line=fgetl(ff);
        if line~=-1
```

```
        char=['s','t','a','r','x','y','p',';','='];
        for k=1:length(char)
            line=erase(line,char(k));
        end
        PartSR(j,:)=str2double(strsplit(line(2:end),','));
        j=j+1;
    end
end
cSR(ii)=length(PartSR);
fclose(ff);
clear ff line j k char

%change directory and start the post-processing of the outputs!
cd('output')

%3-PARTICLES LOST DURING SR RAMP-UP
ff=fopen('trackloss0.txt');
line=fgetl(ff);
j=1;
PartSRlost=zeros(j,12);
PosSRlost=[];
%Delete first lines of the MAD-X output files that are useless
while (line(1)=='@' || line(1)=='*' || line(1)=='$' || line(1)=='#')
    line=fgetl(ff);
    j=j+1;
end
k=1; %Write on a table useful data
while line~=-1
    PartSRlost(k,:)=str2double(strsplit(line(1:end-19),' '));%data
    PosSRlost=[PosSRlost;line(end-18:end)];%position
    index=find(PosSRlost(k,:)=='"');
    if PosSRlost(k,index(1)+1:index(2)-1)=='SE_010A_ESP'
        clostSR(ii)=clostSR(ii)+1;
    else
        celseSR(ii)=celseSR(ii)+1;
    end
    line=fgetl(ff);
    k=k+1;
    clear index
end
PartSRlost(:,1)=[];
PartSRlost(:,end)=[];
fclose(ff);
```

```
clear ff line j k

%4-PARTICLES LOST DURING KICKER RAMP-UP: possible extracted particles!
ff=fopen('trackloss1.txt');
line=fgetl(ff);
j=1;
PartExtr=zeros(j,12);
PosExtr=[];
%Delete first lines of the MAD-X output files that are useless
while (line(1)=='@' || line(1)=='*' || line(1)=='$' || line(1)=='#')
    line=fgetl(ff);
    j=j+1;
end
k=1; %Write on a table useful data
while line~=-1
    PartExtr(k,:)=str2double(strsplit(line(1:end-19),' '));%data
    PosExtr=[PosExtr;line(end-18:end)];%position
    index=find(PosExtr(k,:)=='"');
    if PosExtr(k,index(1)+1:index(2)-1)=='SE_010A_ESP'
        cextr(ii)=cextr(ii)+1;
    else
        clost(ii)=clost(ii)+1;
        PartExtr(k,:)=[];%delete particle if lost somewhere else
    end
    line=fgetl(ff);
    k=k+1;
    clear index
end
PartExtr(:,1)=[];
PartExtr(:,end)=[];
fclose(ff);
%evolution in time of the extracted particles
if cextr(ii)~=0
    bin=15e3;
    int=round(max(PartExtr(:,2)/bin));
    for ll=1:int
        if ll==1
            Part(ll)=length(1:find(PartExtr(:,2)<=bin,1,'last' ));
        else
            if ll==int
                Part(ll)=length(find(PartExtr(:,2)<=(ll-1)*bin,1,'last'):PartExtr(end:2));
            else
                Part(ll)=length(find(PartExtr(:,2)<=(ll-1)*bin,1,'last'):find(PartExtr(:,2)<=ll
```

```
            end
        end
    end
    clear ff line j k
end

%5-PARTICLES STILL AVAILABLE IN THE MACHINE: not extracted & not lost
ff=fopen('tracksumm1.txt');
line=fgetl(ff);
j=1;
AA=zeros(j,11,15);
turns=zeros(1,15);
%Delete first lines of the MAD-X output files that are useless
while (line(1)=='@' || line(1)=='*' || line(1)=='$' || line(1)=='#')
    line=fgetl(ff);
    j=j+1;
end
i=1; %Write on a table useful data
while ((line(1)~='@' || line(1)~='*' || line(1)~='$' || line(1)~='#') &&
    line(1)~=-1)
    k=1;
    while (line(1)~='#' && line(1)~=-1)
        AA(k,:,i)=str2double(strsplit(line(1:end),' '));%data
        turns(i)=AA(1,3,i);
        line=fgetl(ff);
        k=k+1;
    end
    i=i+1;
    line=fgetl(ff);
end
fclose(ff);
index=find(turns==0);
turns(index(2):end)=[];
AA(:,:,index(2):end)=[];
AA(:,1,:)=[];
clear ff line j k index

%6-TRACKING OF PARTICLES BETWEEN SEPTA
if exist('tracksumm_setti.txt','file')==2
    ff=fopen('tracksumm_setti.txt');
    line=fgetl(ff);
    j=1;
    BB=zeros(j,11,2);
```

```
    %Delete first lines of the MAD-X output files that are useless
    while (line(1)=='@' || line(1)=='*' || line(1)=='$' || line(1)=='#')
        line=fgetl(ff);
        j=j+1;
    end
    i=1; %Write on a table useful data
    while ((line(1)~='@' || line(1)~='*' || line(1)~='$' || line(1)~='#') &&
        line(1)~=-1)
        k=1;
        while (line(1)~='#' && line(1)~=-1)
            BB(k,:,i)=str2double(strsplit(line(1:end),' '));%data
            line=fgetl(ff);
            k=k+1;
        end
        i=i+1;
        line=fgetl(ff);
    end
    fclose(ff);
    BB(:,1,:)=[];
    clear ff line j k
elseif exist('tracksumm_setti.txt','file')==0
    sprintf('For the dp/p=%3.2e the track between septa has not been
        performed.\n',momenta(ii));
    sprintf('It is probable that particles have been lost somewhere else rather
        than the electrostatic septum.\n');
    sprintf('Please check the trackloss1.txt file');
end
cd ..
cd ..
%% figures
cd('RESULTS');
%Available particles 4 extraction, 3pict->3mom
h1=figure(ii);
hold on
grid on
box on
for i=1:length(turns)
    hold on
    title(sprintf('%s
        %3.2e',names(ii,:),momenta(ii)));%sprintf('dp/p=%2.1e',momenta(ii)));
    xlabel 'x'
    ylabel 'px'
    h1=plot(AA(:,3,i),AA(:,4,i),'Marker','.','LineStyle','none', ...
```

```
    'MarkerFaceColor',col1(i,:),'DisplayName',sprintf('turn: %i',turns(i)));
    legend '-DynamicLegend'
    if i==1
       if ii==1
           gif('mom-5e-4.gif','DelayTime',0.4,'frame',gcf);%gif('csi_x@-2.gif','DelayTime',0.4);
        elseif ii==2
           gif('mom-1e-3.gif','DelayTime',0.4,'frame',gcf);%gif('csi_y@-01.gif','DelayTime',0.4);%
        elseif ii==3
           gif('mom-1,5e-3.gif','DelayTime',0.4,'frame',gcf);%gif('qy@-1,87.gif','DelayTime',0.4);%
        elseif ii==4
           gif('mom-2e-3.gif','DelayTime',0.4,'frame',gcf);
        elseif ii==5
           gif('mom-2,5e-3.gif','DelayTime',0.4,'frame',gcf);
       end
    else
        gif;
    end
end
hold off
%Histogram extracted particles w. #
h2=figure(10);
hold on
subplot(1,length(momenta),ii)
plot(PartExtr(:,9),PartExtr(:,1),col(ii,:),'DisplayName',sprintf('%s
    %3.2e',names(ii,:),momenta(ii)));
title ('Extracted particles');
legend '-DynamicLegend'
grid on
box on
xlabel 's'
ylabel 'particle'
txt=(sprintf('%i over %i',cextr(ii),cSR(ii)));
text(0.4,500,txt);
xlim([0, max(PartExtr(:,9)+0.2)]);
hold off
if ii==length(momenta)
    maximize(h2);
    saveas(h2,'HistogramExtracted','jpg');
end
%Histogram SR lost particles w. #
h3=figure(11);
hold on
subplot(1,length(momenta),ii)
```

```
plot(PartSRlost(:,9),PartSRlost(:,1),col(ii,:),'DisplayName',sprintf('%s
    %3.2e',names(ii,:),momenta(ii)));
title ('Particles lost in SR ramp-up');
legend '-DynamicLegend'
grid on
box on
xlabel 's'
ylabel 'particle'
txt=(sprintf('%i over %i',clostSR(ii)+celseSR(ii),cIn(ii)));
text(0.4,500,txt);
xlim([0, max(PartSRlost(:,9)+0.2)]);
hold off
if ii==length(momenta)
    maximize(h3);
    saveas(h3,'HistogramLostSR','jpg');
end
%Time evolution extr particles (bin=15e3)
if cextr(ii)~=0
    h4=figure(12);
    hold on
    title 'Distribution of extracted particles vs turns'
    plot(1:bin:bin*int,Part,coltt(ii,:),'DisplayName', sprintf('%s
        %3.2e',names(ii,:),momenta(ii)));
    legend ('-DynamicLegend');
    xlabel '# turns'
    ylabel '# particles'
    hold off
    saveas(h4,'TimeEvolutionExtracted','jpg');
end
%Transport between septa SUPERIMPOSED
if exist('tracksumm_setti.txt','file')==2
    h5=figure(13);
    hold on
    plot(BB(:,3,1),BB(:,4,1),col(ii,:));
    txt='Before septum';
    text(0.035,2.5e-3,txt);
    plot(BB(:,3,2),BB(:,4,2),col(ii,:));
    txt='After septum';
    text(0.06,2.5e-3,txt);
    line([0.04945, 0.04945], [-0.5e-3,4e-3], 'LineWidth', 2, 'Color', 'k');
    title (sprintf('Transport through septum'));
    xlim([0.03 0.065]);
    xlabel 'x'
```

```
        ylabel 'px'
        grid on
        hold off
        saveas(h5,'Transport_Septa_SuperimposedMom','jpg');
    end
    %Superimposed triangles after SR ramp-up
    h6=figure(14);
    hold on
    plot(PartSR(:,1),PartSR(:,2),col(ii,:),'DisplayName',sprintf('%s
        %3.2e',names(ii,:),momenta(ii)));
    grid on
    xlabel 'x'
    ylabel 'px'
    legend '-DynamicLegend'
    title('Initial p. distribution');
    hold off
    saveas(h6,'Triangles@SR','jpg');
%     if ii==1
%         cd ..
%         cd ..
%         cd 'Variables'
%         save(['bin_',dir,'.mat'],'bin');
%         save(['particles_',dir,'.mat'],'Part');
%     end
    cd ..
    clear PartIn PartSR PartSRlost PosSRlost PartExtr PosExtr AA turns BB Part
end
```

APPENDIX C

APPENDIX C: MATLAB CODE FOR KICKER RAMP-UP

```
%ATTENTION MAD-X and this code MUST BE in the same folder when you try to
%make MatLab run!
tic
clearvars
close all
clc

found=zeros(1,2);
%% It automatically gets the # of turns written in MAD-X
ff=fopen('extraction_makethin_v3.madx');
ll=fgetl(ff); %take the first line
while (found(1)==0 || found(2)==0)
    if (isempty(ll)==1 || ll(1)=='!' || ll(1)==' ' || ll(1)=='a' || ll(1)=='o' ||
        ll(1)=='T')
        ll=fgetl(ff);
    else
        iitemp=find(ll=='=');
        jjtemp=find(ll==';');
        if strcmp(ll(1:iitemp-1),'Nturns')==1
            found(1,1)=1;
            Nturns=str2double(ll(iitemp+1:jjtemp(1)-1)); %tot # turns
        elseif strcmp(ll(1:iitemp-1),'Nturns0')==1
            found(1,2)=1;
            Nturns0=str2double(ll(iitemp+1:jjtemp(1)-1)); %# turns no kicker, yes SR
        end
        ll=fgetl(ff);
```

```
    end
end
fclose(ff);
%% Format output file
s1='@ TYPE           %05s "TWISS"';
s2='@ TITLE          %09s "CNAO SYNC"';
s3='@ ORIGIN         %18s "5.03.04 Windows 64"';
s4='@ DATE           %08s "11/09/17"';
s5='@ TIME           %08s "16.08.31"';
s6='* KOL';
s7='$ %le';
f1=fopen('input_kick0.txt','w');
fprintf(f1,'%s \r\n%s \r\n%s \r\n%s \r\n%s \r\n%s \r\n',s1,s2,s3,s4,s5,s6,s7);
f2=fopen('input_kick1.txt','w');
fprintf(f2,'%s \r\n%s \r\n%s \r\n%s \r\n%s \r\n%s \r\n',s1,s2,s3,s4,s5,s6,s7);
%% Values of k
%Nturns=1e6;
%Nturns0=6e3;
kk=ones(1,Nturns);
kmax=0.9e-6;
kmin=0.3e-6;
i=1;
%% Type of kick ramp-up
%% Constant @k=kmin
%%Impose index=0
%% Parabola: index=1
a=(kmax-kmin)/(Nturns^2-2*Nturns*Nturns0+Nturns0^2);
b=-2*a*Nturns0;
c=kmin+a*Nturns0^2;
funct=@(a,b,c,i) (a*i.^2+b*i+c);
%% Exponential: index=2
d=1/Nturns*log(kmax/kmin);
funct1=@(d,i) (kmin*exp(d*i));
%% Chose the function
index=1; %Choose the function
%% Code
for i=1:Nturns
        if i<=Nturns0
            kk(i)=0;
            fprintf(f1,'%-i. \r\n',kk(i));
        else
            if index==0
                yy=-kmin+2*kmin*rand();
```

```
            elseif index==1
                yy=-funct(a,b,c,i)+2*funct(a,b,c,i)*rand();
            elseif index==2
                yy=-funct1(d,i)+2*funct1(d,i)*rand();
            end
            flag=0;
            while flag==0
                if index==0
                    if (yy<kmin && yy>-kmin)
                        kk(i)=yy;
                        flag=1;
                        fprintf(f2,'%-9.8E \r\n',kk(i));
                    else
                        yy=-kmin+2*kmin*rand();
                    end
                elseif index==1
                    if (yy<funct(a,b,c,i) && yy>-funct(a,b,c,i))
                        kk(i)=yy;
                        flag=1;
                        fprintf(f2,'%-9.8E \r\n',kk(i));
                    else
                        yy=-funct(a,b,c,i)+2*funct(a,b,c,i)*rand();
                    end
                elseif index==2
                    if (yy<funct1(d,i) && yy>-funct1(d,i))
                        kk(i)=yy;
                        flag=1;
                        fprintf(f2,'%-9.8E \r\n',kk(i));
                    else
                        yy=-funct1(d,i)+2*funct1(d,i)*rand();
                    end
                end
            end
        end
end
fclose(f1);
fclose(f2);
toc
figure
hold on
plot(1:100:Nturns,kk(1:100:end),'.r');
if index==0
    plot([1 Nturns],[kmin kmin],'-k');
```

```
    plot([1 Nturns],[-kmin -kmin],'-k');
elseif index==1
    plot(1:200:Nturns,funct(a,b,c,1:200:Nturns),'.k');
    plot(1:200:Nturns,-funct(a,b,c,1:200:Nturns),'.k');
elseif index==2
    plot(1:200:Nturns,funct1(d,1:200:Nturns),'.k');
    plot(1:200:Nturns,-funct1(d,1:200:Nturns),'.k');
end
xlabel '#turns'
ylabel 'kick'
hold off
```

APPENDIX D

APPENDIX D: MAD-X CODE FOR PARTICLE TRACKING AT THE LAST THREE TURNS BEFORE THE EXTRACTION

```
system,"mkdir output";

assign, echo=output\results.out;

call, FILE="Elements-I_APERTURE.txt";
call, FILE="k_quads_a_mano.txt";
call, FILE="sextupole.txt";
call, FILE="linea-ESE.txt";!name seq:CNAO3ESE

beam;

use, SEQUENCE=CNAO3ESE;

SELECT, FLAG=TWISS, RANGE=#s/#e,
    column=name,parent,s,betx,bety,alfx,alfy,dx,dy,dpx,dpy,mux,muy;
TWISS, SEQUENCE=CNAO3ESE, FILE="output\twiss.txt";

CNAO3turns: LINE=(3*CNAO3ESE);
use, SEQUENCE=CNAO3turns;
SELECT, FLAG=TWISS, RANGE=#s/#e,
    column=name,parent,s,betx,bety,alfx,alfy,dx,dy,dpx,dpy,mux,muy;
TWISS, SEQUENCE=CNAO3turns, FILE="output\twiss_checknewline.txt";

assign, echo=output\results.out;
```

```
bxES=16.50118429; !da sim precedente
byES=7.209367591;

x0=0.0350039448;
px0=0.000360475927;
SELECT, FLAG=TWISS, RANGE=#s/#e,
    column=name,parent,s,x,px,betx,bety,alfx,alfy,dx,dy,dpx,dpy,mux,muy;
TWISS, LINE=CNAO3turns, betx=bxES,bety=byES,x=x0,px=px0,
    FILE="output\twiss_IC0005.txt";

/*SENSITIVITY ANALYSIS PARTICLE*/
x0=0.03500080537;
px0=0.0002818268497;
SELECT, FLAG=TWISS, RANGE=#s/#e,
    column=name,parent,s,x,px,betx,bety,alfx,alfy,dx,dy,dpx,dpy,mux,muy;
TWISS, LINE=CNAO3turns, betx=bxES,bety=byES,x=x0,px=px0,
    FILE="output\twiss_SensAnalysis_csi-2.txt";

/*
x0=0.03500298439;
px0=0.0006971642493;
SELECT, FLAG=TWISS, RANGE=#s/#e,
    column=name,parent,s,x,px,betx,bety,alfx,alfy,dx,dy,dpx,dpy,mux,muy;
TWISS, LINE=CNAO3turns, betx=bxES,bety=byES,x=x0,px=px0,
    FILE="output\twiss_IC0010.txt";

x0=0.03500082978;
px0=0.00103967663;
SELECT, FLAG=TWISS, RANGE=#s/#e,
    column=name,parent,s,x,px,betx,bety,alfx,alfy,dx,dy,dpx,dpy,mux,muy;
TWISS, LINE=CNAO3turns, betx=bxES,bety=byES,x=x0,px=px0,
    FILE="output\twiss_IC0015.txt";
*/
```

APPENDIX E

APPENDIX E: MATLAB CODE FOR POST-PROCESS MAD-X RESULTS FOR THE LAST THREE TURNS ANALYSIS

```
%Remember to change the index according to the analysis you wanna perform
%1:3 if 1 part for each dp/p to study
%1:1 if sensitivity analysis has to be done
clearvars
close all
clc

cd ..
cd('!Last3Twiss');
cd('output');

% Load 3files for the 3 mom for the closest p to septum
% mom=['0005';'0010';'0015'];
col=['.b';'.r';'.g'];
for i=1:1
%     ff=fopen(strcat('twiss_IC',mom(i,:),'.txt'));
    ff=fopen('twiss_SensAnalysis_csi-2.txt');
    %delete first lines written by MAD-X
    j=1;
    line=fgetl(ff);
    while (line(1)=='@' || line(1)=='*' || line(1)=='$' || line(1)=='#')
           line=fgetl(ff);
           j=j+1;
    end
    k=1;
```

```
    part=zeros(1172,3);
    while (line(1)~='#' && line(1)~=-1)
        temp=str2double(strsplit(line(1:end),' '));%data
        part(k,1)=temp(4);%save s
        part(k,2:3)=temp(end-1:end);%save x and px
        line=fgetl(ff);
        k=k+1;
        clear temp
    end
    figure(1)
    hold on
    plot(part(:,1),part(:,2),col(i,:));
    xlabel 's'
    ylabel 'x'
    title 'Closest p. to septum'
    hold off

    clear part
end
fclose('all');
cd ..
%% To draw APERTURES
ff=fopen('linea_ingrombri.txt','r');
line=fgetl(ff);
i=1;
while line~=-1
    ind=find(line==',');
    ind1=find(line==';');
    if i~=1
        if length(line(1:ind(1)-1))<length(pos(1,:))
            temp=zeros(1,length(pos(1,:))-length(line(1:ind(1)-1)));
            pos(i,:)=[temp line(1:ind(1)-1)];
        else
            pos(i,:)=line(1:ind(1)-1);
        end
    else
        pos(i,:)=line(1:ind(1)-1);
    end
    ESE(i,1)=str2double(line(ind(1)+1:ind(2)-1));
    ESE(i,2)=str2double(line(ind(2)+1:ind(3)-1));
    ESE(i,3)=str2double(line(ind(3)+1:ind1-1));
    negESE(i,1)=str2double(line(ind(1)+1:ind(2)-1));
    negESE(i,2)=-str2double(line(ind(2)+1:ind(3)-1));
```

```
    negESE(i,3)=-str2double(line(ind(3)+1:ind1-1));
    if pos(i,:)=='SE_010A_ESP'
        ESE(i,2)=0.035;
        negESE(i,2)=-0.07;
    end
    if pos(i,:)=='S0_016A_MSP'
        ESE(i,2)=0.0289;
        negESE(i,2)=-0.07;
    end
    if pos(i,:)=='S0_023A_ESP'
        ESE(i,2)=0.07;
        negESE(i,2)=-0.0424;
    end
    if pos(i,:)=='SC_023A_DPH'
        negESE(i,2)=-0.059;
        ESE(i,2)=0.0325;
    end
    i=i+1;
    line=fgetl(ff);
end
ll=cumsum([ESE(:,1);ESE(:,1);ESE(:,1)]);
ESE=[ESE;ESE;ESE];
negESE=[negESE;negESE;negESE];

h1=figure(1);
hold on
for i=1:length(ll)
    if i==1
        plot([ll(i),ll(i)],[0.07,ESE(i,2)],'-k');
        plot([0,ll(i)],[ESE(i,2),ESE(i,2)],'-k');
        plot([0,ll(i)],[-0.07,negESE(i,2)],'-b');
        plot([0,ll(i)],[-0.07,negESE(i,2)],'-b');
    elseif i~=length(ll)
        plot([ll(i-1),ll(i)],[ESE(i,2),ESE(i,2)],'-k');
        plot([ll(i),ll(i)],[ESE(i,2),ESE(i+1,2)],'-k');
        plot([ll(i-1),ll(i)],[negESE(i,2),negESE(i,2)],'-b');
        plot([ll(i),ll(i)],[negESE(i,2),negESE(i+1,2)],'-b');
    else
        plot([ll(i-1),ll(end)],[ESE(i,2),ESE(i,2)],'-k');
        plot([ll(end),ll(end)],[ESE(i,2),ESE(i,2)],'-k');
        plot([ll(i-1),ll(end)],[negESE(i,2),negESE(i,2)],'-b');
        plot([ll(end),ll(end)],[negESE(i,2),negESE(i,2)],'-b');
    end
```

```
end
ylim([-0.1 0.1]);
grid on
hold off
saveas(h1,'Last3p_Last3turns','jpg');
cd ..
```

BIBLIOGRAPHY

[1] *Fast picture shot from: wiki/linear particle accelerator*.

[2] *Image from the web: Accelerators for society*.

[3] *Image from the web: Chang gung memorial hospital, international medical center*.

[4] *Image from the web: cyberphysics.co.uk*.

[5] *Image from the web: lhc-closer.es*.

[6] *Image from the web: nuclphys.ru*.

[7] *Image from the web: Particle therapy co-operative group*.

[8] *Image from the web: psi.ch*.

[9] *Image from the web: Radiation biology chapter 7*.

[10] *Image from the web: starsdestination.blogspot.com*.

[11] *Image from the web: teslaresearch.com*.

[12] *Image from the web: triumf.ca/*.

[13] *Image from the web: uspas.fnal.gov/materials/*.

[14] *National institue of standards and technology*.

[15] M. J. BARNES, *Beam trasnfer devices: septa*.

[16] M. CRESCENTI, P. KNAUS, AND S. ROSSI, *The rf cycle of the PIMMS synchrotron*, CERN-PS 99-060-DI, p. 26.

[17] J. L. DUFF, *Longitudynal beam dynamics and stability*, in Small Accelerators Course, Zeegse, 24th May - 2nd June 2005.

[18] W.-M. Y. ET AL., *Review of particle physics*, Journal of Physics, p. 1232.

[19] G. FLOQUET, *Sur les équations différentielles linéaires à coefficients périodiques*, Annales scientifiques de l'E.N.S. 2e série, pp. 47 – 88.

[20] T. FURUKAMA, K. NODA, T. H. UESUGI, S. SHIBUYA, T. NARUSE, M. KANAZAWA, E. TAKADA, AND S. YAMADA, *Recent improvement of slow-extraction at HIMAC synchrotron*.

[21] L. GREVILLOT, M. STOCK, AND S. VATNITSKY, *Evaluation of beam delivery and ripple filter design for non-isocentric proton and carbon ion therapy*, Physics in Medicine and Biology, Vol. 60.

[22] A. C. S. GROUP, *Proton-Ion medical machine study PIMMS - Part I*, CERN, 2005.

[23] T. LAWRENCE, *Introduction to radiation oncology pre-clinical*, University of Michigan Medical School.

[24] C. B. MEINHOLD, S. ABRAHAMSON, S. J. ADELSTEIN, W. J. BAIR, J. J. D. BOICE, R. M. FRY, E. J. HALL, E. W. WEBSTER, AND W. K. SINCLAIR, *Limitation of exposure to ionizing radiation (supersedes NCRP report no. 91)*, (1993).

[25] E. B. PODGORSAK, *Radiation Oncology: a handbook for teachers and students*, IAEA, 2005.

[26] M. G. PULLIA, *Synchrotron for hadrontherapy*, Reviews of Accelerators Science and Technology, Vol. 2, pp. 157–178.

[27] S. ROSSI, *The status of CNAO*, The European Physiscal Journal Plus, p. 78.

[28] TURNER AND STUART, *CAS – CERN accelerator school: 5th general accelerator physiscs course*, in CERN-94-01, 1994.

Ringraziamenti

Vorrei ringraziare il centro CNAO per avermi ospitata in questi mesi. In particolare, il Dr. Marco Pullia e Simone Savazzi per avermi guidata nello studio di argomenti per me nuovi e per avermi dato la possibilità di studiare un argomento così stimolante. Federica Carnevale, Daniele Introini e l'Ing. Michele Ferrarini per aver reso la mia permanenza al CNAO lieta e essere stati i colleghi perfetti con cui condividere le giornate.

Vorrei inoltre ringraziare i miei relatori, Prof.ssa Sandra Dulla e il Prof. Stefano Agosteo, per aver appoggiato la mia scelta di una tesi svolta in un centro di ricerca così all'avanguardia. Dunque, il Politecnico di Torino e i suoi docenti per avermi istruita per quattro anni e per avermi dato la possibilità di partecipare ad un programma di scambio con il Politecnico di Milano dove ho avuto modo di crescere ulteriormente. Infine, il Professor Gianni Coppa per avermi guidata nella strada verso il dottorato di ricerca.

A questo punto vorrei ringraziare i miei colleghi, soprattutto coloro che sono stati da vicino i compagni di questa avventura: Daniele, Vincenzo, Samuele e Gabriele. Ma più di tutti Anna, Enrica ed Emanuele che dai primi anni sono stati colleghi e poi amici fidati. A Claudia e Carlotta che ho incrociato nel mio percorso e che hanno deciso di rimanere. Le mie amiche di sempre, Veronica e Maura, perché nonostante la distanza e i periodi di assenza sono sempre state pronte a ricominciare esattamente da dove eravamo rimaste.

A tutta la mia numerosa famiglia va un grande e sentito grazie. Perché sono loro che, a prescindere dal legame di sangue, sono stati sempre al mio fianco dal primo giorno di scuola elementare ad oggi in cui concludo il mio percorso di studi universitari.

Infine, vorrei spendere due parole per i miei genitori, Michele e Maria Gabriella. Sono stati la mia guida e il mio più grande appoggio. Vorrei dire loro grazie per avermi fornito supporto quando ne avevo bisogno ma, soprattutto, per avermi lasciata libera di scegliere permettendomi così di fallire e di rialzarmi. Sono loro sinceramente grata per avermi dato la possibilità di crescere e di inseguire i miei sogni nonostante significasse allontanarmi da casa. Nonostante la distanza sapevo che sarebbero sempre stati al mio fianco per superare con me le difficoltà e so che sempre ci saranno.

I would also like to thank my supervisors, Prof. Sandra Dulla and Prof. Stefano Agosteo, for supporting my choice of a thesis carried out in such a cutting-edge research centre. So, Politecnico di Torino and its teachers for having instructed me for four years and for giving me the opportunity to participate in an exchange program with Politecnico di Milano where I had the opportunity to grow further. Finally, Prof. Gianni Coppa for guiding me on my way to my PhD.

At this point I would like to thank my colleagues, especially those who have been close companions of this adventure: Daniele, Vincenzo, Samuele and Gabriele. But above all Anna, Enrica and Emanuele who from the early years were colleagues and then trusted friends. To Claudia and Carlotta that I crossed in my path and who have decided to stay. My friends of all time, Veronica and Maura, because despite the distance and periods of absence have always been ready to start exactly where we were left.

A large and heartfelt thanks go out to my whole family. Because it is they who, irrespective of the blood bond, have always been by my side from the first day of elementary school to today when I finish my university studies.

Finally, I would like to spend some words for my parents, Michele and Maria Gabriella. They were my guide and my greatest support. I would like to say thank you for giving me support when I needed it but, above all, for leaving me free to choose, allowing me to fail and get up again. I am sincerely grateful to you for giving me the opportunity to grow up and pursue my dreams even though it meant leaving home. Despite the distance I knew that you would always be by my side to overcome difficulties with me and I know you will always be there.*I would like to thank the CNAO centre for hosting me in these months. In particular, Dr. Marco Pullia and Simone Savazzi for having guided me in the study of new topics and for giving me the opportunity to study such a stimulating topic. Federica Carnevale, Daniele Introini and Ing. Michele Ferrarini for making my stay at CNAO happy and being the perfect colleagues to share the days with.*

I would also like to thank my supervisors, Prof. Sandra Dulla and Prof. Stefano Agosteo, for supporting my choice of a thesis carried out in such a cutting-edge research centre. So, Politecnico di Torino and its teachers for having instructed me for four years and for giving me the opportunity to participate in an exchange program with Politecnico di Milano where I had the opportunity to grow further. Finally, Prof. Gianni Coppa for guiding me on my way to my PhD.

At this point I would like to thank my colleagues, especially those who have been close companions of this adventure: Daniele, Vincenzo, Samuele and Gabriele. But above all Anna, Enrica and Emanuele who from the early years were colleagues and then trusted friends. To Claudia and Carlotta that I crossed in my path and who have decided to stay. My friends of all time, Veronica and Maura, because despite the distance and periods of absence have always been ready to start exactly where we were left.

A large and heartfelt thanks go out to my whole family. Because it is they who, irrespective of the blood bond, have always been by my side from the first day of elementary school to today when

I finish my university studies.

Finally, I would like to spend some words for my parents, Michele and Maria Gabriella. They were my guide and my greatest support. I would like to say thank you for giving me support when I needed it but, above all, for leaving me free to choose, allowing me to fail and get up again. I am sincerely grateful to you for giving me the opportunity to grow up and pursue my dreams even though it meant leaving home. Despite the distance I knew that you would always be by my side to overcome difficulties with me and I know you will always be there.